University of Tennessee, Knoxville

TRACE: Tennessee Research and Creative Exchange

Doctoral Dissertations

Graduate School

5-2021

# Wide Area Damping Control to Improve Transient Stability and Hardware-In-the-Loop (HIL) Implementation

Ibrahim Abdullah Altarjami
ialtarja@vols.utk.edu

Follow this and additional works at: https://trace.tennessee.edu/utk_graddiss

Part of the Power and Energy Commons

## Recommended Citation

Altarjami, Ibrahim Abdullah, "Wide Area Damping Control to Improve Transient Stability and Hardware-In-the-Loop (HIL) Implementation. " PhD diss., University of Tennessee, 2021.
https://trace.tennessee.edu/utk_graddiss/6671

This Dissertation is brought to you for free and open access by the Graduate School at TRACE: Tennessee Research and Creative Exchange. It has been accepted for inclusion in Doctoral Dissertations by an authorized administrator of TRACE: Tennessee Research and Creative Exchange. For more information, please contact trace@utk.edu.

To the Graduate Council:

I am submitting herewith a dissertation written by Ibrahim Abdullah Altarjami entitled "Wide Area Damping Control to Improve Transient Stability and Hardware-In-the-Loop (HIL) Implementation." I have examined the final electronic copy of this dissertation for form and content and recommend that it be accepted in partial fulfillment of the requirements for the degree of Doctor of Philosophy, with a major in Engineering Science.

Yilu Liu, Major Professor

We have read this dissertation and recommend its acceptance:

Seddik Djouadi, Lin Zhu, Evangelos Farantatos

Accepted for the Council:

Dixie L. Thompson

Vice Provost and Dean of the Graduate School

(Original signatures are on file with official student records.)

# Wide Area Damping Control to Improve Transient Stability and Hardware-In-the-Loop (HIL) Implementation

A Dissertation Presented for the

Doctor of Philosophy

Degree

The University of Tennessee, Knoxville

Ibrahim Abdullah Altarjami

May 2021

© by Ibrahim Abdullah Altarjami, 2021
All Rights Reserved.

*dedication...*

*To my beloved parents, my supportive siblings, my lovely wife, and my astonishing kids.*

# Acknowledgments

First and foremost, all praises to Allah, for giving me the health and the will to finish this academic work successfully.

I would like to express my deepest gratitude to my advisor Dr.Yilu Liu for her professional guidance and unlimited support throughout my Ph.D. journey. No words can express how grateful I am.

Special thanks to Dr.Seddik Djouadi, Dr.Lin Zhu, and Dr.Evangelos Farantatos for being in my dissertation committee. I greatly appreciate their insightful suggestions throughout dissertation preparation.

My sincere thanks also go to all my colleagues in the Power IT Lab. I am very grateful to all group members for their productive discussions and comments during the research progress. Special thanks to Dr.Lin Zhu for his time, effort, and patience with providing advice, comments, and feedback on my research works. I profoundly appreciated and valued what you have done with me.

My heartfelt thanks and appreciation go to my parents, Abdullah and Aydah, who have unlimitedly supported me with love and prayers throughout my academic journey. I am genuinely grateful for their sacrifices and endless support. Moreover, I would like to express my sincere appreciation to all my brothers and sisters for their tremendous motivation and best wishes.

My affectionate thanks go to my amazing wife Afaf, who has been supportive since I started pursuing graduate studies. Her selfless care for our children and me made it possible to accomplish this degree. I am truly blessed to have her in my life. To the joy of my life, my two astonishing kids, Abdulmalik and Heba, thanks for being patient with me!

I would like to thank my sponsor, Taibah University represented by the Saudi Arabian Cultural Mission in the United States, for giving me the opportunity to study abroad and the generous financial support.

# Abstract

In this dissertation, the impacts of WADCs on system transient stability are investigated, including system separation prevention under large disturbances and tie-line power transfer limit enhancement with consideration of a three-phase fault on one of the two tie-lines. The full Saudi power grid model in PSS/e is reduced for the real-time simulation on the Real-Time Digital Simulator (RTDS), and thus the developed WADCs can be tested in a controller hardware-in-the-loop environment in the future. The RTDS model is validated by comparing the full PSS/e model and the reduced PSS/e model under different contingencies. The WADCs are designed using a measurement-driven approach. The system separation prevention and tie-line power transfer limit by these WADCs are demonstrated by the real-time simulations on the RTDS. Moreover, the performance of the developed WADC was validated on the HIL test setup under different scenarios, including measurement error/noise, constant and stochastic time delay, consecutive and stochastic data package loss, and multiple PMUs as a backup. The experiment results demonstrate that the developed WADC can provide sufficient damping to suppress the targeted oscillation mode. Meanwhile, with multiple WADCs, the system separation after a large amount generation trips can be prevented. Also, the transfer limit of the tie-line can be further enhanced. The WADC performance will be evaluated under realistic operating conditions, including communication uncertainties and measurement error. The CompactRIO system was used to implement the WADC. The CompactRIO system is a general-purpose controller provided by National Instruments (NI) for prototyping. Using a hybrid TSAT-RTDS simulation, a HIL testing platform was built to imitate realistic conditions with several communication network uncertainties and impairments. The hardware WADC was tested in the HIL setup, where several auxiliary function modules were implemented within the WADC. The WADC

was validated during testing to ensure satisfactory performance under realistic operating conditions. The impacts of the higher PV penetration on the rotor angle stability and inter-area oscillations are also investigated. It has been known that the inter-area oscillations are significantly affected by the increasing amount of PV generation since the system inertia is reduced. The impacts of WADCs on small-signal stability and system transient stability are investigated when the SEC system is integrated with high PV penetration. The marginal generation trip and tie-line power transfer limit enhancement considering a three-phase fault on one of the major tie-line.

# Table of Contents


**1 Introduction** **1**

1.1 Background . . . . . 1

1.2 Motivation . . . . . 2

1.3 Contributions . . . . . 3

1.4 Dissertation Outline . . . . . 4

**2 Literature Review** **6**

2.1 Low-Frequency Oscillations in Power Systems . . . . . 6

2.2 Wide-Area Damping Control Design . . . . . 8

2.3 System Identification . . . . . 9

2.4 Impact of high renewable resources on system interarea oscillations . . . . . 11

**3 Wide Area Damping Control Design** **15**

3.1 Introduction . . . . . 15

3.2 Transfer function model construction and validation . . . . . 15

3.2.1 Transfer function model construction . . . . . 15

3.2.2 Transfer function model validation . . . . . 18

3.3 Optimal signal selection . . . . . 20

3.3.1 Optimal observation signal selection . . . . . 20

3.3.2 Optimal actuation signal selection . . . . . 21

3.4 Wide Area Damping Controller Design . . . . . 22

3.5 Summery . . . . . 27

**4 Impact of WADC on rotor angle stability: Case Study Saudi System** **29**
4.1 Introduction Of Saudi System . . . . . 29
4.1.1 Saudi Electricity Company (SEC) Model Validation . . . . . 31
4.2 WADC design for Saudi System . . . . . 34
4.2.1 Optimal Observation Signal Selection . . . . . 34
4.2.2 Optimal Actuation Signal Selection . . . . . 37
4.2.3 Model validation in time domain and frequency domain . . . . . 45
4.3 WADC design and impact on the system oscillations . . . . . 48
4.3.1 Control effect of single plant WADC . . . . . 48
4.3.2 Comparison of WADCs via different actuators . . . . . 57
4.3.3 Control effect of multiple WADCs . . . . . 57
4.3.4 Control effect of the WADC via HVDC . . . . . 61
4.4 Transient Stability Improvement with the designed WADC . . . . . 65
4.4.1 Impact of WADC on system separation condition . . . . . 65
4.4.2 Impact on the tie-line active power transfer limit . . . . . 66
4.5 Improving the robustness of the WADC . . . . . 70
4.5.1 Improving the performance of the used controller . . . . . 70
4.5.2 Developing a robust controller using H-infinity . . . . . 73
4.6 Summary . . . . . 78

**5 Implementation of the WADC using Real Time Simulator (RTS) and Hardware-In-the-Loop (HIL) testing** **79**
5.1 Introduction . . . . . 79
5.2 SEC pure RTDS model development . . . . . 80
5.2.1 WADC development in the pure RTDS model . . . . . 85
5.2.2 Performance of the WADCs using pure RTDS . . . . . 85
5.3 SEC hybrid TSAT-RTDS model development . . . . . 91
5.3.1 WADC development through Hardware-In-the-Loop . . . . . 95
5.3.2 Performance of the WADCs using HIL testing . . . . . 102
5.4 Summary . . . . . 112

**6 Impact of WADC on the system with high PV** **113**

6.1 Introduction . . . . . 113

6.2 Impact of high PV on SEC oscillation modes . . . . . 114

6.3 The Impact of WADC on high PV system oscillation . . . . . 117

6.3.1 Using synchronous machine as WADC actuator . . . . . 117

6.3.2 Using Battery Electric Storage System (BESS) as WADC actuator . . 124

6.4 Transient stability improvement with the designed WADC . . . . . 131

6.4.1 Impact of WADC on system marginal generation trip . . . . . 131

6.4.2 Impact on the tie-line active power transfer limit . . . . . 133

6.5 Summary . . . . . 136

**7 Conclusion** **137**

**Bibliography** **140**

**Appendices** **156**

A SEC Coherent groups . . . . . 157

B Addition Results for Impact of the WADC (Base Case) . . . . . 158

C Addition Results of impact for the WADC (HVDC, PV cases, and BESS) . . 163

D Data Loss Handling Process . . . . . 169

**Vita** **170**

# List of Tables


4.1 Oscillation comparison between measurement PSSe model . . . . . 32
4.2 Candidate Observation Signals In Central Area . . . . . 35
4.3 Candidate Observation Signals In Western Area . . . . . 36
4.4 Top 10 generator exciter actuators based on bus frequency magnitude . . . 39
4.5 Top 10 generator exciters actuator based on residue magnitude . . . . . 39
4.6 Top 10 generator governor actuators based on bus frequency magnitude . . 42
4.7 Top 10 generator governor actuators based on residue magnitude . . . . . 43
4.8 Model validation in time domain and frequency domain . . . . . 47
4.9 Prony analysis results tie-line fault (WADCs via single plant exciters) . . . . 50
4.10 Prony analysis results single generation trip (WADCs via single plant exciters) 52
4.11 Prony analysis results tie-line fault (WADCs via single plant governors) . . . 54
4.12 Prony analysis results single generation trip (WADCs via single plant governors) 55
4.13 Prony analysis results tie-line fault (WADCs via governor and exciter) . . . . 58
4.14 Prony analysis results single generation trip (WADCs via governor and exciter) 59
4.15 Prony analysis results tie-line fault (Multiple WADCs) . . . . . 60
4.16 Prony analysis results for single generation trip (Multiple WADCs) . . . . . 62
4.17 Marginal amount of generation trip With WADCs . . . . . 67
4.18 Active power transfer limit With WADCs . . . . . 69

5.1 Prony analysis of system responses in three models . . . . . 84
5.2 Active power transfer limit With WADCs For the three models . . . . . 89

6.1 The generation amount of the solar PV penetration levels . . . . . 115
6.2 Prony analysis results of tie-line fault (PV level comparison) . . . . . 116

6.3 Prony analysis results of tie-line fault (20% PV) . . . . . 119
6.4 Prony analysis results of tie-line fault (40% PV) . . . . . 121
6.5 Prony analysis results of tie-line fault (60% PV) . . . . . 122
6.6 Top 10 buses based on residue magnitude of the BESS placement . . . . . 127
6.7 Prony analysis results of tie-line fault (BESS cases) . . . . . 130
6.8 Marginal amount of generation trip With WADCs (PV cases) . . . . . 134
6.9 Active power transfer limit With WADCs (PV cases) . . . . . 135

B.1 Transfer function model for each selected generator exciter actuator . . . . . 161
B.2 Transfer function model for each selected generator governor actuator . . . . 162
B.3 WADC parameters . . . . . 162

# List of Figures


3.1 Transfer function model structure for damping control. . . . . 17
3.2 WADC block diagram. . . . . 24
3.3 WADC closed loop structure of the system. . . . . 24
3.4 Flowchart of the WADC design method. . . . . 28

4.1 SEC System grid. . . . . 30
4.2 SEC FDR Results . . . . . 32
4.3 Frequency response for different line fault (coherent group analysis). . . . . 33
4.4 Central buses FFT. . . . . 35
4.5 West buses FFT. . . . . 36
4.6 Step down response - Exciter. . . . . 38
4.7 Transfer function model identification using probing signal. . . . . 38
4.8 Controllability comparison (frequency magnitude comparison - Exciter). . . . 40
4.9 Controllability comparison (residue magnitude comparison - Exciter). . . . . 40
4.10 Step down frequency response - Governor. . . . . 42
4.11 Controllability comparison (frequency magnitude comparison - Governor). . 43
4.12 Controllability comparison (residue magnitude comparison - Governor). . . . 44
4.13 Input and output signal for Identified model. . . . . 46
4.14 Fitness index for Identified model. . . . . 46
4.15 Exciter WADC. . . . . 49
4.16 Frequency response during Tie-line fault (WADCs via single plant exciters). 49
4.17 Angle difference response during tie-line fault (WADCs via single plant exciters). 50

4.18 Frequency response during single generation trip (WADCs via single plant exciters). . . . . 52
4.19 Governor WADC. . . . . 53
4.20 Frequency response during Tie-line fault (WADCs via single plant governors). 53
4.21 Angle difference response during tie-line fault (WADCs via single plant governors). . . . . 54
4.22 Frequency response during single generation trip (WADCs via single plant governors). . . . . 55
4.23 Angle difference response during single generation trip (WADCs via single plant governors). . . . . 56
4.24 Frequency response during Tie-line fault (WADCs via governor and exciter). 58
4.25 Frequency response during single generation trip (WADCs via governor and exciter). . . . . 59
4.26 Frequency response during Tie-line fault (WADCs via multiple actuators). . 60
4.27 Frequency response during single generation trip (WADCs via multiple actuators). . . . . 62
4.28 SEC HVDC links. . . . . 63
4.29 Frequency response during line fault (HVDC case). . . . . 63
4.30 HVDC PSSE model. . . . . 64
4.31 WADC via multiple actuators frequency response after large generation trip (2040 MW). . . . . 67
4.32 WADC via HVDC frequency response after large generation trip (2040 MW). 68
4.33 Marginal generation trip at the western area. . . . . 68
4.34 Transfer limit of the major tieline. . . . . 69
4.35 Gain uncertainty function implementation. . . . . 71
4.36 Frequency response after line fault disturbances with gain robustness function (WADCs via exciters). . . . . 71
4.37 Frequency response after single generator trip with gain robustness function (WADCs via exciters). . . . . 72

4.38 Frequency response after three generators trip with gain robustness function (WADCs via exciters). . . . . 72
4.39 Hinf Control structure. . . . . 75
4.40 System response with H-infinity controller after line fault. . . . . 76
4.41 System response with H-infinity controller after generation trip (680 MW). . 77

5.1 Model reduction using DYNRED. (Source: Powertech Labs Inc.) . . . . . 82
5.2 Models comparison after a single-generator trip (680 MW). . . . . 83
5.3 Models comparison after large generation trip (2,040 MW). . . . . 83
5.4 WADC block diagram. . . . . 86
5.5 WADCs via Exciters and Governors on RTDS. . . . . 86
5.6 WADC performance after a single-generator trip (pure RTDS). . . . . 87
5.7 System response after large generation trip 2040 MW(pure RTDS). . . . . 89
5.8 Transfer limit of the major tieline for the three models. . . . . 90
5.9 Hybrid TSAT-RTDS simulation overview. (Source: RTDS). . . . . 93
5.10 TRI links for hybrid simulation. . . . . 93
5.11 Frequency response comparison of TSAT-RTDS hybrid and the full PSSE model during a single generation trip. . . . . 94
5.12 HIL test setup based on hybrid TSAT-RTDS simulation. . . . . 96
5.13 Analogue Input Output of RTDS (Picture source: RTDS). . . . . 96
5.14 Overall structure of the controller. . . . . 98
5.15 The delay compensator process. . . . . 101
5.16 WADCs via exciters after single-generator trip (TSTA-RTDS Hybrid). . . . . 103
5.17 WADCs via governors after single-generator trip (TSTA-RTDS Hybrid). . . . 103
5.18 System response during large generation trip of 2040 MW (TSTA-RTDS Hybrid). . . . . 104
5.19 WADCs via exciters with constant delay during single-generator trip. . . . . 106
5.20 Control effect of WADCs via exciters with random time delay during single-generator trip. . . . . 107

5.21 Control effect of WADCs via exciters with random time delay and occasional data drop during single-generator trip. . . . . 109
5.22 Control effect of WADCs via exciters intolerable time delay with supervisory control during single-generator trip. . . . . 110
5.23 Control effect of WADCs via exciters with data drop with supervisory control during single-generator trip. . . . . 111

6.1 Frequency response during tie-line fault (PV level comparison). . . . . 115
6.2 Residue Mag. of system identification (Exciters case). . . . . 118
6.3 Frequency response during tie-line fault (20% PV). . . . . 118
6.4 Angle difference response during tie-line fault (20% PV). . . . . 119
6.5 Frequency response during tie-line fault (40% PV). . . . . 121
6.6 Frequency response during tie-line fault (60% PV). . . . . 122
6.7 Exciter Control Signal during line fault (No PV vs 60%PV). . . . . 123
6.8 BESS Model in the PSSE. . . . . 126
6.9 Controllability comparison of the BESS based on residue analysis. . . . . 126
6.10 Frequency response during line fault for BESS optimal placement. . . . . 127
6.11 Frequency response during tie-line fault (20% PV with BESS). . . . . 129
6.12 Frequency response during tie-line fault (40% PV with BESS). . . . . 129
6.13 Frequency response during tie-line fault (60% PV with BESS). . . . . 130
6.14 Actuator output Active Power comparison. . . . . 132
6.15 Marginal generation trip at the western area with PV. . . . . 134
6.16 Transfer limit of the major tieline with PV. . . . . 135

A.1 SEC Coherent groups . . . . . 157
B.2 Angle difference response during single generation trip (WADCs via single plant exciters). . . . . 158
B.3 Angle difference response during tie-line fault (WADCs via governor and exciter). . . . . 158
B.4 Angle difference response during single generation trip (WADCs via governor and exciter). . . . . 159

B.5 Angle difference response during tie-line fault (WADCs via multiple actuators). 159
B.6 Angle difference response during single generation trip (WADCs via multiple actuators). . . . . 160
B.7 WADC via multiple actuators angle difference after large generation trip (2040 MW). . . . . 160
C.1 Angle difference comparison response during line fault (HVDC case). . . . . 163
C.2 WADC via HVDC angle difference after large generation trip (2040 MW). . 163
C.3 Frequency response after two generators trip with gain robustness function (WADCs via exciters). . . . . 164
C.4 Tie-line angle difference response during tie-line fault (PV level comparison). 165
C.5 Angle difference response during tie-line fault (40% PV). . . . . 165
C.6 Angle difference response during tie-line fault (60% PV). . . . . 166
C.7 Frequency response during line fault (WADC via BESS). . . . . 166
C.8 Angle difference response during tie-line fault (20% PV with BESS). . . . . 167
C.9 Angle difference response during tie-line fault (40% PV with BESS). . . . . 167
C.10 Angle difference response during tie-line fault (60% PV with BESS). . . . . 168
C.11 Angle difference response during tie-line fault (60% PV with BESS). . . . . 168
D.1 The missing data handling process. . . . . 169

# Chapter 1

# Introduction

## 1.1 Background

The power grid is growing towards a complex and widely geographical distributed network with uncertainty in generation and load behaviors. Increased penetration of renewable energy resources and the deployment of distributed generation have introduced uncertainty and variability on the generation side. Adapting these changes and maintaining system balance demand additional operational flexibility. The integration of renewable energy resources also modifies the behavior of the power system's dynamic. Furthermore, renewable resources mainly interact with the power system through power electronic devices, which are characterized by lower short circuit power and lack of inertia, causing more complications to the power system operation. The power grid load side is also experiencing substantial changes. New types of loads like electric vehicles are altering the traditional consumption trends.

There are numerous reasons, other than the imbalance between the load and generation, that power systems are operating closer to their stability limits, such as the restructuring, deregulation, environmental, and economic constraints for transmission infrastructure development [1]. Therefore, critical system modes near stability with limited performance could be affected by random disturbances and cause severe complications like cascading failures and blackouts [2]. Consequently, security boundaries need to be maintained based on a reliable control infrastructure.

Variations in power system operations' demands have radically reformed the expectations from control mechanisms and presented their deficiencies [3]. Conventionally, power system control has been mainly dependent on local input signals. These local controllers are not able to counter the effects of system-wide contingencies. With the increasing growth of Phasor Measurement Units(PMUs) and advancements in the communication technologies, power system monitoring has improved the power system operation awareness and introduced a platform for adaptive and flexible control.

Furthermore, the operator's responses cannot stand solely in the face of events and assure reliability for a complex interconnected power system. Therefore, there is a necessity for improving the wide-area control designs to automatically taking actions to ensure reliable and secure operations by utilizing the modern wide-area monitoring system.

## 1.2 Motivation

One of the primary concerns for the reliable and secure power systems' operation is the small-signal stability issues associated with inter-area oscillations [4]. In the future grid, improving the transfer capability while maintaining system stability requires a significant enhancement of the existing control infrastructure to damp these low-frequency oscillations [5]. Due to the complex operational nature of the existing interconnected power system, deployment of wide-area control schemes is essential for a self-healing grid.

Extensive research has investigated different aspects of wide-area damping control design (WADC) to enhance small signal stability [6]. Some studies have been primarily focused on selections of various actuators such as PSS [7, 8, 9, 10],HVDC [11, 12, 13] or FACTS devices [14, 15]. Other studies deeply discuss the selection of the feedback signal and input placement [16, 17, 18]. The control design methods have also been considered, such as the residue method [19], pole-placement [15, 20], and robust control approaches [7, 17]. Since the communication issue is considered one of the challenges of the wide-area controllers, some studies have examined the controller performance under different time delay conditions [21, 22, 23].

However, one of the main obstacles of WADC design is the assumption of having access to accurate system-wide dynamic models. Recently, the power systems' models have become insufficient to represent the complexity of the power system due to several factors such as the renewable distributed resources deployment and the launching of new models' varieties. Hence, highly reliable controls cannot be built based on inaccurate models. Measurement-based models estimated directly from the measurements can be an outstanding complement to traditional models [24]. With the increasing growth of Phasor Measurement Units(PMUs) and the evolving estimation of model techniques, there are insufficient methods to fill the gap between power system control design and online model estimation. This dissertation aims to propose a wide-area damping control approach that ensures the system's small-signal stability with the desired performance and slightly enhancing the system's transient stability while taking into account the future trend of the power grid with high renewable energy penetration. Moreover, I'll be implementing the wide-area control design in the real-time simulator and Hardware in the loop testing.

## 1.3 Contributions

This dissertation aims to propose a wide-area damping control systematic strategy for power system inter-area oscillations. The contributions of this dissertation are:

- Demonstrated a systematic strategy to design wide-area damping control and presented its effectiveness in enhancing small signal stability and damping out inter-area oscillations by providing system-wide measurements for the controller and control actions through generator excitation systems and governors.

- Demonstrated a measurement-driven identification model for the Saudi Electric System using probing data with modal controllability/observability analysis and then selection of the optimal observation and actuation signals for the WADC design.

- Studied the impact of implementing the WADC on the SVCs, generator exciters, and generator governors.

- Studied the impacts of time-delays on the performance of WADC and proposed a method to handle time-delays.
- Studied the impact of large-scale solar generation on the inter-area oscillations.
- Studied the impact of WADC on the Saudi Electric System integrated with large-scale solar generation at the critical clearing time and system separation.
- Studied the impact of implementing the WADC on the energy storage system and investigated the effect on small-signal and transit stability.
- Demonstrated the WADC design in Hardware in the loop controller and real-time digital simulator (RTDS).

## 1.4 Dissertation Outline

This dissertation is organized as follows:

- **Chapter 2** reviews the low-frequency oscillation problems in power systems and conventional control methods for limiting its consequences. It then presents a comprehensive review of wide-area damping control (WADC) designs and describes the challenging features covered in the literature. Methods to find power system dynamic models from the measurements are reported as well. After that, this chapter summarizes the literature that covered the system identification for oscillation purposes in the power system. Finally, the literature about the impact of high penetration of photovoltaic on system oscillation is presented.
- **Chapter 3** describes the used methodology of designing damping controllers for low-frequency inter-area oscillations. It covers the transfer function model construction, validation, optimal observation and actuation signal selection, and controller design.
- **Chapter 4** studies the impact of WADC on rotor angle stability. The study scope covers transient and small-signal stability by observing the impact on the major tieline power transfer limit, system separation, and inter-area oscillations.

- **Chapter 5** presents the implementation of the wide-area control design (WADC) in the real-time simulator (RTDS) and Hardware in the loop testing.

- **Chapter 6** investigates the impact of high renewable penetration on the system oscillation. The case study presented in this chapter is the Saudi Electric System. Moreover, the chapter studies the impact of WADC on a system with high renewable penetration. The WADC actuators used in the chapter are the energy storage system, exciter, and governor. The study scope covers transient and small-signal stability by observing the impact on the major tieline power transfer limit, system separation, and inter-area oscillations.

- **Chapter 7** summarizes the dissertation's main contributions and suggests recommendations for possible future work.

# Chapter 2

# Literature Review

## 2.1 Low-Frequency Oscillations in Power Systems

One of the primary concerns regarding a secure and reliable power system operation is the small-signal stability problem. In the complex interconnected power system, an unstable mode can have immediate consequences across a wide area and may even lead to cascading failures and blackouts [25]. In the US, past blackout events mostly exhibited sustained low-frequency oscillations [26]. The famous blackout that happened on August 10, 1996, for the Western Electricity Coordinating Council (WECC) system, was due to undamped oscillations [27]. Other major oscillation events involve a generation loss like the one on October 9, 2003, the BC-Alberta separation event on August 4, 2000 [28], or multiple lines tripping on June 4, 2003 [29]. These events bring up considerable concerns about the adverse impact of oscillations on power system operation. Inter-area and local oscillations are two different kinds of oscillations that have led to problems in power systems. Local mode oscillations are caused by a generator or small group of generators swinging against the rest of the system. Local plant modes are usually induced by the action of Automatic Voltage Regulators (AVRs) operating at high output [30]. Natural frequencies of the Local modes are generally in the range of 1 to 3 Hz. Their characteristics are adequately understood and analyzed using a detailed representation [31]. Power system stabilizers (PSS) can be used to achieve satisfactory damping for local modes.

Inter-area oscillations involve a large group of machines oscillating against other large groups of machines in other parts of the system. They may be caused by either improper exciter's gain or groups of machines tightly coupled but interconnected by weak tie lines [2]. Inter-area modes have frequencies typically in the range of 0.1 to 1 Hz. The characteristics of these modes and the factors that influenced them are not fully understood, making them way more complex to study and control. A detailed model of the entire system is required to study inter-area modes [32].

Complex power systems regularly exhibit multiple dominant inter-area oscillation modes. Insufficient damping of these types of oscillations may drive the system to its limitation of power transfer capability or an increment in the amplitude of the oscillations, which could even lead the system to collapse [33]. With the growing power exchange between electric utilities over the transmission network, power systems are pushed to their boundaries, precisely the capacity of transmission lines. Therefore, improving the power transfer capability, while maintaining system stability, dramatically relies on damping these inter-area oscillations.

The traditional approach for damping inter-area oscillations is by installing PSS to provide supplementary control to the excitation generators. Due to the observability lack of specific inter-area modes in local measurements, conventional PSS with local measurements as input, cannot efficiently damp these oscillations. An inter-area mode may be observable from one area and controllable from another [34]. Furthermore, conventional PSS performance is highly sensitive to operating point variations in the system dynamics, which leads to significant challenges in the design process [35]. PSS's practical feasibility is also limited since power system models have been found unsatisfactory for representing real-time operating conditions [27]. To overcome the deficiencies of the conventional control methods, wide-area control methodologies need to be improved for enhancing the inter-area oscillations' damping.

## 2.2 Wide-Area Damping Control Design

The benefits of the growing deployment of Phasor Measurement Units (PMUs) offer the feasibility of control based on Wide-area Measurements (WAMs) and afford the great potential to overcome conventional controllers' shortcomings. North America Synchrophasor Initiative (NAPSI) has identified real-time automated and adaptive wide-area grid controls for interarea oscillation damping as one of the top priority applications to be developed utilizing the phasor data [36]. Wide-area Damping Control (WADC) design involves three primary steps [6]. Before the control design, the feedback signal and control inputs are chosen based on the controllability and observability of the dominant oscillation modes, respectively. In the following step, the system model defining the input-output relationships is identified. Then, the control can be designed using the desired control methodologies.

Researchers achieved promising results by applying WAMs to Wide-area Damping Control (WADC) of inter-area oscillations. Generator PSSs, FACTS devices, and HVDC are three primary actuators used in WADC design. A Linear Matrix Inequality (LMI) based centralized wide-area damping control was proposed in [7] that provides supplementary damping signals to AVRs of selected generators and their local PSS signal. In the proposed design procedure, only a few measurements with high observability of inter-area modes are chosen, and only a few generators with the high controllability of those modes are selected as control locations. A novel control inversion framework was proposed in [37], which can invert PMU-based control designs developed for reduced-order power systems to controllers in actual higher-order systems via optimization methods. In practice, to enhance inter-area oscillations' damping performance, a WADC framework was designed to modulate multiple HVDC systems and was implemented in China Southern Power Grid (CSG) [11].

Although various other studies also prove that remote measurement signals could increase the damping of inter-area modes beyond that achievable by local signals [38, 39, 40], wide-area damping control (WADC) still has many challenges associated with its design and implementation. Since power networks are considered large-scale systems, the centralized structure for wide-area control proposed by many previous studies [7, 41, 42], notwithstanding showing optimal performance, is quite challenging to perform in practice.

On the other hand, there is a lack of research efforts in using distributed control schemes for wide-area damping control design that can afford near-optimal performance by exploiting limited communication and limited model data sufficiently [43].

## 2.3 System Identification

The order of a detailed complex power system model could reach a vast number; also, it is difficult to get the precise controller parameters. Consequently, it is unreliable to design WADC using a detailed model. The dominant modes in a single power system are not many and could be represented using a reduced-order model [6].

Accurate power system dynamic models are the primary stage of power system analysis, control, and operation [27, 44]. Traditionally, power system dynamic responses can be achieved by the time-domain simulation using theoretical models and parameters for a given operating condition. However, the time-domain simulation approach has two significant limitations [45]. First, the simulated dynamic model cannot cover all the power systems details. Second, the operating point and the topology of the power system change quite frequently. These two aspects can never be captured entirely by existing circuit-based models. System identification is a suitable method for obtaining the power system's dynamic behaviors based on real measurement data.

Random load changes occur regularly in power systems and are imagined as an unknown input noise, which is the primary excitation source of the electromechanical dynamics. In the measured data, this excitation is translated into ambient noise. Using ambient data to estimate the electromechanical mode in real-time is described in [46]; also, the study illustrated three-mode meter algorithms to utilize the ambient data for automated assessment of dynamic system stability. A comparison study is conducted between several methods that have been employed for ambient data analysis [47], which are The Yule-Walker (YW), Yule-Walker with spectral analysis (YWS), and subspace system identification (N4SID). These algorithms have been performed in the Real-Time Dynamic Monitoring System (RTDMS). One advantage of utilizing ambient data is that measurement data are always available [48]. One of the recent approaches to enhance electromechanical mode identification is

through injecting probing signals into power systems. Rich information regarding the electromechanical modes is obtained when a well-designed probing signal is injected [43]. The probing signals design for estimation accuracy were also studied [46]. One critical improvement in the analysis of ambient data is the feasibility of mode shapes' estimation [49]. The mode shape estimation could further provide advanced control application possibilities [49].

For identifying a reduced-order model, perturbation is injected into the power system to excite system response [50]. Impulse perturbation is used as the injection signal to obtain system model identification in early studies. Prony analysis method is considered the first method used in analyzing system state-space identification [51]. Later, some other techniques have been used to identify the system model using the system response after disturbance such as Eigensystem Realization Algorithm(ERA) [52], Steiglitz–McBride Method,[53], Artificial Neural Network(ANN) [54], and the transfer function method [51]. The system identification methods that can be used with measurement-based models include autoregressive moving average exogenous inputs (ARMAX) and the subspace state-space model. The subspace state-space methods usually use numerical algorithms such as the stochastic subspace identification method [55, 56], or the subspace state-space system identification (N4SID) method [57, 58, 48].

The other subspace methods have earned much recognition recently due to the simplicity of their algorithms [59] and are famous for Multi-Input-Multi-Output systems (MIMO). A literature review of a popular method is presented in [60]. Besides the N4SID and ERA, fundamental algorithms that utilize the subspace method are the Canonical Variate Algorithm (CVA) and the MIMO output-error state-space model identification (MOESP). Single-Input-Multi-Output (SIMO) subspace algorithm is presented in [48], whereas [61] studies MIMO systems.

Another method used to determine the stability limit of the system is Stochastic subspace identification (SSI), which is illustrated in [55]. The main advantages of using SSI are that there is no need for disturbance to obtain information from the measured data, the short computational time, and its capability to handle the signals that contain noise. In [48], the

study proposed that the subspace method should have a continuously exciting input that may offer a promising alternative for the online identification of MIMO systems.

Fast online identification that captures all power system oscillation modes is the core of the adaptive and coordinated oscillation damping controller. Nevertheless, slow computation speed is the primary concern of subspace methods due to the singular value decomposition (SVD) of a large-dimensional matrix. Therefore, to minimize the computation time, a recursive adaptive stochastic subspace identification method is used in [56].

On the other hand, the ARMAX model identification method can be used as an alternative to reduce computational time [62, 63]. The family of "auto-regressive" models has been used for system identification in the oscillation damping controllers [20, 10]. The identified ARMAX model is usually a SISO model, reflecting only one mode, which is considered one of the main shortcomings of this method. [45] proposes a methodology to identify a multi-input multi-output (MIMO)ARMAX-based transfer function model using measurement data to capture all the dominant oscillation modes where ring-down data and ambient data are used for system identification. [45] results prove that using ARMAX for system identification may describe the power system's oscillatory responses accurately. The ARMAX model has comparable accuracy but lower order and enhanced computational efficiency compared to the subspace state-space model.

## 2.4 Impact of high renewable resources on system interarea oscillations

Since the PV system dynamics are fully decoupled from the power system grid synchronization, removing synchronous machines from the grid and replacing them with PV units will affect the system critical modes [64]. Specifically, the reduction of the overall system inertia due to replacing the synchronous generators with PV units will reduce the damping power of the modes [6, 65]. Most of the literatures studied the impact of high PV penetration on oscillation damping and some literature studied the eigenvalues sensitivity analysis to improve the damping. Some researchers studied the impact of high PV penetration, but the

impact on the system oscillation was not the main concern. These studies as well as other partial impacts of the high penetration of PV on oscillation are the focal concerns of the literature highlighted in this section.

Paper [66] focused on the small signal stability of both rooftop and utility PV units through measuring the influence of various percentages of PV (up to 50%) on the small signal stability of the studied system and investigating the impact of high penetration of PV on the oscillation modes in the 0.01-2 Hz range with lower damping (¡ 10%). Its outcomes indicate that higher PV penetration has a negative impact on small signal stability. Similarly, in paper [67], the damping of the mode dropped as the percentage level of PV penetration increased in the system. This indicates that the damping of the system is significantly influenced by the reduction of the system inertia. Similar results can be seen in [68, 69, 70]. Moreover ,in [64], the authors studied the impact of the high penetration of PV in the inter-area oscillation modes of the IE system, defining simulation scenarios of IE systems with high PV based on the percentage of the PV penetrations (5%, 25%,45%, or 65%). The paper reveals that the frequency oscillation increased from 0.20 Hz (dominant inter-area oscillation mode) to 0.28 Hz, with the increment of PV penetration behaving linearly. However, the damping ratio of the oscillation mode decreased when the percentage of PV penetration increases.

However, Reference [65] investigates the system stability of distributed PV and large plants and concludes that the damping ratio of the critical mode is not significantly impacted by increasing any type of PV generation. Similarly, Authors in [71] studied the impact of the high penetration of PV on the low frequency oscillation mode. The paper outcomes show that the damping ratio of the mode is unaffected as the PV penetration increased, whereas the frequency oscillation of the mode increased compared to the one in the non-PV case. Reference [70] studied the impact of the high penetration of PV on the low frequency oscillation mode. The results show that the frequency oscillation of the mode remained unchanged and equivalent to the cases without PV. In [72], the author studied the impact of increasing PV on one machine infinite bus system. The results show that (1) the local electromechanical modes (EM) were significantly affected and (2) the PV system controller parameter significantly impacted the damping ratio of the local modes. Similarly, in [65, 73]

it is also observed that the control method influenced the mode shape and could introduce a new oscillation mode.

On the other hand , some research indicate that increasing PV led to increase the damping. For instant, the authors in [74] studied the impact of the PV on the critical mode of the system. Adding PV generation in the system resulted damping to the critical mode. As such, the impact of concentrated PV integration was less beneficial than scattered integration. [75] and [76] have similar conclusions. Interestingly, other literature found out that the impact of PV could be positive or negative. Reference [77] examines the impact of a PV generator a single-machine infinite-bus system. The paper concludes that PV can either positively or negatively influence oscillation damping. Moreover, other studies found both beneficial and detrimental impacts of PV on oscillations [73]. It is clear that, so far, the literature on the impact of PV on power system oscillations has been inconsistent. In some cases, it finds that the increased penetration of solar PV has a detrimental impact on power system oscillation due to the reduction in the system inertia. Meanwhile, in others, it shows beneficial impacts that depend mainly on the studied system, the penetration percentage of PV penetration, the dispatch of the existing conventional machines, and the PV location. Furthermore, as the literature on the impact of high penetration of PV has been mainly limited to case studies, there are no clear theories to represent this field.

In response to the negative impact of the reduction of inertia on the studied system, paper [68] examined the sensitivity analysis of the interested modes for the system generators and then ranked them based on their sensitivity to the inertia. Redispatching the generators based on their sensitivity to inertia led to improve the damping compared to the base case of PV penetration. Similarly, the authors of paper [70, 74] conducted a sensitivity analysis of the generators by ranking them based on their sensitivity to the inertia. Based on that analysis, the damping ratio of the modes increased after re-dispatching the generators while the damping of the other modes remained almost unchanged.

The DC/AC converter mainly influences PV systems' transient characteristics while the dynamic behavior of a PV system is dominated by the converter associated control [77]. Solar PV is converter-based generation with system dynamics that depend on the state variables of the converter [78]. Some researches introduces two new kinds of identified oscillation

modes that are dominated mainly by converter state variables [64, 65, 73]. These oscillation modes fit in the same range as inter-area oscillation modes, and some of the new oscillation modes are poorly damped [73]. Unlike conventional electromechanical modes, these new oscillation modes in which initiated by the converter dynamic variables and do not involve a large number of participating state variables. [65] Also observed that the control method influenced the mode shape and could introduce a new oscillation mode [64].

Converter oscillation modes are defined based on whether or not synchronous machines participate in the mode. In the first category, all the participating variables of the mode are converter state variables. In the second, the synchronous generators' state variables participate in the oscillation mode. A key trait of the new oscillation modes is their high sensitivity to control parameter variations [73]. Its implications include that the mode shapes could change dramatically due to tuning of the system parameter, making the system unpredictable and hard to monitor [73]. Morover,though some control parameters can improve mode damping significantly, improper tuning could lead to mode instability and the potential introduction of a new oscillation mode [70, 64, 73]. Since many conventional generators are being replaced with PV, Eigenvalue sensitivity analysis is important for dealing with the high penetration of PV due to the high sensitivity of the control parameters that attached with the rest of conventional generators.

# Chapter 3

# Wide Area Damping Control Design

## 3.1 Introduction

The used methodology comprises five stages: transfer function model construction, validation, optimal observation signal selection, optimal actuation signal selection, and controller design. The relevant approaches for each step are presented in this chapter.

## 3.2 Transfer function model construction and validation

### 3.2.1 Transfer function model construction

System identification is a process of building mathematical models for a dynamic system from measurement data. A measurement-based model's development includes three steps, which are data type, model input/output, and model structure and parameter identification.

Three measurement data types (ambient data, probing data, and ringdown data) can be employed to excite oscillatory system modes [79, 63, 48]. For a complex and large interconnected power grid, probing data are theoretically perfect for developing the model since the system response to the injected probing signal contains most of the system's typical modes [45]. Ambient data are primarily produced through generation regulation or load switching within a small range, but they could be very low to observe all the system modes

[80]. However, ringdown data are more comfortable to be collected since they can be observed during large contingencies like generation trips, load shedding, and line trips.

The next step is selecting the proper model input/output. In this dissertation, the excitation system voltage and governor power reference were chosen as the input of the transfer function model, while bus frequency (f) was selected as the output, as shown in Figure 3.1.

If probing data or ambient data are used to construct the transfer function model, a probing signal (or ambient signal) will be combined with Vref or Pref, whereas the system response could be observed from the bus frequency. Therefore, the sum of the reference value and the probing signal (or ambient signal) can be selected as the transfer function model's input.

Bus frequency,tie-line active power, and rotor angular speed are the common observation signals in the power system field. In this dissertation, the high voltage bus frequency was selected as the transfer function model's output signal.

The representation of the measurement-driven model can be achieved using two methodologies. First is the transfer function model, which is a set of difference equations, and the other is the sub-space state-space model, which is a set of differential equations [81]. Then, the measurement-driven model is built using system identification techniques [10]. The output error (OE) polynomial model is chosen as the measurement-driven model structure for model identification using probing measurements, which is a typical type of transfer function model. Output-error (OE) model is a special configuration of the polynomial model. The conventional transfer functions are represented using OE models between the measured inputs, which is white noise, and the outputs [82].

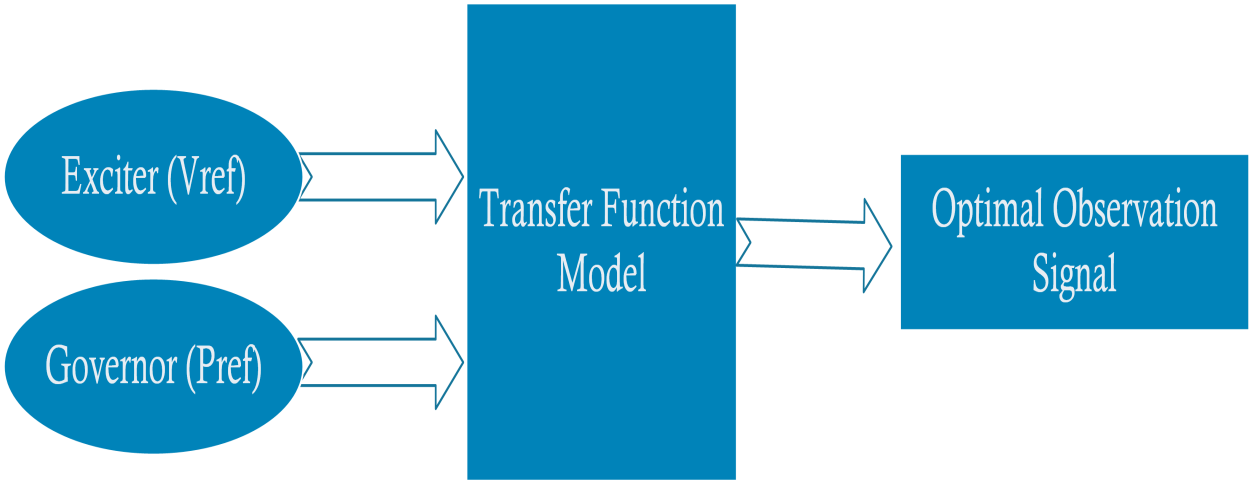


**Figure 3.1:** Transfer function model structure for damping control.

Considering that the input signal is informative enough to identify a system model with n orders or even larger orders, an output error (OE) model structure is chosen with n orders as the identified system model. The system structure is described as follows [83]:

$$y(k) = \frac{B(z,\theta)}{F(z,\theta)}u(k) + e(k) \quad = \frac{b_1 z^{-1} + \cdots + b_n z^z \cdot n_b}{1 + f_1 z^{-1} + \cdots + f_n z^{-n}}u(k) + e(k) \tag{3.1}$$

The mathematical extensive expression of the OE model is described by the following equation:

$$\bar{y}(t) + \sum_{k=1}^{n} a_k \bar{y}(t-k) = \sum_{j=1}^{n} b_j u(t-j) + e(t) \tag{3.2}$$

where : $t$ is the sampled data index $e(t)$ is a white noise process $u$ and $\bar{y}$ are the model input and output, $a_k$ is the coefficient denominator $b_j$ is the coefficient numerator

In case the system is described using Equation (3.2), the inputs and outputs relationship can be described as a set of discrete-time difference equations, as shown in the following equations:

$$\begin{aligned}
&x_{i,1}(n) + \textstyle\sum_{l=1}^{p} a_p(l) x_{i,1}(n-l) = \sum_{l=1}^{q} b_{i,1}(l) u_{i,1}(n-l) + e_1 \\
&x_{i,2}(n) + \textstyle\sum_{l=1}^{p} a_p(l) x_{i,2}(n-l) = \sum_{l=1}^{q} b_{i,2}(l) u_{i,2}(n-l) + e_2 \\
&\vdots \quad \vdots \\
&x_{i,N}(n) + \textstyle\sum_{l=1}^{p} a_p(l) x_{i,N}(n-l) = \sum_{l=1}^{q} b_{i,N}(l) u_{i,N}(n-l) + e_N
\end{aligned} \tag{3.3}$$

Where $x_{i,1}(n)$ is the contribution of the $j-th$ input to the $i-th$ output at the sampling time, $p$ and $q$ are autoregressive and moving average model orders, respectively, with corresponding coefficients $a_p(l)$ and $b_{i,i}(l)$, and $e_i$ is the error.

### 3.2.2 Transfer function model validation

After identifying the system model, it is critical to validate whether the model is accurate enough to describe the system's oscillatory behaviors. The developed transfer function model contains numerator (zeros) and denominator (poles). To validate the poles, eigenvalues are determined by the denominator polynomials and then compared with the Prony analysis

results of measurement data. It is challenging to validate the zeros part of the transfer function model immediately. Alternatively, it is feasible to compare the time-domain response of the developed model and actual system with the same external inputs, which is an indirect approach to validate the zeros part if the poles have already been validated. Therefore, these two validation methods provide more confidence that the developed transfer function model has captured the required behaviors.

### Validation in the frequency domain

The OE model can be converted into a complex frequency domain; hence, the eigenvalues can be obtained directly. If the eigenvalues of interest are similar to those of the actual system, it means that the constructed OE model can describe the dominant dynamic behaviors of the system. Since the eigenvalues of the oscillation modes may change due to the variation of operation conditions, the Prony analysis results are selected as the benchmark. For convenience, the eigenvalue comparison can be performed using oscillation frequency and damping ratio comparison.

### Validation in the time domain

The response of the actual system and constructed model are compared during the same external excitation for the time domain validation purpose. The response of the actual system is obtained using the actual system model simulation. If the constructed model response is similar to the actual system when encountering multiple disturbances, it enhances the confidence that the constructed model can represent the actual system dynamics. In other words, the constructed models should have robustness even if the operating point has changed from the initial one. To obtain how well the constructed model response matches the actual system, a fit accuracy is defined based on the following equation [57].

$$\text{Accuracy Index } = \left(1 - \frac{\left\|Y_i - \hat{Y}_i\right\|}{\left\|Y_i - \bar{Y}_i\right\|}\right) \times 100 \tag{3.4}$$

Where $Y_i$ is the constructed model response , $\hat{Y}_i$ is the actual system response, and $\bar{Y}_i$ is the actual system response mean over several periods. As the index is getting close to 1, it indicates that the constructed model response is valid to match the actual system.

## 3.3 Optimal signal selection

### 3.3.1 Optimal observation signal selection

Observation and actuation signals selection is a significant step for proper damping controller design. With exploiting the benefits of increasing deployment of Phasor Measurement Units (PMUs), a complex power system involves significant observation signals candidate for controller design analysis. Nevertheless, considering only some of the candidates that have sufficient observability of the interested mode, a proper method is required to choose the optimal observation signal for the interested oscillation mode among all the candidate observation signals. Fast Fourier Transform (FFT) method is used in this work to choose optimal observation signal.

FFT is widely used for numerous studies in engineering, mathematics, and science [84]. Fourier analysis transforms the sampling rate to the frequency domain and vice versa. The FFT algorithm quickly computes such transformations through factorizing the discrete Fourier transform matrix into a product of sparse factors. The function $Y = fft(x)$ is given for vectors of length $N$ by:

$$X(k) = \sum_{j=0}^{N-1} x(j)\omega_N^{jk} \tag{3.5}$$

where

$$\omega_N = e^{(-2\pi i)/N} \tag{3.6}$$

is an N-th root of unity.

In this work, FFT is used to choose the damping control loop's observation signals by converting the measurement signals into the frequency domain. The measurement signals

are sorted from high to low according to the magnitude of the dominant frequency mode. Finally, the one with the highest magnitude is chosen as the optimal observation signal.

A series of typical disturbances are used to excite the interested oscillation mode, e.g., tie-line trip, generation trip, and load shedding. During each case, the measurement signals are ranked based on the magnitude of the dominant frequency mode from high to low. Eventually, after combining the magnitude of different case studies, the one with the highest magnitude will be selected as the optimal observation signal to suppress the interested mode.

### 3.3.2 Optimal actuation signal selection

Damping control can be implemented using PSS, HVDC, or FACTS devices. The Exciter and governor are used as potential actuation signals in this dissertation. Since these generator devices react differently to system oscillation modes, a sensitivity analysis of all actuation signals' candidates to the optimal observation signal was developed to select the optimal actuation signal.

After selecting the optimal observation and actuation signals, the Power system identification regarding the optimal signals can be described as Single-Input-Single-Output (SISO) system :

$$G(s) = \frac{R_1}{s - \lambda_1} + \frac{R_2}{s - \lambda_2} + \ldots + \frac{R_m}{s - \lambda_m} \tag{3.7}$$

Where $\lambda_i$ is the eigenvalue of the system and $R_i$ is the system residue, which is the product of mode observability and controllability. $|R_1| \geq |R_2| \geq \ldots \geq |R_m|$. When $\lambda_i$ is unobservable or uncontrollable,$R_i = 0$. In complex power systems, any generator is typically engaged with one or multiple modes in the system. Inter-area oscillation modes can be observed from controlled system $G(s)$ with stronger mode observability and controllability than other modes.

The transfer function $G_{ij}$ is obtained from the transfer function model from the input $u_i$ to the output $y_j$, and it can be represented as a sum of partial fractions of the following form [85]:

$$G_{ij}(s) = \sum_{k=1}^{n} \frac{R_k}{s - \lambda_k} \tag{3.8}$$

where $R_k$ is the residue associated with the mode $\lambda_k$. The residue $R_k$ provides an idea of how the mode $\lambda_k$ is influenced by the input $u_i$ and how much is observed from the output $y_j$. Therefore, the residues are considered precise measures of controllability and observability relation of a particular oscillation mode. For this purpose, residues are mostly utilized in damping oscillation analysis [82, 2].

For most of the state-of-the-art research, the residues are computed directly from the state-space representation by using:

$$R_k = c_j \emptyset_k \varphi_k b_k \tag{3.9}$$

where $\emptyset_k$ and $\varphi_k$ are the right and left eigenvectors of the state matrix A, respectively, corresponding to the eigenvalue $\lambda_k$.

Generally, the residues are complex numbers, and the optimal input-output signal impact is given by the maximum value of the residue magnitude [86]. The residues depend on the input and output signals scale. However, theyit does not provide a clearn exact comparison among transfer functions associated with variables ofwith different units. Therefore, the residue is only used to select the optimal actuation signal corresponding to the optimal selected observation signal. Another practical method is to inject an up/down step signal into the preferred setpoint of each actuator. Then, the frequency responses of the optimal observation signal are compared. The bus frequency response with a higher magnitude means higher controllability of the corresponding actuator.

## 3.4 Wide Area Damping Controller Design

In existing power grids, the PSSs based on local signals can provide sufficient damping to suppress local oscillation modes. However, they usually have a limited control impact on the inter-area mode due to the lack of the observability of the inter-area mode from the local signals.

In this dissertation, a supplementary damping controller (WADC) using remote PMU measurements is designed to suppress the inter-area oscillation mode. The classical lead-lag structure is employed to design the WADC.

As shown in Figure 3.2, the controller has a band-pass filter, a gain block, a washout block, two lead-lag structures, and a deadband block. The band-pass filter is centered at the frequency of the target oscillation mode to eliminate impacts on other oscillation modes. The washout block is used to remove the direct current component in the observation signals. The time constant of the washout block is set to 10s. The upper limit and lower limit of the WADC are set to 0.1 p.u. and -0.1 p.u., respectively. The deadband is set to [-0.01 p.u., 0.01 p.u.].

A simple block diagram of the WADC structure for the controlled system shown in Figure 3.3. $G(s)$ describes the power system dynamics that connect to the generator exciter or governor, and $K(s)$ is the WADC transfer function.

Assuming that the system model $G(s)$ is a reduced-order model with r oscillation modes, the transfer function of the system can be represented in the following form:

$$G(s) = \frac{R_1}{s-\lambda_1} + \frac{R_1^*}{s-\lambda_1^*} + \ldots + \frac{R_r}{s-\lambda_7} + \frac{R_r^*}{s-\lambda_r^*} \tag{3.10}$$

Where $\lambda_i$ and $\lambda_i^*$ are a conjugate pair eigenvalues which describe one mode, and $R_i$ and $R_i^*$ are the mode conjugate residues.

$G(s)$ can be expressed in a state-space linearizaion form:

$$\begin{aligned} \dot{x}(t) &= Ax(t) + Bu(t) \\ y(t) &= Cx(t) \end{aligned} \tag{3.11}$$

The Eigen-properties of the matrix A can be represented briefly using a new state vector $z(x)$ [87], related to the original state vector $x(t)$ through the transformation $x(t) = \Phi z(x)$ , which is presented in [2]. Equations (3.11) can be reformed using the term $z(x)$ as :

$$\begin{aligned} \dot{z}(t) &= \Lambda z(t) + \Phi^{-1} bu(t) \\ y(t) &= cz(t) \end{aligned} \tag{3.12}$$

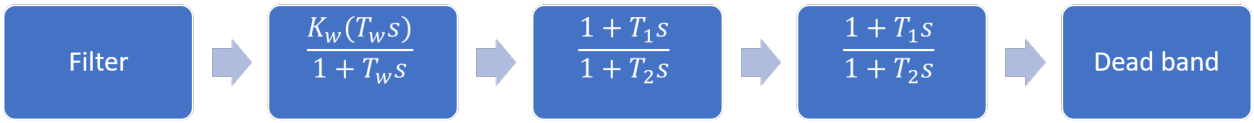


**Figure 3.2:** WADC block diagram.

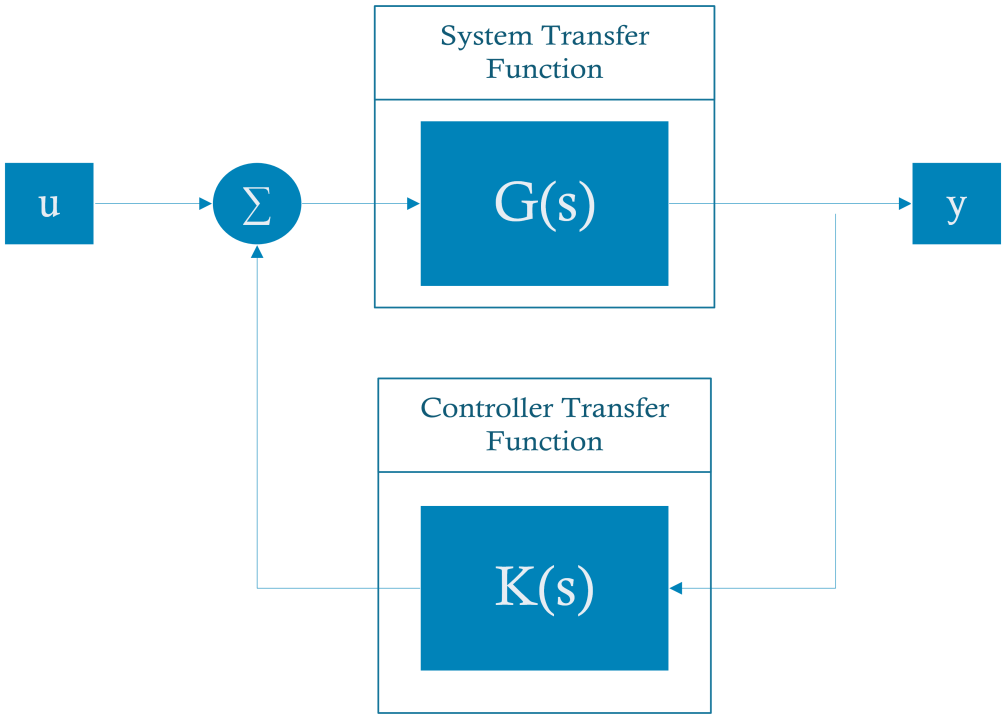


**Figure 3.3:** WADC closed loop structure of the system.

Where $\Phi$ is the modal matrix, and $\Lambda$ is a diagonal matrix using the eigenvalues of A as the diagonal elements.

Applying Laplace transform for equations (3.12) with adding one more equation describing the control law $U(s) = K(s)Y(s)$ [87], the resulting equations can be written as:

$$\begin{aligned} sz(s) &= \Lambda z(s) + \Phi^{-1} bU(s) \\ Y(s) &= c\Phi z(s) \\ U(s) &= K(s)Y(s) \end{aligned} \tag{3.13}$$

Using $A_z = \Lambda + K(s)\Phi^{-1}bc\Phi$ , equation (3.13) can be simplified as [87]:

$$sz(s) = \Lambda z(s) + K(s)\Phi^{-1}bc\Phi z(s) = A_z z(s) \tag{3.14}$$

Where the eigenvalues of $A_z$ describes the closed-loop system modes.

Using the eigenvalues characteristic equation $|A_z - \lambda I| = 0$ [2] , eigenvalues of the closed-loop system is

Assuming that $\lambda_d = -\zeta_d\omega_n \pm j\sqrt{1-\zeta_d^2\omega_n}$ [5] are the designed dominant poles, $\zeta_d$ is the designed damping ratio, and $\omega_n$ is the natural oscillation frequency. Assuming that $\lambda_i = -\zeta_i\omega_n \pm j\sqrt{1-\zeta_i^2\omega_n}$ are the interested mode dominant poles, $\zeta_d$ is the interested mode damping ratio.

WADC design needs to fulfill the two essential constraints [87]. First,the damping ratio of closed-loop needs to be improved from $\zeta_i$ to the desired value $\zeta_d$ , and that means :

$$\mathrm{Re}\left(\lambda_i + K(s)\Psi_i bc\Phi_i\right) - \mathrm{Re}\left(\lambda_i\right) = -\left(\zeta_d - \zeta_i\right)\omega_n \tag{3.15}$$

Second, the oscillation frequency of the closed-loop mode has to be close to the open-loop oscillation frequency, which means:

$$\sqrt{\left|\mathrm{Im}\left(\lambda_i + K(s)\Psi_i bc\Phi_i\right)\right|^2 - \left|K(s)\Psi_i^* bc\Phi_i\right|^2} = \left|\mathrm{Im}\left(\lambda_i\right)\right| \tag{3.16}$$

Using equations (3.15) (3.16), if $K(s)\Psi_i bc\Phi_i$ is a real number number with $\mathrm{Re}(K(s)\Psi_i bc\Phi_i) \neq 0$ , $\mathrm{Im}(K(s)\Psi_i bc\Phi_i) = 0$, then equations (3.15) (3.16) can be reformed as :

$$\mathrm{Re}\left(K(s)\Psi_i bc\Phi_i\right) \neq 0, \mathrm{Im}\left(K(s)\Psi_i bc\Phi_i\right) = 0 \tag{3.17}$$

$$\begin{aligned} &\mathrm{Re}\left(K(s)\Psi_i bc\Phi_i)\right) = -\left(\zeta_d - \zeta_i\right)\omega_n \\ &\sqrt{\left|\mathrm{Im}\left(\lambda_i\right)\right|^2 - \left|K(s)\Psi_i^* bc\Phi_i\right|^2} \approx \left|\mathrm{Im}\left(\lambda_i\right)\right| \end{aligned} \tag{3.18}$$

It is evident that the first constraint can be satisfied using the first equation in (3.17) , which is enhancing the desired damping ratio of the closed-loop oscillation mode.

Considering that

$$\left|K(s)\Psi_i^* bc\Phi_i\right|^2 = \left|K(s)\Psi_i bc\Phi_i\right|^2 = \left|-\left(\zeta_d - \zeta_i\right)\omega_n\right|^2 << \left|\mathrm{Im}\left(\lambda_i\right)\right|^2 \tag{3.19}$$

while the second equation in (3.18) can be written as

$$\sqrt{\left|\mathrm{Im}\left(\lambda_i\right)\right|^2 - \left|K(s)\Psi_i^* bc\Phi_i\right|^2} \approx \left|\mathrm{Im}\left(\lambda_i\right)\right| \tag{3.20}$$

Which also satisfies the second constraint.

Using the previous analysis, $K(s)$ can be written as

$$\begin{aligned} &\mathrm{Re}\left(K(s)\Psi_i bc\Phi_i\right) = -\left(\zeta_d - \zeta_i\right)\omega_n \\ &\mathrm{Im}\left(K(s)\Psi_i bc\Phi_i)\right) = 0 \end{aligned} \tag{3.21}$$

Where $\Psi_i bc\Phi_i$ is the open-loop dominant oscillation mode residue. Since the residue of the open-loop oscillation mode is known, the compensation angle of WADC satisfies:

$$\angle K\left(j\omega_d\right) + \angle\left(\Psi_i bc\Phi_i\right) = -180^\circ \tag{3.22}$$

and the amplitude satisfies:

$$\left|K\left(j\omega_d\right)\right| \cdot \left|\Psi_i bc\Phi_i\right| = \left|-\left(\zeta_d - \zeta_i\right)\omega_n\right| \tag{3.23}$$

The parameters of the WADC can be determined using the following equations [85]:

$$T_1 = \alpha T_2, \quad T_2 = \frac{1}{\sqrt{\alpha}\omega_d} \tag{3.24}$$

Where $T_1$ and $T_2$ are the time constants of the lead-lag structure, $\omega_d$ is the dominant oscillation frequency, and

$$\alpha = \frac{1 + \sin\theta_{\max}}{1 - \sin\theta_{\max}}, \theta_{\max} = \angle K\left(j\omega_d\right)/2 \tag{3.25}$$

Where $\theta_{\max}$ is the compensation phase of each lead-lag block and $K\left(j\omega_d\right)$ is the residue magnitude.

$$K_a = \frac{\left|K\left(\omega_d\right)\right|}{\left(\left|\frac{1+T_1 s}{1+T_2 s}\right|_{s=j\omega_d}\right)^2} \tag{3.26}$$

The transfer function of the filter is [88]:

$$K_f(s) = \frac{\frac{\omega_n}{Q}s}{s^2 + \frac{\omega_n}{Q}s + \omega_n^2} \tag{3.27}$$

Where $Q$ is the quality factor, which is usually set to 1.

## 3.5 Summery

This chapter summarized the methodology to design WADC using a measurement-based transfer function model. Figure 3.4 [85] presents the general design flow of a WADC. The method utilizes ambient data to develop the transfer function model in which the system dynamics are represented. Then, the developed transfer function model will be validated in both frequency and time domains to ensure that the developed model can capture the dominant system modes. The residue method is used to compute the WADC parameters for the target oscillation mode.

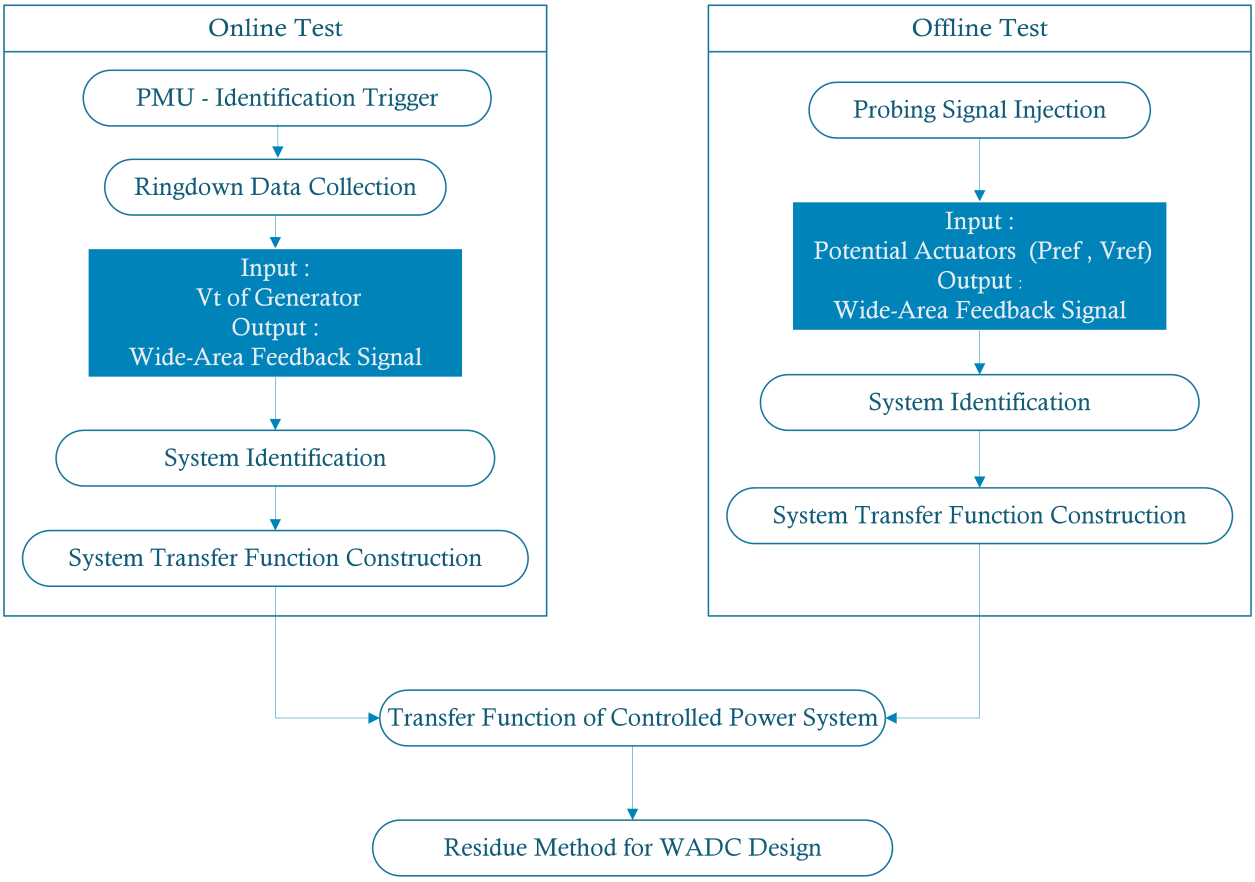


**Figure 3.4:** Flowchart of the WADC design method.

# Chapter 4

# Impact of WADC on rotor angle stability: Case Study Saudi System

## 4.1 Introduction Of Saudi System

Saudi Arabia is considered one of the largest countries in western Asia and the Middle East and also among the top countries in the world in oil production besides having about 20 % of the world's oil reserves [89]. However, it is one of the top countries that directly burn oil and natural gas to generate electrical power. The country is anticipated to consume more energy sources to serve the massive increase in electricity consumption. Consequently, the Saudi government intends to enhance the existing grid efficiency. Thus, the existing grid needs to be robust enough to withstand the predicted future changes, like integrating renewable energy resources and interconnection with neighboring countries.

Saudi system frequency is 60 Hz, and the peak electricity demand reached approximately 62 GW in 2017 [90]. There are five main operation areas in the Saudi Electricity Company (SEC) system; Central, East, West, North, and South, as shown in Figure 4.1. The dominant oscillation mode in the system is around 0.30 Hz between the West and Central areas. There is one tie-line (double circuit) that connects these areas. The power flow of the tie-line is typically from the Central region to the West region. The primary SEC grid will separate into two groups if the tie-line is tripped. The SEC can be conceptualized as the Kundur system since the tie-line links two major groups.

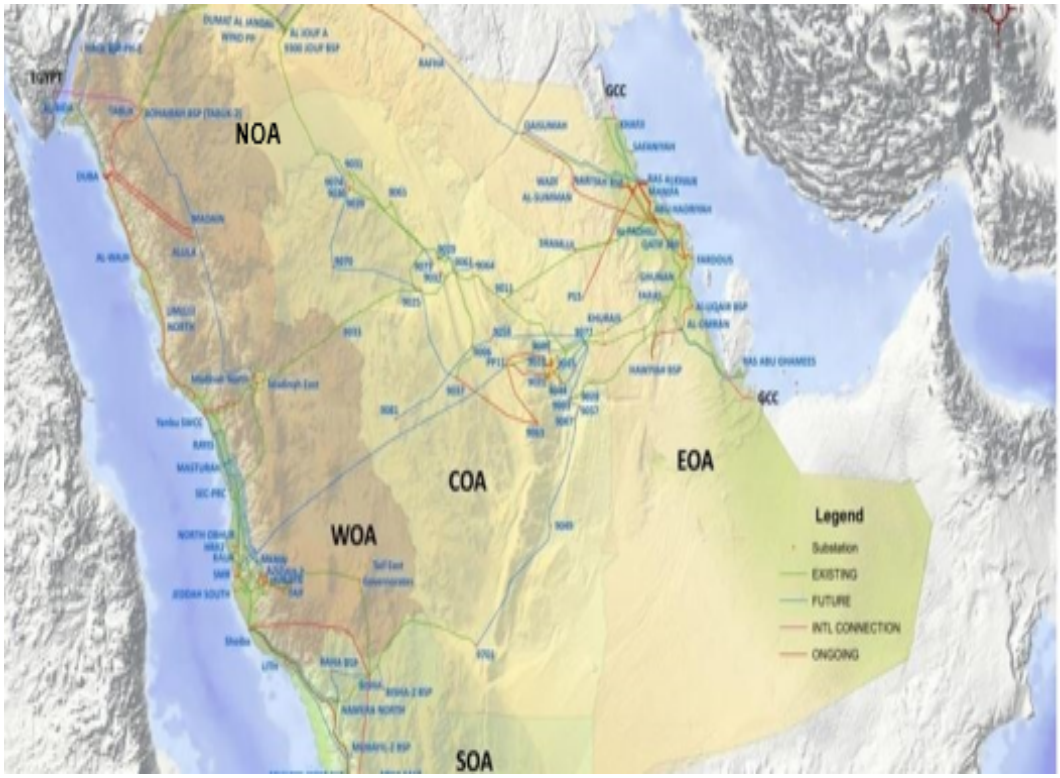


**Figure 4.1:** SEC System grid.

### 4.1.1 Saudi Electricity Company (SEC) Model Validation

This section presents the dynamic model validation of the Saudi national grid. Simulated frequency responses are modified and validated to match the accumulated measurements by the frequency monitoring network (FNET/GridEye). This section aims to demonstrate that the PSSE model can rationally match the output of the real system. Two single-phase PMUs, so-called Frequency Disturbance Recorders (FDRs), are deployed in the Saudi distribution grid; one is in the western area, and the other is in the central area.

FDRs can measure grid frequency, voltage, and the angle at an outlet on the wall to detect system disturbances [91]. Figure 4.2 lists some of oscillation events detected by the FDR, which has exhibited the dominant oscillation mode around 0.3 Hz between the western and central areas. Table 4.1 presents validation results in the frequency domain. The PSS/e model has a similar dynamic behavior as the measurement cases regarding the frequency oscillation and the damping ratio.

#### Coherent group analysis for SEC model

Identifying the coherent group helps to understand the dynamic behavior and reduces the system's complexity into a couple of coherent groups. One high voltage bus frequency signal was selected as the representative signal for each area to identify coherent groups. These buses frequency response to line trip disturbances and temporary 3-phase fault on all system tie-lines were used to identify coherent groups. For instance, the responses to a temporary 3-phase fault on the tie-line are shown in Figure 4.3. Based on the analysis, it is concluded that the SEC power system can be divided into five coherent groups: Central, West, East, South, and North, as shown in Figure A.1.

**Figure 4.2:** SEC FDR Results

**Table 4.1:** Oscillation comparison between measurement PSSe model

| No. | **Case** | **Oscillation Frequency(Hz)** | **Damping Ratio(%)** |
|---|---|---|---|
| 1 | PSSe Model | 0.288 | 11.45 |
| 3 | FDR Measuremnt 1 | 0.275 | 9.281 |
| 4 | FDR Measuremnt 2 | 0.291 | 8.747 |
| 5 | FDR Measuremnt 3 | 0.294 | 8.301 |
| 6 | FDR Measuremnt 4 | 0.288 | 9.961 |
| 7 | FDR Measuremnt 5 | 0.282 | 11.189 |
| 8 | FDR Measuremnt 6 | 0.313 | 11.293 |

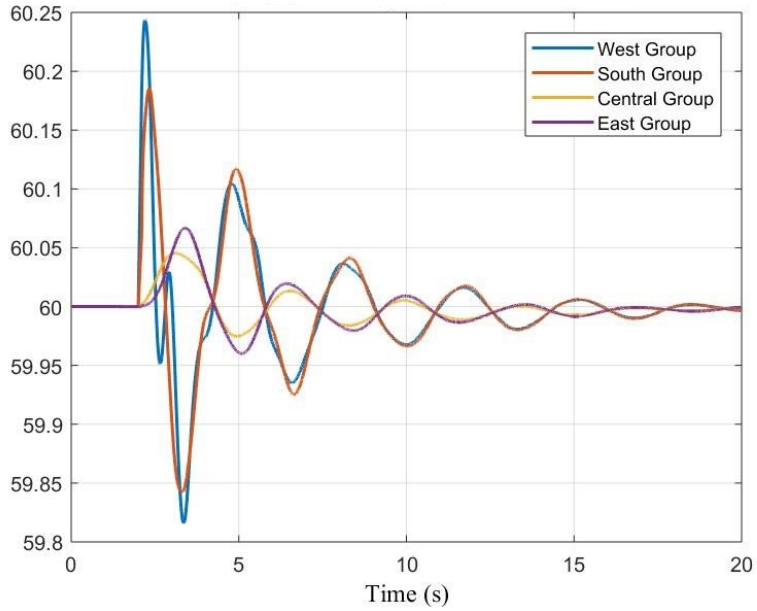


**(a)** Line fault South-West

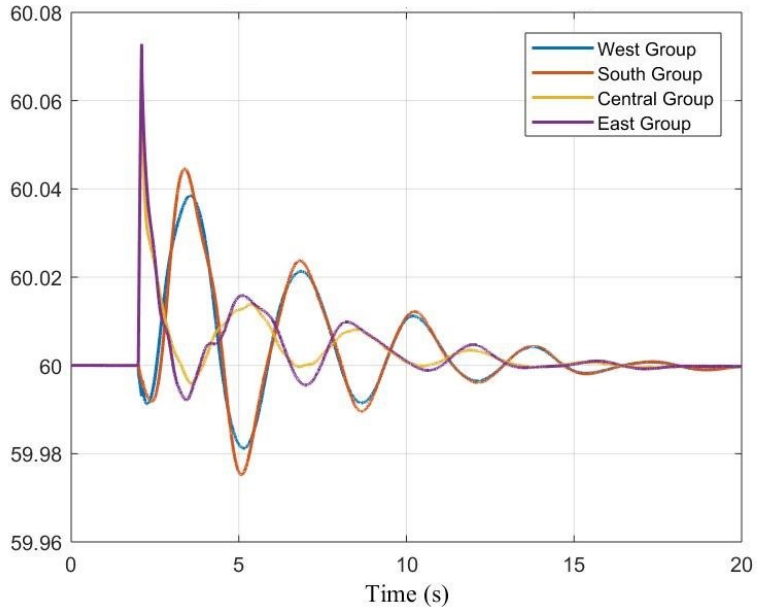


**(b)** Line fault Central-East

**Figure 4.3:** Frequency response for different line fault (coherent group analysis).

## 4.2 WADC design for Saudi System

This section presents the selection of the optimal observation and actuation signals for the Saudi system's WADC design. Also, system identification and validation are presented in this section.

### 4.2.1 Optimal Observation Signal Selection

As mentioned in Chapter 3, Fast Fourier Transform (FFT) is applied to select the damping control optimal observation signals by converting the measurement signals to the frequency domain. Since the target mode is the oscillation between western and central areas, the frequencies at high voltage buses in these areas are initial observation signals.

Numerous temporary line fault disturbances are applied to excite the target oscillation mode. During each disturbance, bus frequency signals are ranked high to low based on the dominant mode's frequency magnitudes. The bus with the highest-ranking signal is chosen as the optimal observation signal for the controller design, as listed in Table 4.2 and Table 4.3. In the central area, bus Area-C5 has the highest mean frequency amplitude, as shown in Figure 4.4, where the FFT results are presented. The magnitude of bus Area C-5 for all tested cases are circled in the Figure 4.4 where the average magnitude is the highest among all central area buses.

Similarly, the frequency at bus Area-W6 has the highest magnitude in the western area, as shown in Figure 4.5. Since the bus frequency in the west area has a higher amplitude than in the central area bus, bus Area-W6 is chosen as the optimal observation signal. Moreover, the frequency difference between Area-W6 and Area-C6 is used as a wide-area observation signal for designing the controller.

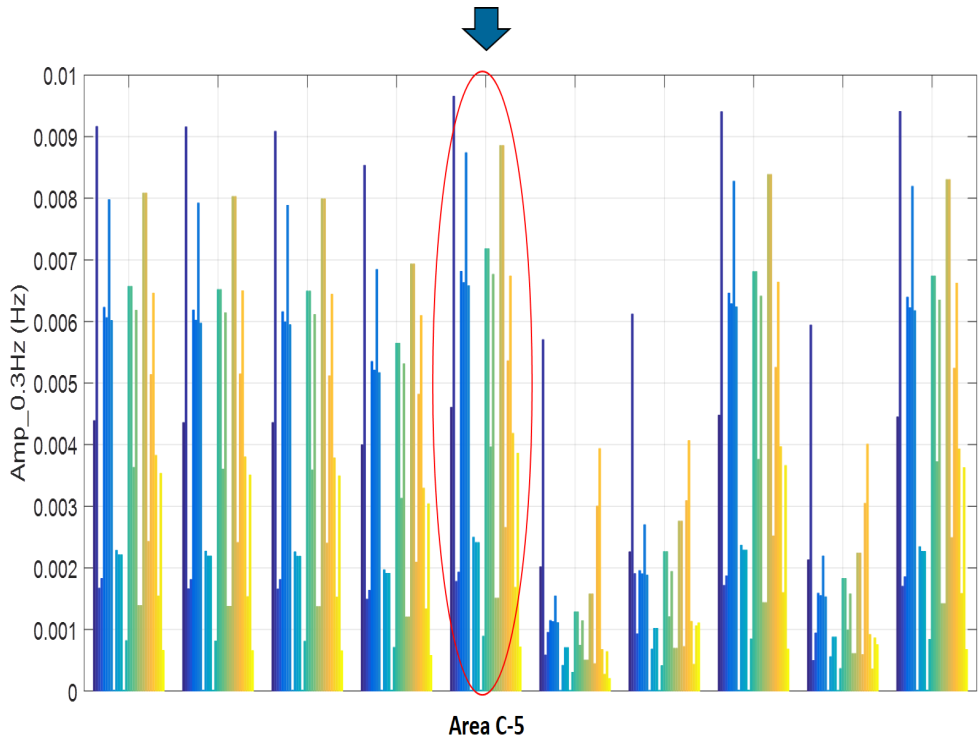


**Figure 4.4:** Central buses FFT.

**Table 4.2:** Candidate Observation Signals In Central Area

| No. | **Bus Number** | **Mean Amp. (Hz)** |
|---|---|---|
| 1 | Area-C1 | 0.0040 |
| 2 | Area-C2 | 0.0040 |
| 3 | Area-C3 | 0.0040 |
| 4 | Area-C4 | 0.0035 |
| **5** | **Area-C5** | **0.0043** |
| 6 | Area-C6 | 0.0012 |
| 7 | Area-C7 | 0.0017 |
| 8 | Area-C8 | 0.0041 |
| 9 | Area-C9 | 0.0014 |

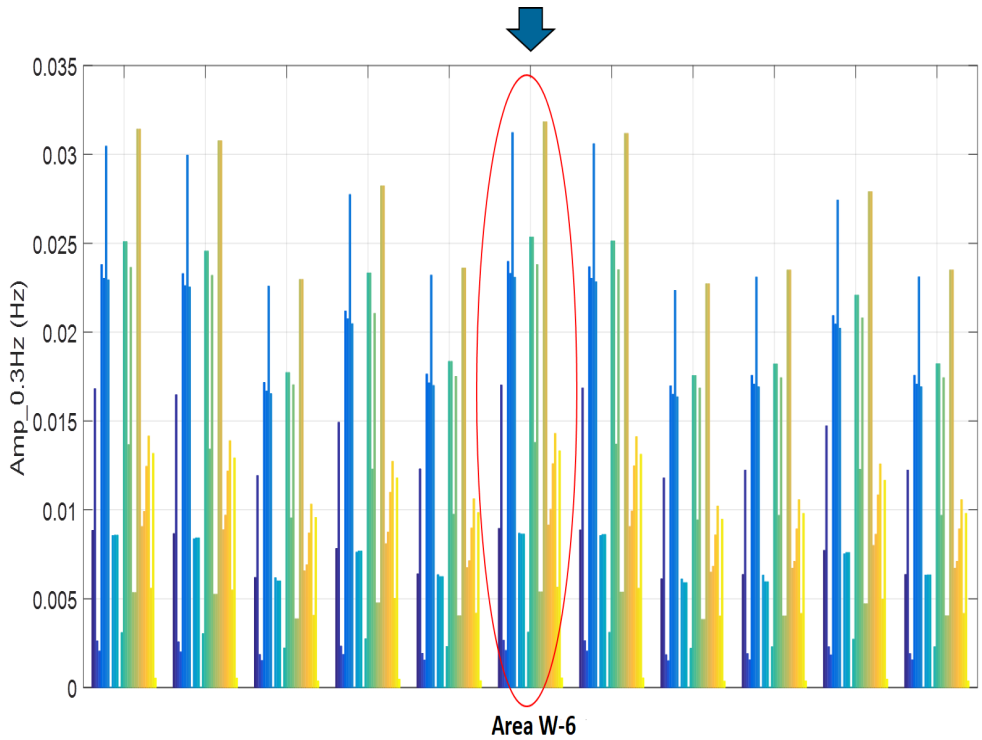


**Figure 4.5:** West buses FFT.

**Table 4.3:** Candidate Observation Signals In Western Area

| No. | **Bus Number** | **Mean Amp.(Hz)** |
|---|---|---|
| 1 | Area-W1 | 0.0133 |
| 2 | Area-W2 | 0.0130 |
| 3 | Area-W3 | 0.0096 |
| 4 | Area-W4 | 0.0120 |
| 5 | Area-W5 | 0.0098 |
| **6** | **Area-W6** | **0.0134** |
| 7 | Area-W7 | 0.0133 |
| 8 | Area-W10 | 0.0117 |
| 9 | Area-W11 | 0.0098 |

### 4.2.2 Optimal Actuation Signal Selection

This section presents the results of selecting the optimal actuation signal, as discussed in Chapter 3. The WADCs could provide supplementary control via generator exciters and generator governors. In this dissertation, generator exciters and governors will be used to equip the WADC control commands, and two methods are used to obtain optimal actuators.

#### Generators Exciter as Target Actuators

Generator excitation determines the voltage and reactive power output values for the generator. An excitation system's primary purpose is to provide direct current to the synchronous field winding of the machine [92]. Also, the automatic voltage regulator (AVR), with an excitation system, performs control and protective functions, which are essential to the satisfactory output of the power system by regulating the field voltage and thus the field current. The excitation system must supply and automatically adjust the synchronous generator's field current to maintain terminal voltage under steady-state conditions, as the output varies continuously within the generator's capacity [93].

There are two methods used in the dissertation to detect the optimal exciters among all generators. One approach is to inject an up/down step signal into the preferred reference of the actuators. Then, the frequency responses of bus Area-W6 (based on the optimal observation signal analysis) are compared. The bus frequency response with a higher magnitude means higher controllability of the corresponding generator actuators. Figure 4.6 illustrates the frequency response at bus Area-W6 when each generator's exciter is subjected to a 0.05 down step signal. Table 4.4 lists the top 10 generator exciter actuators based on their magnitudes.

The other method is to inject color noise to the exciter voltage set point and then compare the calculated residue magnitudes with the identified transfer function models. Color noise is a white noise after a low pass filter (0-2Hz), as shown in Figure 4.7a. This probing signal is injected to the voltage setpoint of each generator exciter. Based on the probing signal and the collected frequency at bus Area-W6, a single-input single-output transfer function model can be identified, as shown in Figure 4.7b.

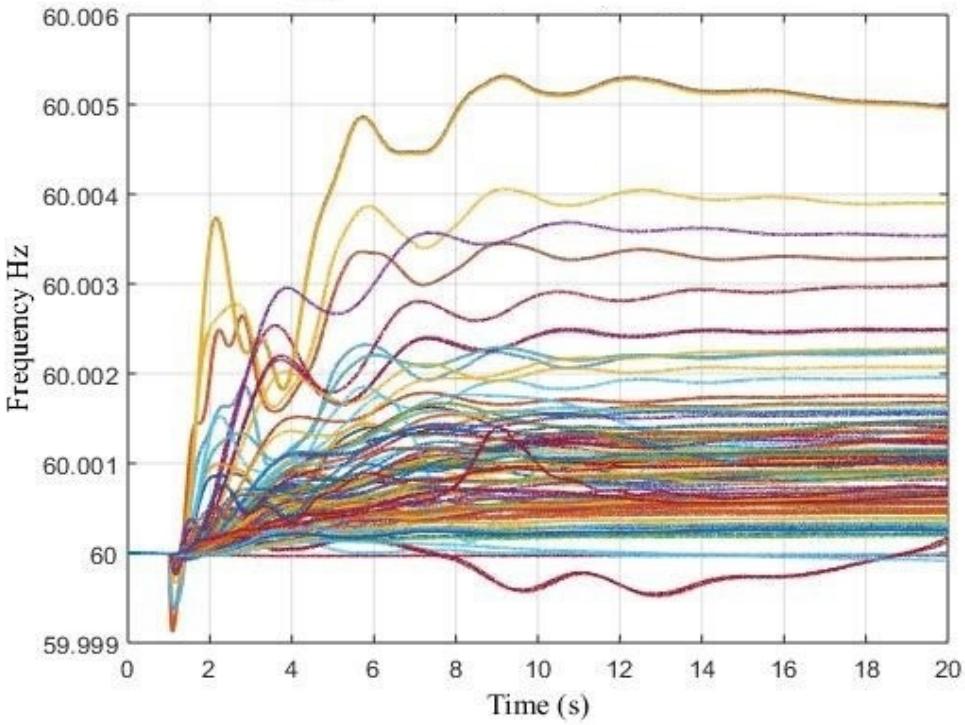


**Figure 4.6:** Step down response - Exciter.

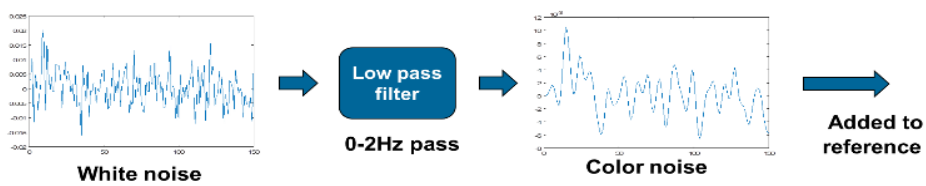


**(a)** Color noise as probing signal

**(b)** Identified model structure

**Figure 4.7:** Transfer function model identification using probing signal.

**Table 4.4:** Top 10 generator exciter actuators based on bus frequency magnitude

| No. | Bus NO. | Gen. ID |
|---|---|---|
| 1 | South57 | 1 |
| 2 | West17 | 1 |
| 3 | East81 | 1 |
| 4 | West55 | 1 |
| 5 | East88 | 5 |
| 6 | East37 | 1 |
| 7 | West94 | 1 |
| 8 | West80 | 1 |
| 9 | West69 | 3 |
| 10 | East481 | 1 |

**Table 4.5:** Top 10 generator exciters actuator based on residue magnitude

| No. | Bus NO. | Gen ID | Residue Magnitude(Normalized) |
|---|---|---|---|
| 1 | South57 | 1 | 1.0000 |
| 2 | West17 | 1 | 0.9368 |
| 3 | West55 | 1 | 0.8250 |
| 4 | East88 | 5 | 0.8015 |
| 5 | East37 | 1 | 0.7609 |
| 6 | West94 | 1 | 0.6390 |
| 7 | West80 | 1 | 0.6302 |
| 8 | South11 | 1 | 0.4705 |
| 9 | East44 | 20 | 0.4600 |
| 10 | South07 | 5 | 0.4512 |

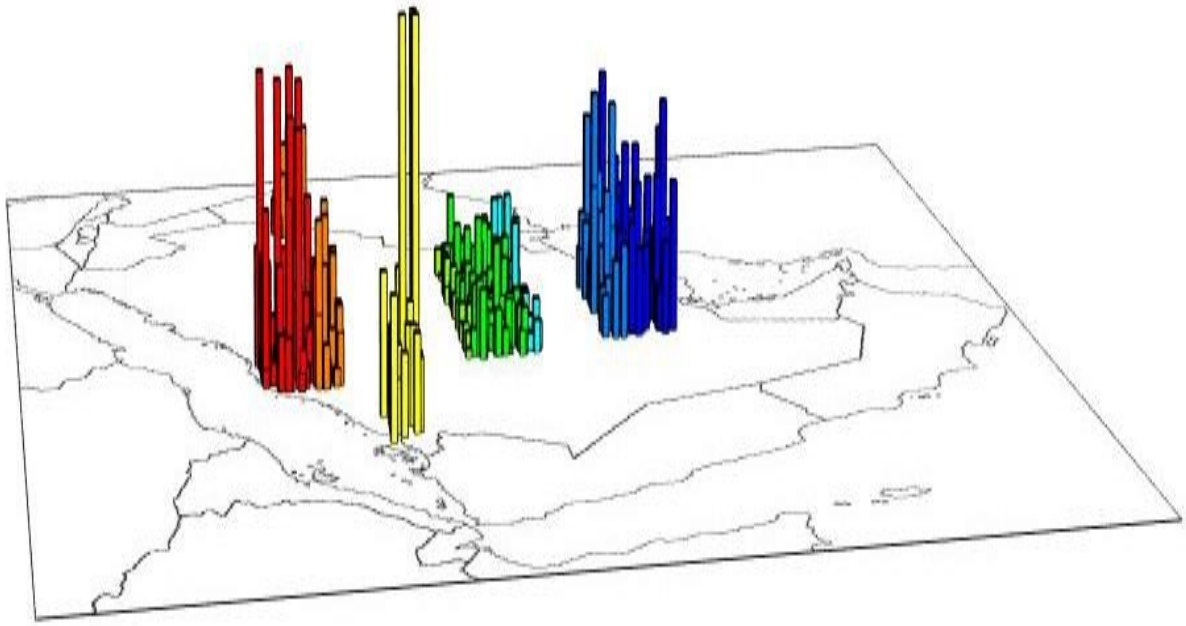

**Figure 4.8:** Controllability comparison (frequency magnitude comparison - Exciter).

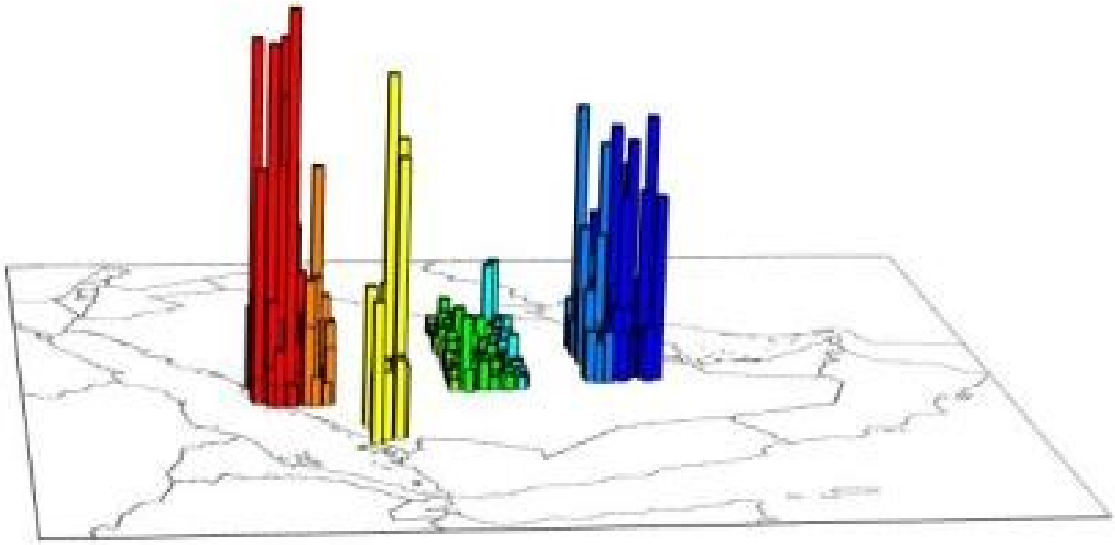

**Figure 4.9:** Controllability comparison (residue magnitude comparison - Exciter).

After the transfer function models are identified, the residue magnitudes of the models are compared. Note that residue magnitude is a joint measure of controllability and observability. Given that the same bus frequency signal is selected as the observation signal, the controllability can be compared indirectly by comparing residue magnitude. Table 4.5 lists the top 10 generator exciter actuators based on the calculated residue magnitudes.

The selected top 10 generator exciter actuators from both methods are quite similar to each other. Moreover, the comparison between the two methods is conducted. Figure 4.8 shows the results from the response magnitude comparison method, while Figure 4.9 shows the results from the residue magnitude comparison method. Both indicate that generators in eastern, western, and southern areas have higher controllability of the target oscillation mode than those in the central area.

#### Generators governor as target actuators

The governor is a device that varies the amount of fuel delivered to the engine to maintain a constant speed. The primary purpose of the governor is to regulate the active power of the machine based on the system frequency variations. Similarly, refining the governors of the system units to possible actuators can be done using the same two methods that were used for the exciter case. Figure 4.10 illustrates the bus frequency responses to a 0.5 down step signal at the generator governor set point and the Table 4.6 lists the top 10 generator governor actuators based on bus frequency response magnitude to the step signal.

Using the residue method similar to the exciter case, Table 4.7 lists the top 10 generator governor actuators based on their residue magnitude when the color noise injected the governor set point. The results from the two methods are similar. Figures 4.11 ,4.12 compare controllability of all generator governors using the two methods. Generally, the residue magnitude comparison method is more accurate.

The Final optimal actuators are chosen based on the the two used methods. Usually, the residue magnitude comparison is more accurate. Two plant at the western area and one plant at the southern area are used as the optimal actuators in this dissertation.

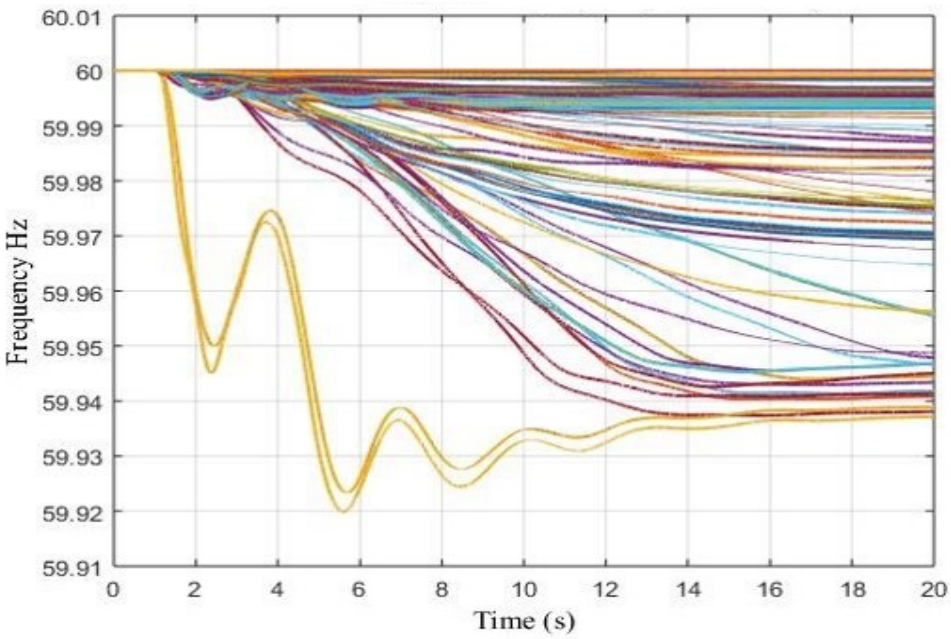


**Figure 4.10:** Step down frequency response - Governor.

**Table 4.6:** Top 10 generator governor actuators based on bus frequency magnitude

| No. | Bus NO. | Gen. ID |
|---|---|---|
| 1 | West17 | 1 |
| 2 | South57 | 1 |
| 3 | East88 | 5 |
| 4 | West55 | 1 |
| 5 | East37 | 1 |
| 6 | West80 | 1 |
| 7 | West94 | 1 |
| 8 | East77 | 41 |
| 9 | West20 | 10 |
| 10 | West15 | 11 |

**Table 4.7:** Top 10 generator governor actuators based on residue magnitude

| No. | Bus NO. | Gen ID | Residue Magnitude(Normalized) |
|---|---|---|---|
| 1 | South57 | 1 | 1.0000 |
| 2 | West17 | 1 | 0.9813 |
| 3 | East88 | 5 | 0.8759 |
| 4 | West55 | 1 | 0.8726 |
| 5 | West94 | 1 | 0.8546 |
| 6 | West80 | 1 | 0.8236 |
| 7 | South11 | 1 | 0.8136 |
| 8 | West20 | 10 | 0.8015 |
| 9 | West69 | 3 | 0.8007 |
| 10 | West15 | 11 | 0.7598 |

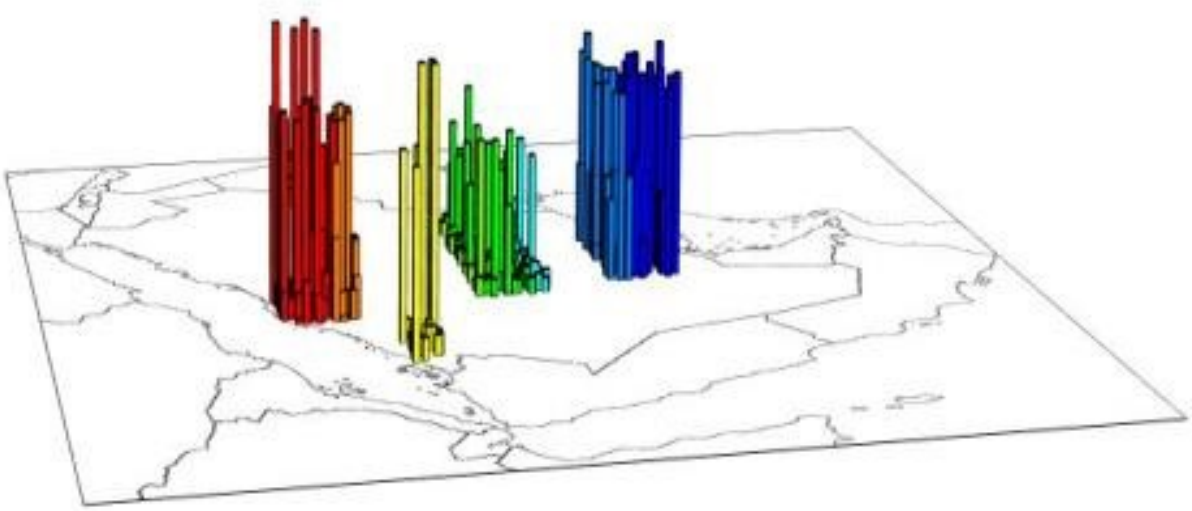

**Figure 4.11:** Controllability comparison (frequency magnitude comparison - Governor).

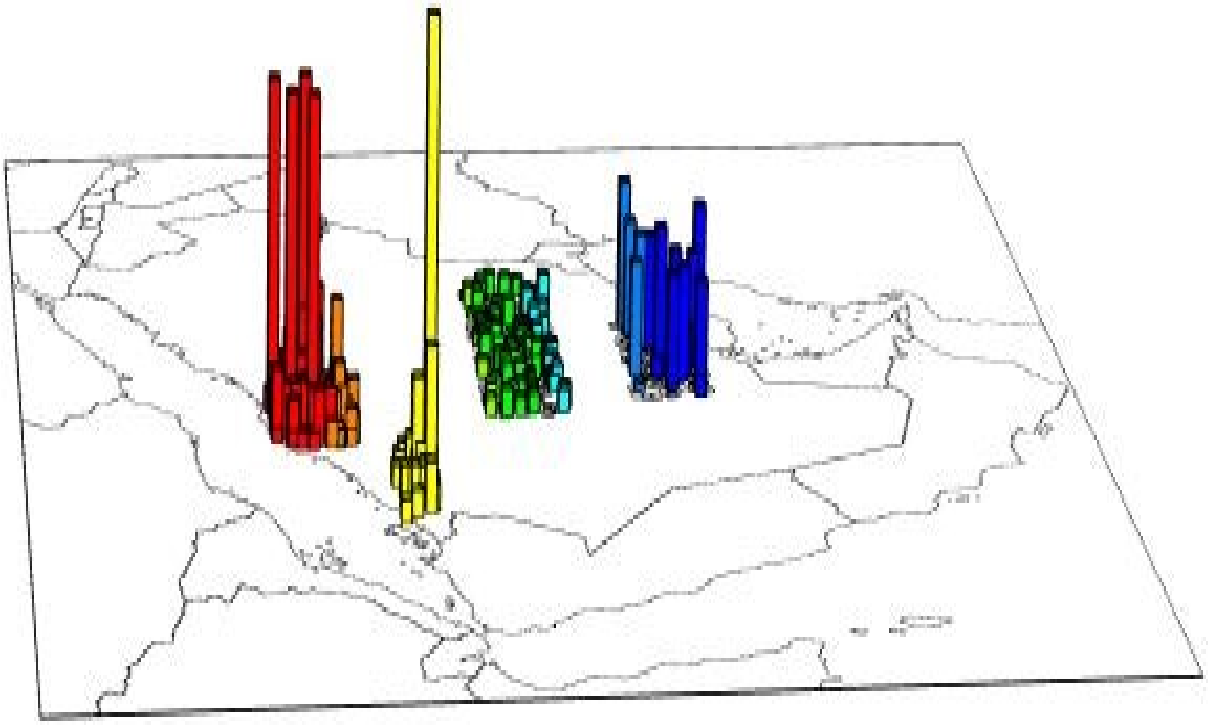

**Figure 4.12:** Controllability comparison (residue magnitude comparison - Governor).

### 4.2.3 Model validation in time domain and frequency domain

As introduced in Chapter 3, color noise is injected into the preferred set point of the actuator. Based on the probing signal and the collected frequency at Bus Area-W6, a single-input single-output model can be identified as shown in Figure 4.13. As a typical transfer function model, the output error (OE) polynomial model is chosen as the measurement-driven model structure for model identification using probing measurements.

After the OE model is identified, it is necessary to validate the model to make sure the model is accurate enough to depict the oscillatory behavior in the original system. The identified model is validated in both the time and frequency domain. In the time domain, the responses of the original model and the developed model are compared. The fitness index is used to measure how similar the two responses are. For instance, as shown in Figure 4.14, when the OE model has 7 order, the fitness index is 91.71%. Usually, a model with fitness higher than 80% is considered a good model. OE models with different orders can be identified. Table 4.8 provides the identified models of order 4 to 10. In the frequency domain, the residue angle, residue magnitude, oscillation frequency, and damping ratio can be compared to validate the model. As shown in Table 4.8, the models with orders 7, 8, and 9 have similar residue angle, residue magnitude, oscillation frequency, and damping ratio. Their fitness indices are all higher than 80%. Therefore, the model with order 7 is selected as the validated model for further WADC design.

Ten generator exciter actuators have been selected using two methods. Although the selection results from both methods are similar, there are still some discrepancies. Hence, the actuators chosen by both methods are evaluated in this section. The transfer function models are identified by injecting color noise signals to the generator exciter voltage set point. Moreover, the models are validated in both the time domain and frequency domain. Table B.1 gives the identified models of each selected generator exciter actuator.

Similar to the exciter case, ten generator governor actuators have been picked using two methods, and the transfer function models are identified by injecting a color noise signal to the generator governor set point and validated both in time and frequency domain. Table B.2 gives the identified models of each generator governor chosen actuator.

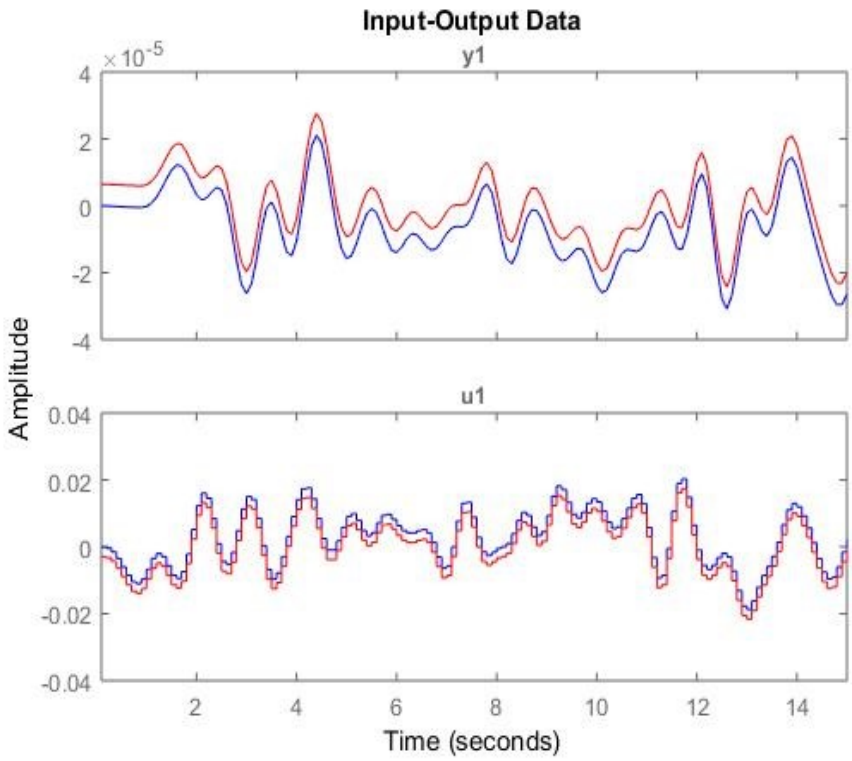


**Figure 4.13:** Input and output signal for Identified model.

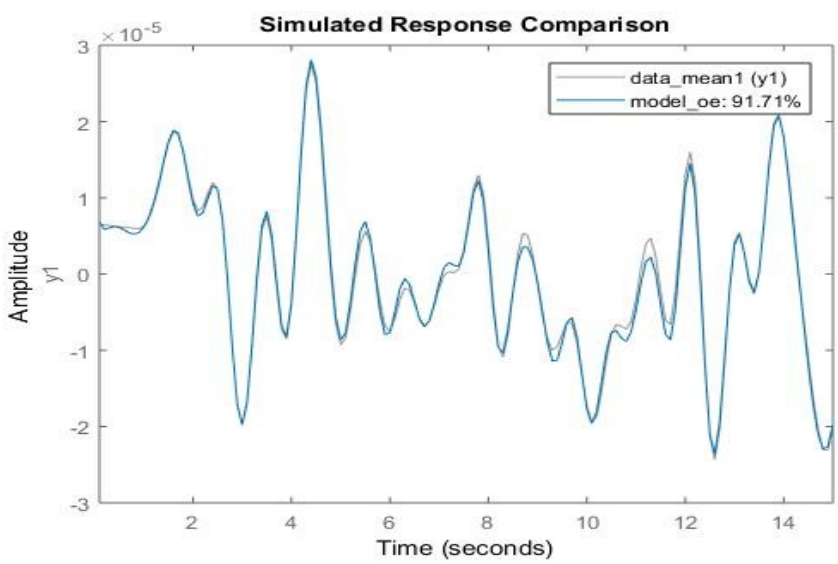


**Figure 4.14:** Fitness index for Identified model.

**Table 4.8:** Model validation in time domain and frequency domain

| **Order** | **Fitness (%)** | **Residue Angle(deg)** | **Residue Mag.** | **Oscillation Freq(Hz)** | **Damping ratio(%)** |
|---|---|---|---|---|---|
| 4 | 75.3811 | 121.9963 | 0.0019 | 0.2632 | 0.2433 |
| 5 | 82.5676 | 148.5648 | 0.0014 | 0.2805 | 0.1898 |
| 6 | 82.8362 | 146.3235 | 0.0013 | 0.2788 | 0.1773 |
| 7 | 85.7721 | 148.0735 | 0.0016 | 0.2805 | 0.2024 |
| 8 | 85.9431 | 147.6656 | 0.0016 | 0.2804 | 0.2072 |
| 9 | 83.2410 | 148.7078 | 0.0016 | 0.2808 | 0.2023 |
| 10 | 79.9621 | 156.5048 | 0.0011 | 0.2908 | 0.1424 |

## 4.3 WADC design and impact on the system oscillations

A WADC is designed to suppress the dominant target mode of the system. A classical lead-lag structure is employed to develop the WADC, as presented in chapter 3. The concluded equations were used to compute the controller parameters based on the identified transfer function model using the residue analysis of the actuator. Using wide-area measurement, the bus frequency difference between the two optimal observation buses of the western and central area is selected as the optimal observation signal. Table B.3 shows the calculated parameters of the WADC when the exciters and governors are used as an actuator for multiples locations. The listed plants in Table B.3 are chosen based on the analysis of the optimal actuators in the previous section.

### 4.3.1 Control effect of single plant WADC

In this section, based on the transfer function models presented in the previous section, a WADC is designed for each actuator and tested under two events: temporary line fault and single machine trip to study the impact on system dominant oscillation. The control effect of WADCs on generators' exciter and governor is presented.

#### Impact of WADCs via single plant exciters

Using the exciter as WADC actuators, the output of the WADC is combined with the PSS output and then added to the set point of the exciter to manipulate reactive power, as shown in Figure 4.15. The frequency of the optimal observation bus under temporary line fault is given in Figure 4.16 and the angle difference between the tie line buses is given in Figure 4.17 whereas Table 4.9 shows the Prony analysis for the cases in Figure 4.16. When only one plant WADC is activated, the damping ratio of the dominant oscillation mode can be improved compared to no WADC case. Moreover, when WADCs are activated on the WestJ plant, the damping ratio could be further enhanced more than the other two cases.

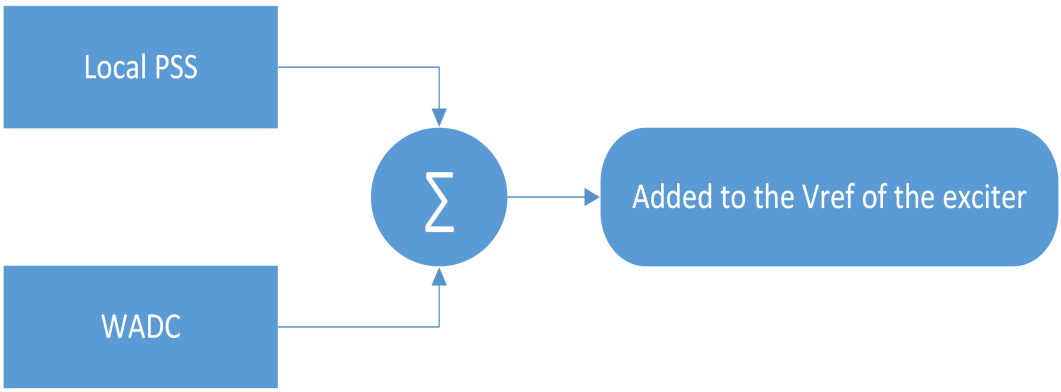


**Figure 4.15:** Exciter WADC.

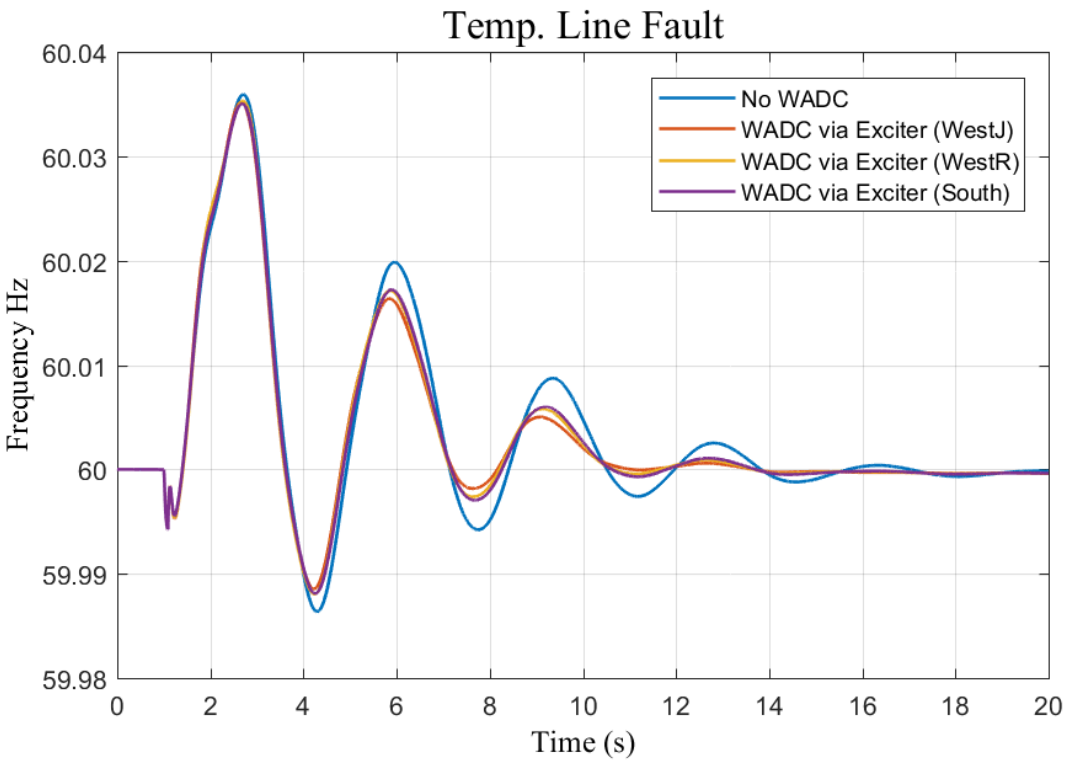


**Figure 4.16:** Frequency response during Tie-line fault (WADCs via single plant exciters).

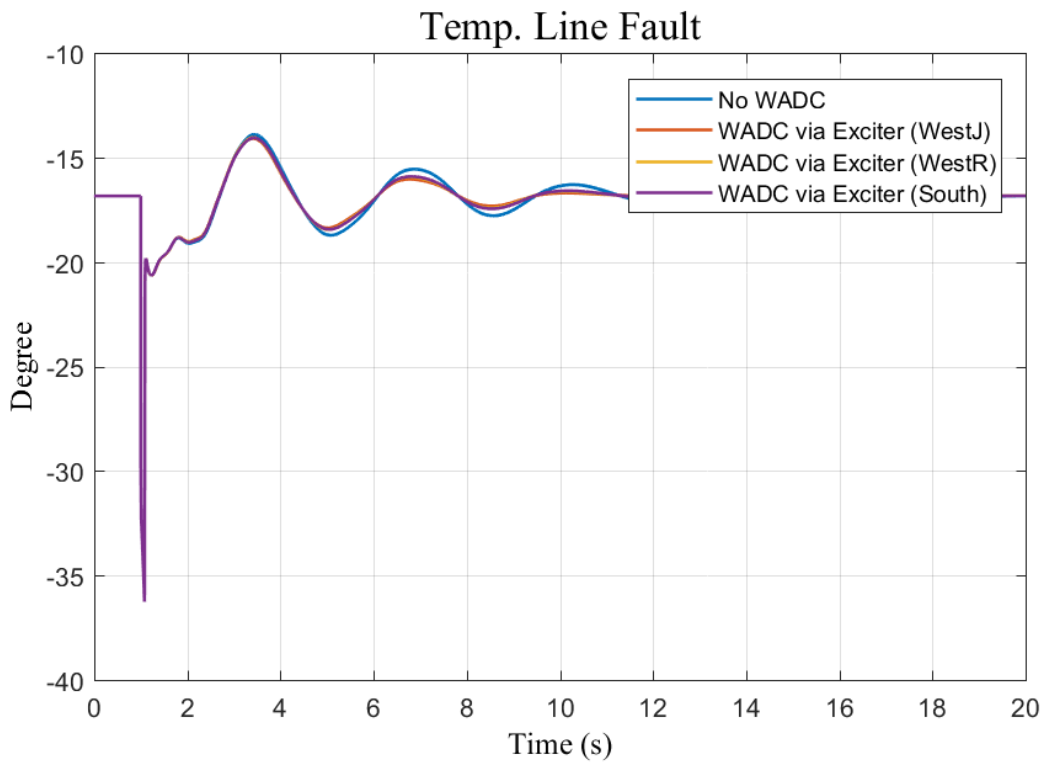


**Figure 4.17:** Angle difference response during tie-line fault (WADCs via single plant exciters).

**Table 4.9:** Prony analysis results tie-line fault (WADCs via single plant exciters)

| No. | **Case** | **Oscillation Frequency(Hz)** | **Damping Ratio(%)** |
|---|---|---|---|
| 1 | No WADC | 0.288 | 11.45 |
| 3 | WADC via Exciter (WestJ) | 0.289 | 17.288 |
| 4 | WADC via Exciter (WestR) | 0.291 | 15.893 |
| 5 | WADC via Exciter (South) | 0.29 | 15.104 |

Similarly, the frequency and the angle difference under temporary single generation trip (680 MW) are provided in Figure 4.18 and Figure B.2 respectively, whereas Table 4.10 presents the Prony analysis for the cases in Figure 4.18. The damping ratio of the dominant oscillation mode can be increased compared to no WADC cases if only one WADC plant is activated. Also, when WADCs are activated at the WestJ plant, the damping ratio can be further improved in comparison to the other cases. It can be conclude that the impact of WADC via exciters at WestJ plant is the best among all three plants.

#### Impact of WADCs via single plant governors

The impact of WADC via governor is directly related to the reserved active power of the generator that equips with a WADC. The headroom availability of the generator that equips with a WADC is important to achieve the optimal control effect of the WADC. Using the governor as WADC actuators, the output of the WADC is combined with the Pref of the governor and then added to the set point of the governor to manipulate the active power, as shown in Figure 4.19.

For the governor case, the frequency of the optimal observation bus and the angle difference between the tie line buses under temporary line fault are provided in Figure 4.20 and Figure 4.21 respectively, whereas Table 4.11 shows the Prony analysis for the scenarios given in Figure 4.20. When a single WADC plant is activated, the dominant oscillation mode damping ratio can be improved compared to no WADC scenario. Moreover, the damping ratio can be further enhanced when WADCs are activated on the WestJ plant.

Similarly, the frequency and the angle difference under temporary single generation trip (680 MW) are provided in Figure 4.22 and Figure 4.23 respectively, whereas Table 4.12 presents the Prony analysis for the cases in Figure 4.22. The damping ratio of the dominant oscillation mode can be improved when only one WADC plant is activated in contrast with no WADC scenarios. Furthermore, the damping ratio can be further enhanced in comparison to other scenarios if WADCs are activated at the WestJ plant.

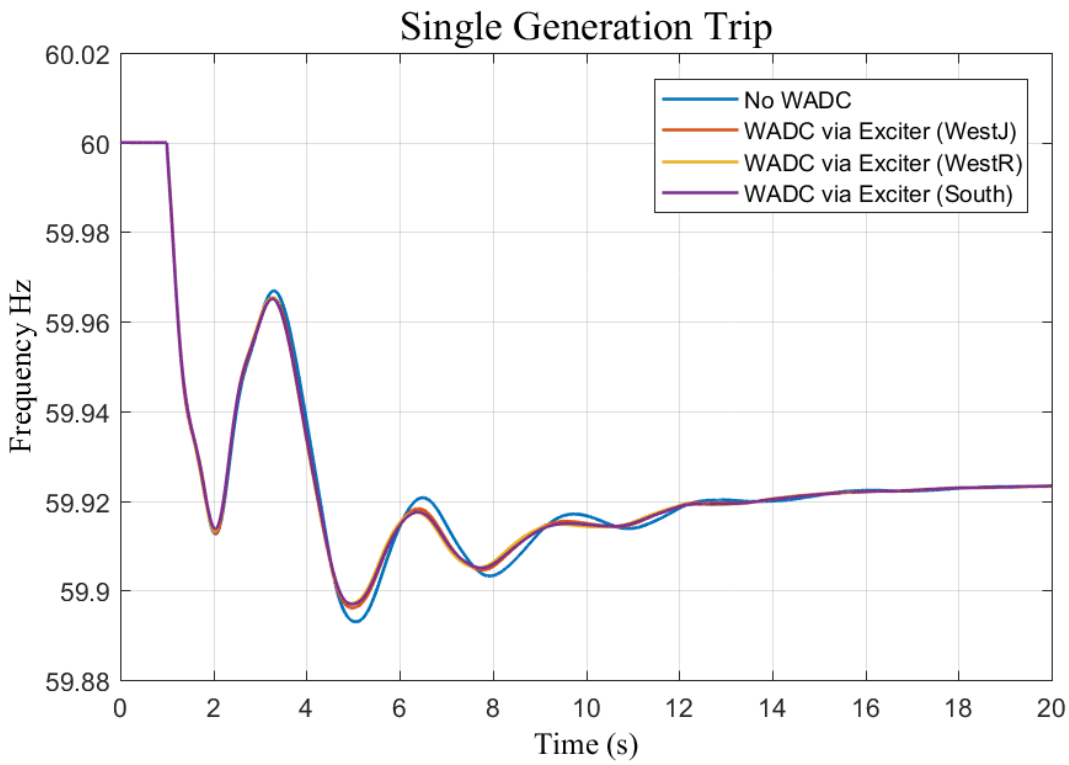


**Figure 4.18:** Frequency response during single generation trip (WADCs via single plant exciters).

**Table 4.10:** Prony analysis results single generation trip (WADCs via single plant exciters)

| No. | **Case** | **Oscillation Frequency(Hz)** | **Damping Ratio(%)** |
|---|---|---|---|
| 1 | No WADC | 0.314 | 13.79 |
| 3 | WADC via Exciter (WestJ) | 0.326 | 16.656 |
| 4 | WADC via Exciter (WestR) | 0.328 | 17.47 |
| 5 | WADC via Exciter (South) | 0.329 | 17.598 |

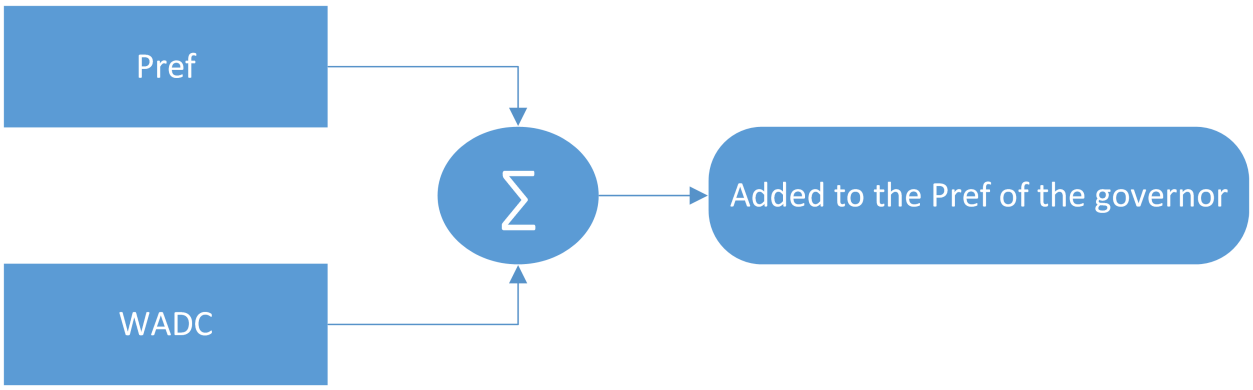


**Figure 4.19:** Governor WADC.

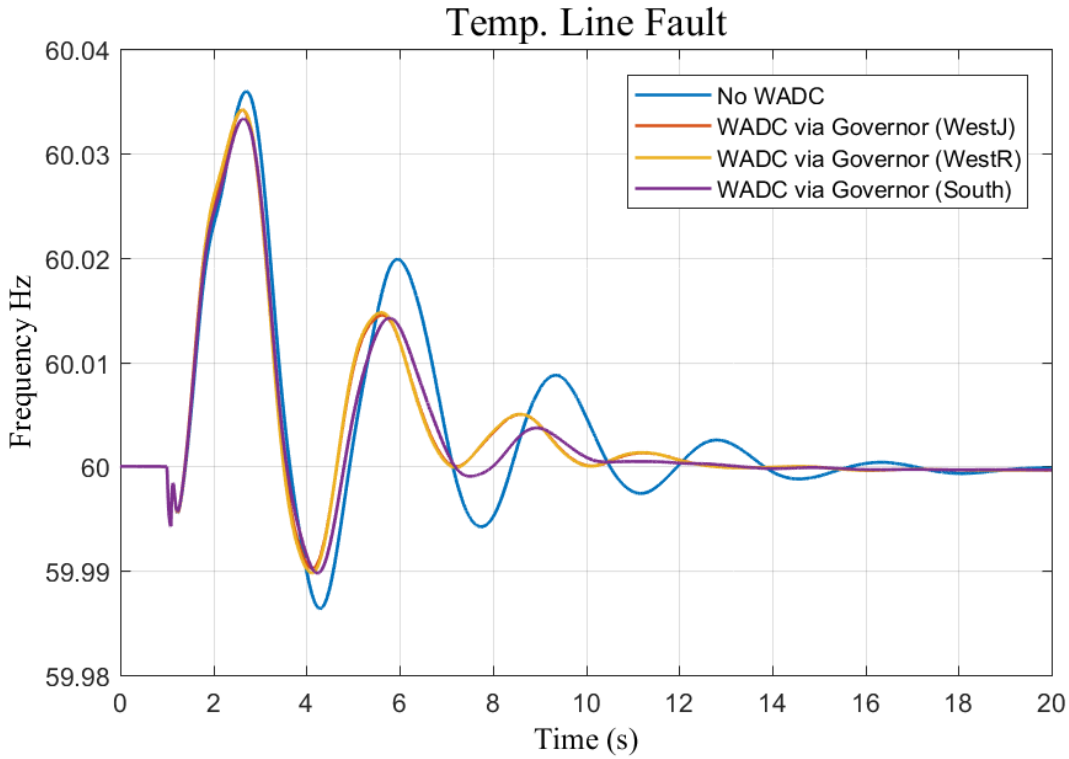


**Figure 4.20:** Frequency response during Tie-line fault (WADCs via single plant governors).

**Table 4.11:** Prony analysis results tie-line fault (WADCs via single plant governors)

| No. | **Case** | **Oscillation Frequency(Hz)** | **Damping Ratio(%)** |
|---|---|---|---|
| 1 | No WADC | 0.288 | 11.45 |
| 3 | WADC via Governor (WestJ) | 0.317 | 20.879 |
| 4 | WADC via Governor (WestR) | 0.316 | 21.033 |
| 5 | WADC via Governor (South) | 0.299 | 21.039 |

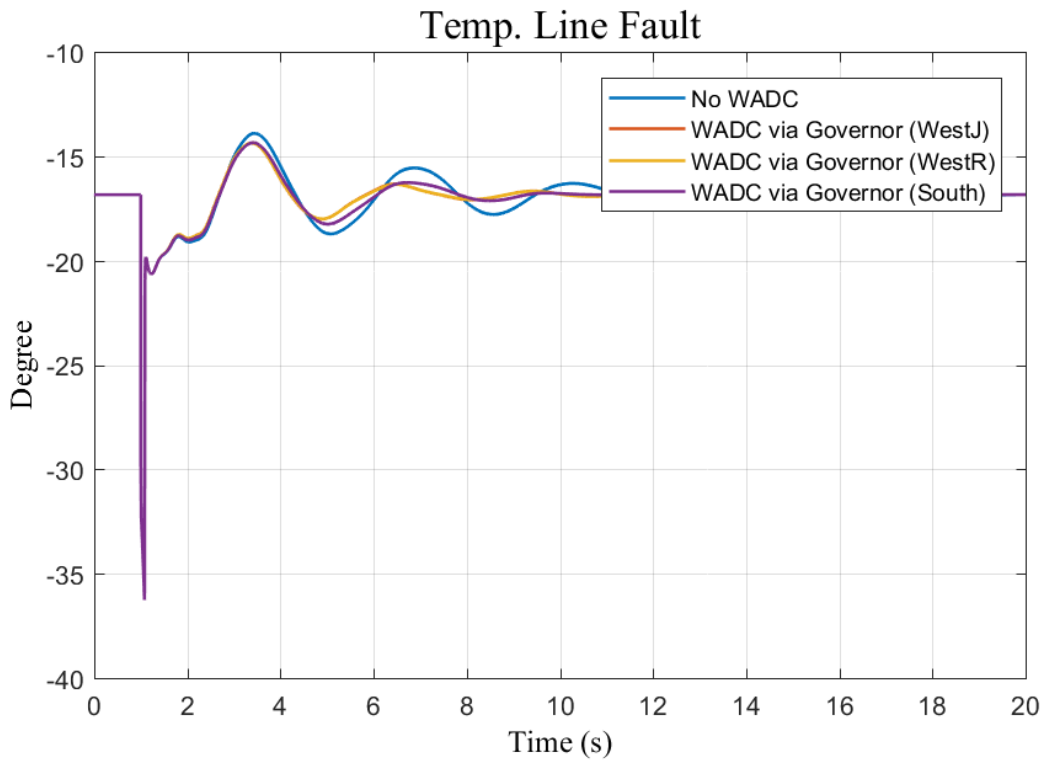


**Figure 4.21:** Angle difference response during tie-line fault (WADCs via single plant governors).

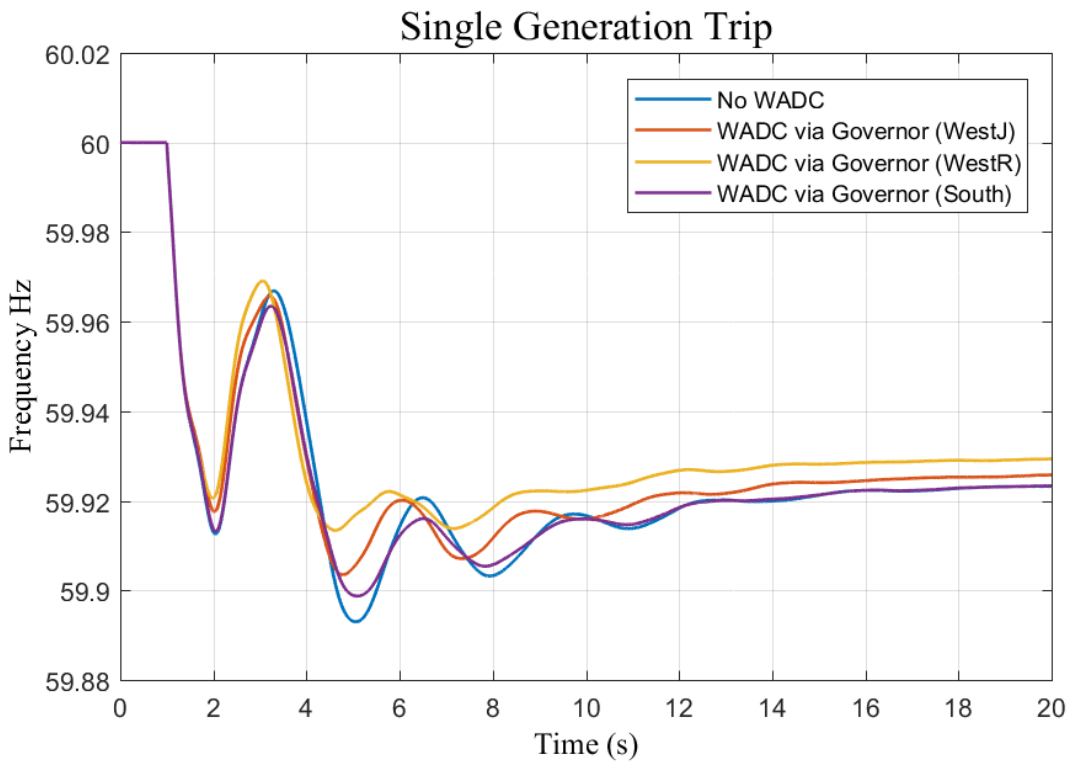


**Figure 4.22:** Frequency response during single generation trip (WADCs via single plant governors).

**Table 4.12:** Prony analysis results single generation trip (WADCs via single plant governors)

| No. | **Case** | **Oscillation Frequency(Hz)** | **Damping Ratio(%)** |
|---|---|---|---|
| 1 | No WADC | 0.314 | 13.79 |
| 3 | WADC via Governor (WestJ) | 0.347 | 17.075 |
| 4 | WADC via Governor (WestR) | 0.354 | 26.685 |
| 5 | WADC via Governor (South) | 0.312 | 21.592 |

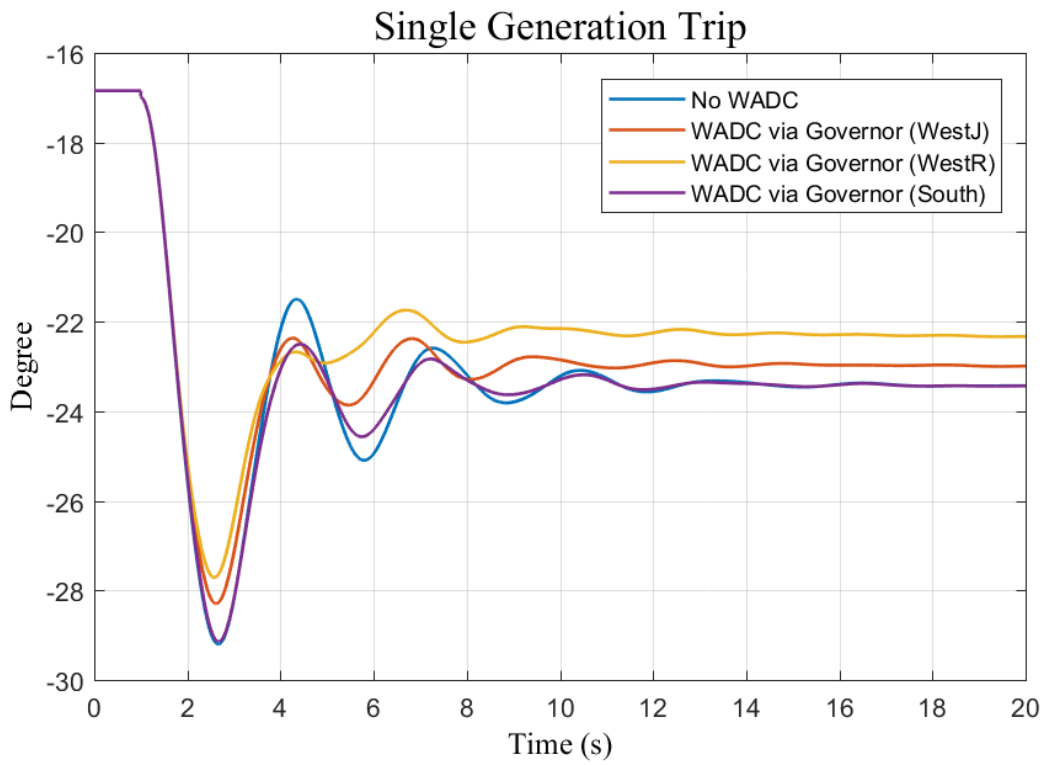


**Figure 4.23:** Angle difference response during single generation trip (WADCs via single plant governors).

### 4.3.2 Comparison of WADCs via different actuators

The control effect when WADC is activated in a different actuator on the same plant is presented in this section. To demonstrate that the control effect can be accumulated when different WADCs are activated, WADCs are equipped with the exciter and governor on each plant individually. The three plants are WestJ, WestR, and South, and WADCs were tested under two disturbances. One is a temporary fault on the tie-line between the central and western areas, and the other is a generator trip at WestJ plant. During a temporary tie-line fault, the control effect of WADCs via a combination of different actuators in the same plant is given in Figure 4.24 and Figure B.3 respectively. The damping ratio of the dominant oscillation mode for WADCs via exciter and governor at all cases is significantly improved compared to the No WADC case. Table 4.13 shows the Prony analysis for the cases in Figure 4.24. Similarly, during a single generation trip, the control effect is given in Figure 4.25 and Figure B.4 respectively. The damping ratio of the dominant oscillation mode at WestR and and South is considerably improved than the No WADC case. The damping ratio when WADCs deployed on the WestJ plant is not as good as the other two cases. The reason might be because the generation trip occurred at WestJ plant, so the impact is reduced since one machine is out. Table 4.14 shows the Prony analysis for the cases in Figure 4.25.

### 4.3.3 Control effect of multiple WADCs

The control effect when WADC is activated in multiple plants is presented in this section. WADCs on WestJ, WestR, and South are activated simultaneously. These three WADCs were tested under two disturbances; a temporary fault and a generator trip. During a temporary tie-line fault, the control effect of WADCs via multiple actuators and their combinations is given in Figure 4.26 and Figure B.5 respectively. The damping ratio of the dominant oscillation mode for WADCs via all plant exciters is improved sharply from 11.45% to 26.988% while the dominant oscillation mode is still closer to the base case. When WADCs are equipped with all the plant governors, the dominant oscillation of the system increased from 0.288 to around 0.4 Hz. Table 4.15 shows the Prony analysis for the cases in Figure 4.26.

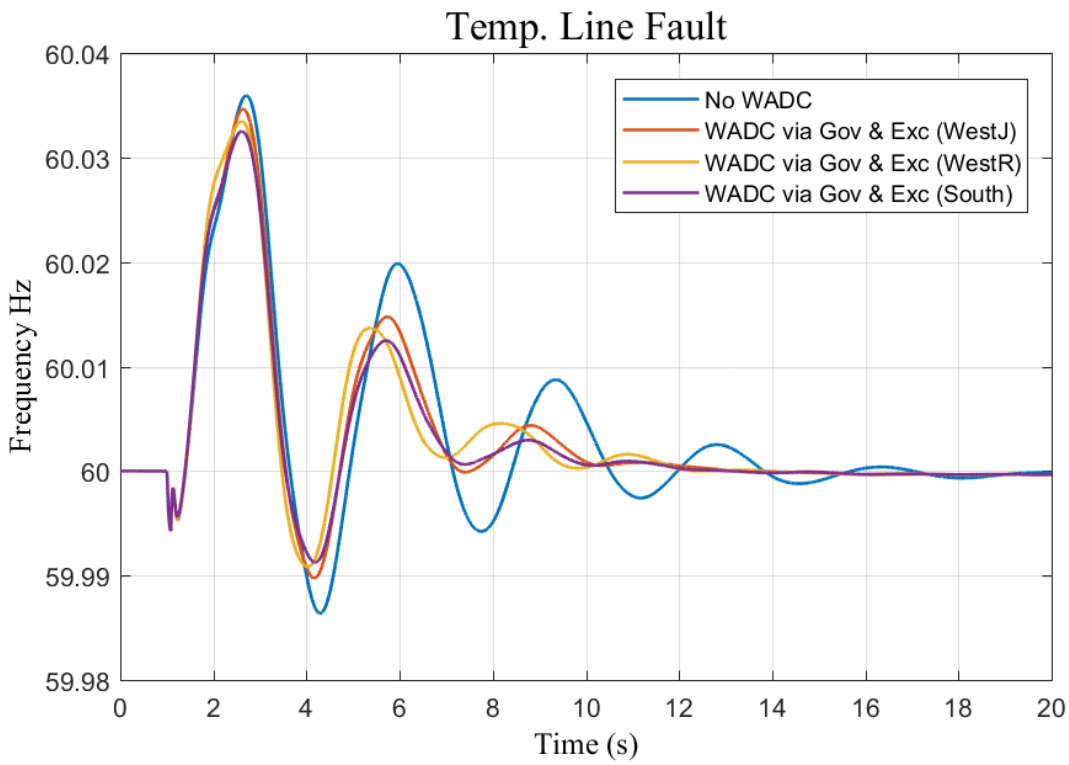


**Figure 4.24:** Frequency response during Tie-line fault (WADCs via governor and exciter).

**Table 4.13:** Prony analysis results tie-line fault (WADCs via governor and exciter)

| No. | **Case** | **Oscillation Frequency(Hz)** | **Damping Ratio(%)** |
|---|---|---|---|
| 1 | No WADC | 0.288 | 11.45 |
| 3 | WADC via Governor and Exciter (WestJ) | 0.296 | 21.658 |
| 4 | WADC via Governor and Exciter (WestR) | 0.331 | 24.159 |
| 5 | WADC via Governor and Exciter (South) | 0.303 | 25.815 |

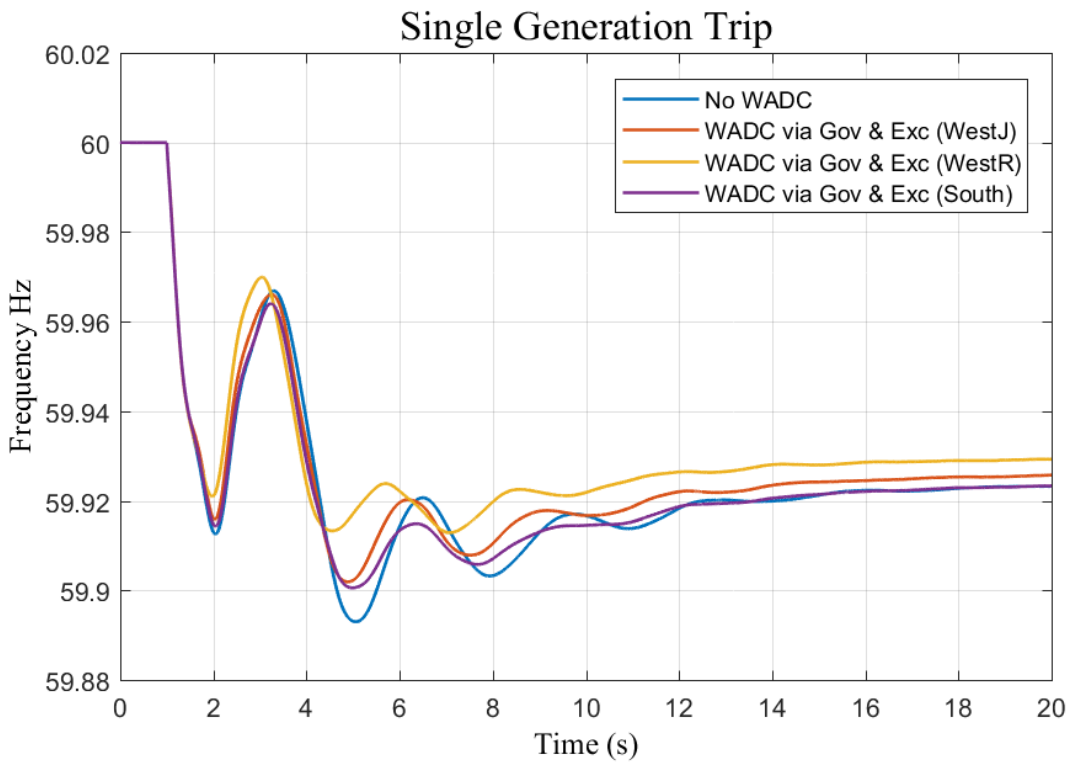


**Figure 4.25:** Frequency response during single generation trip (WADCs via governor and exciter).

**Table 4.14:** Prony analysis results single generation trip (WADCs via governor and exciter)

| No. | **Case** | **Oscillation Frequency(Hz)** | **Damping Ratio(%)** |
|---|---|---|---|
| 1 | No WADC | 0.314 | 13.79 |
| 3 | WADC via Governor and Exciter (WestJ) | 0.339 | 16.702 |
| 4 | WADC via Governor and Exciter (WestR) | 0.367 | 23.569 |
| 5 | WADC via Governor and Exciter (South) | 0.325 | 23.678 |

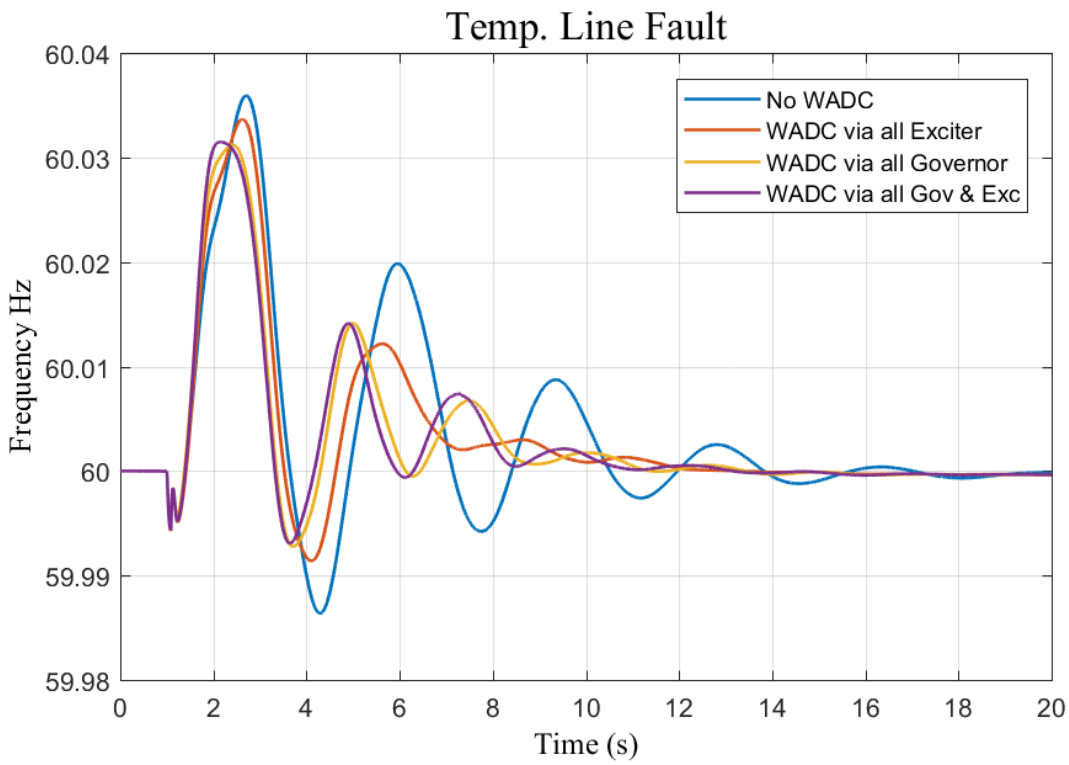


**Figure 4.26:** Frequency response during Tie-line fault (WADCs via multiple actuators).

**Table 4.15:** Prony analysis results tie-line fault (Multiple WADCs)

| No. | **Case** | **Oscillation Frequency(Hz)** | **Damping Ratio(%)** |
|---|---|---|---|
| 1 | No WADC | 0.288 | 11.45 |
| 3 | WADC via all Exciter | 0.299 | 26.988 |
| 4 | WADC via all Governor | 0.409 | 15.699 |
| 5 | WADC via all Governor and Exciter | 0.427 | 14.142 |

Similarly, for the single generation trip case, the control effect of WADCs is given in Figure 4.27 and Figure B.6 respectively. The damping ratio of the dominant oscillation mode for WADCs via all plant exciters is improved from 14.468% to 20.422% while the dominant oscillation mode is increased slightly from 0.32 Hz to 0.358 Hz. When WADCs are equipped with all the plant governors, the oscillation mode increase to 0.409 Hz with 23.552%. Comparing the cases of WADCs with all exciters and all governors during the generation trip, using the governors is better than the exciter one since the governor, regulating the active power, directly impacts the frequency response. Table 4.16 shows the Prony analysis for the cases in Figure 4.27.

### 4.3.4 Control effect of the WADC via HVDC

In this section, the WADC is tested via the HVDC link. In the SEC grid, a long-distance HVDC transmission link is currently under development [94]. It is a 770 km point-to-point link that is embedded in a powerful AC network [94]. The HVDC converter stations are connected to 380 kV existing substations, part of a current network. The HVDC link is planned and designed to connect the central and western areas in the SEC power grid, as shown in Figure 4.28. In this study, the VSCDCT model in PSSE is utilized to model the dynamic characteristics of the VSC-based HVDC system. It is a combination of three modules: one DC transmission line module (DCLINE) for the DC link and two voltage source converter modules (VSCDYN) for the VSCs at each DC line terminal [95]. Figure 4.30 describes the HVDC model for this study which is Voltage Source Converter-based HVDC system [95]. The model describes the general performance to evaluate the interaction of a VSC-based HVDC system with the AC network.

The impact of adding the HVDC with and without WADC on the dominant oscillation mode is studied. The control effect of WADC via HVDC is tested under a line fault event. The frequency response is presented in Figure 4.29, and the angle difference between the western and central areas is shown in Figure C.1. It is evident that the damping ratio of the dominant oscillation mode is improved when the HVDC is added to the SEC grid. Furthermore, when the WADC is activated on HVDC, the damping ratio of the dominant oscillation mode is further improved and the best performance is achieved.

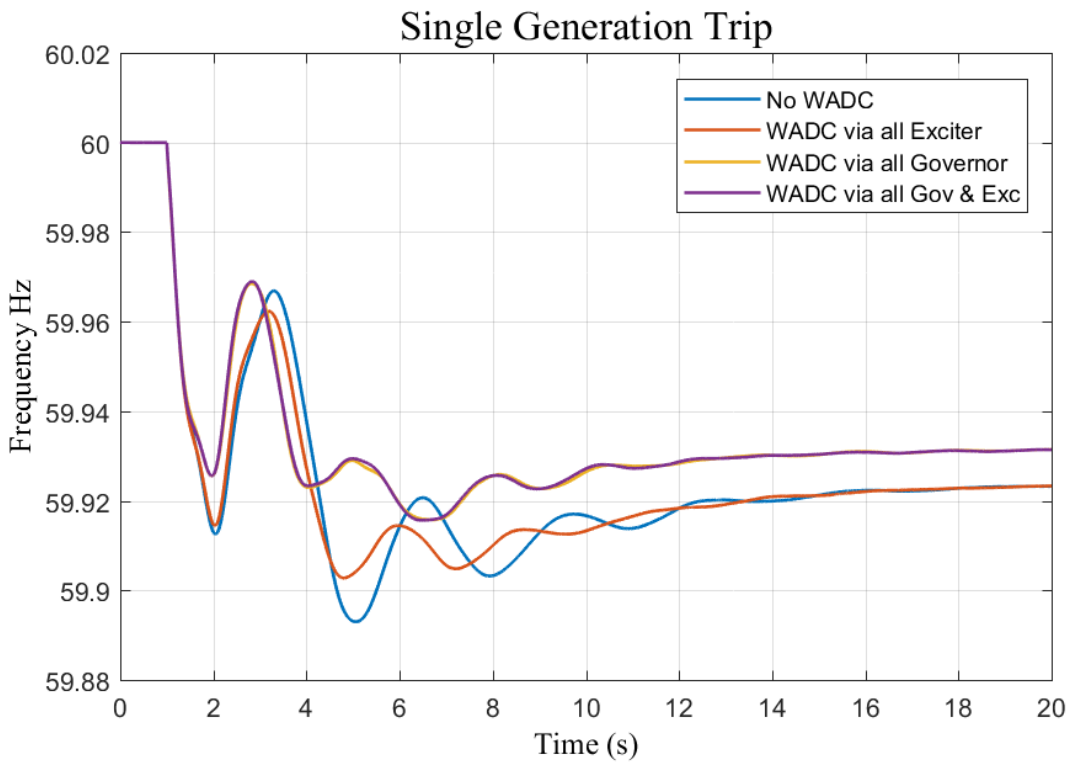


**Figure 4.27:** Frequency response during single generation trip (WADCs via multiple actuators).

**Table 4.16:** Prony analysis results for single generation trip (Multiple WADCs)

| No. | **Case** | **Oscillation Frequency(Hz)** | **Damping Ratio(%)** |
|---|---|---|---|
| 1 | No WADC | 0.314 | 13.79 |
| 3 | WADC via all Exciter | 0.358 | 20.422 |
| 4 | WADC via all Governor | 0.409 | 23.552 |
| 5 | WADC via all Governor and Exciter | 0.395 | 22.186 |

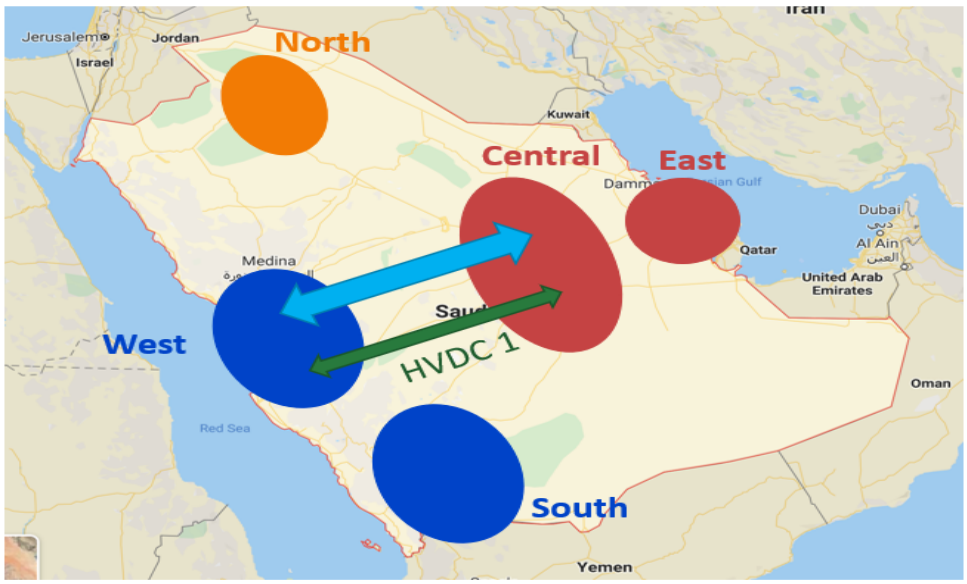


**Figure 4.28:** SEC HVDC links.

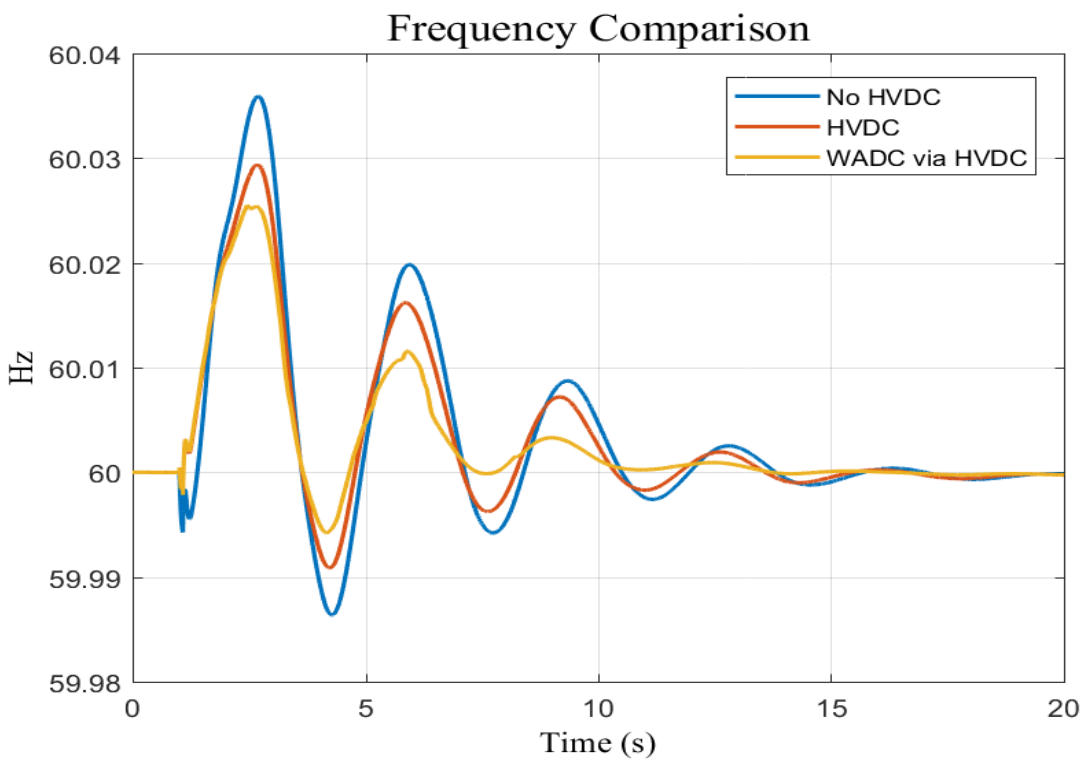


**Figure 4.29:** Frequency response during line fault (HVDC case).

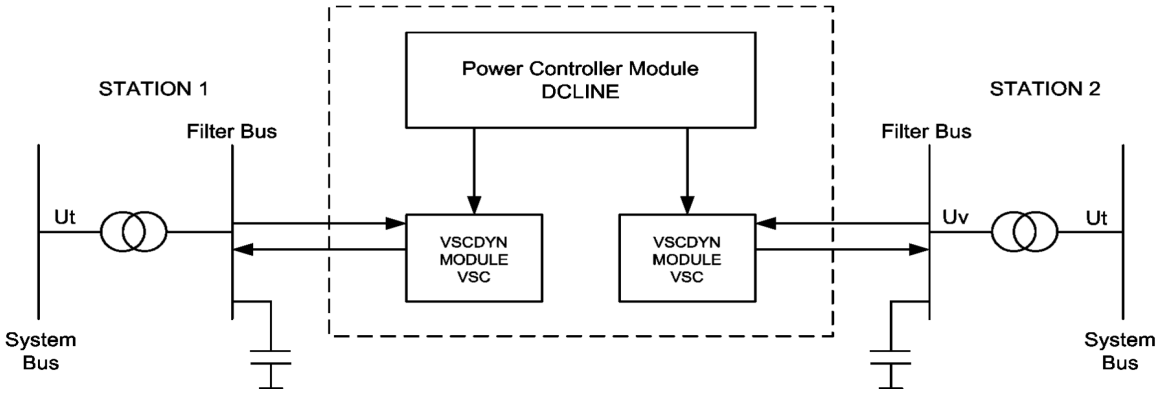


**Figure 4.30:** HVDC PSSE model.

## 4.4 Transient Stability Improvement with the designed WADC

Today's power systems are stressed towards their stability limit due to many reasons, a sudden large disturbance could push the power system to operate closer to its stability limit and may lead to system separation or widespread blackout [96, 97]. Consequently, security precaution measurements are used to prevent the system from separating. The traditional methods such as Special Protection Schemes (SPS) [98] and Remedial Action Schemes (RAS) [98] based on fast generation trip and load shedding are widely used in today's power grids. Some severe contingencies could cause system separation with huge losses. Therefore, it is crucial to keep the two AC transmission lines connected and prevent system separation after various contingencies.

Although small-signal stability and transient stability are two different aspects of power system stability, any measures to enhance system's small-signal stability can usually improve system's transient stability simultaneously. This is because a better damping control could reduce the angle difference in the first swing after a large disturbance. If these WADCs designed to enhance system's small-signal stability can be sufficiently prevent system separation, SPS and RAS may not need to take actions to proactively trip generators and shed loads. This section introduces the benefit of the designed WADCs in improving the SEC's transient stability. The designed WADCs cannot only prevent the system from separation under large generation trips but can also increase the power transfer limit of the tielines between the western and central areas.

### 4.4.1 Impact of WADC on system separation condition

This section presents the cases when the system was separated due to the large generation trip and how WADC prevented the separation with multiple WADCs. The system separation could happen in the Saudi power grid when a large amount of generation trip happens in the western area simultaneously.

Table 4.17 shows the marginal amount of generation trip for different WADC configurations. For instance, when there is no WADC, the system will be separated by the out-of-step relay if the generation trip amount is larger than 1860 MW. The marginal generation trip increases to 1952 MW for the WADC case via exciters and 1968 MW for the WADC case via governors. The system can be saved from separation during a three-generation trip in the west (2040 MW) for the WADC case via exciters and governors. The frequency response is presented in Figure 4.31, and the angle difference between the western and central areas is shown in Figure B.7. These results demonstrated the effectiveness of the designed WADCs in preventing system separation. The system can be saved from separation when HVDC is added to the SEC grid. The frequency response is presented in Figure 4.32, and the angle difference between the western and central areas is shown in Figure C.2. It is clear that the system is still connected after the 2040 MW trip for the HVDC case, while the system is separated for the no HVDC case. Figure 4.33 visualizes the data presented in Table 4.17.

### 4.4.2 Impact on the tie-line active power transfer limit

The impact of WADCs on the transfer limit of the major tie lines between the western area and the central area is also studied. The tie-line power flow is increased by increasing one selected load in the western area and decreasing one selected load in the central area. The impact of WADC on the transfer limit of two tie lines between the western and central areas was studied. The two tie lines carry 1230 MW totally in the base case. A temporary three-phase fault is applied on one of the tie lines followed by tripping the faulted tie line after 80 ms. The transfer limit is determined based on the pre-disturbance power flow when the system is still connected after the disturbance. The simulation results are given in Table 4.18. Without WADC, the system can keep connected after the abovementioned fault and line trip occurs if two tie lines carry 2017.0 MW prior to the disturbance. With WADCs via exciters, WADCs via governors, and WADCs via exciters and governors, the transfer limit can be increased to 2029.0 MW, 2051.2 MW, and 2058.6 MW, respectively. The higher transfer limit can be achieved with the WADC case via exciters and governors. When the HVDC is added to the SEC grid, the transfer limit is significantly increased to more than 2300 MW. Figure 4.34 visualize the cases that presented in Table 4.18.

**Table 4.17:** Marginal amount of generation trip With WADCs

| Case | Marginal amount of generation trip in west (MW) |
|---|---|
| No WADC | 1860 |
| WADC via Exciters | 1952 |
| WADC via Governors | 1968 |
| WADC via Exciters & Governors | <2040 |
| WADC via HVDC | <2040 |

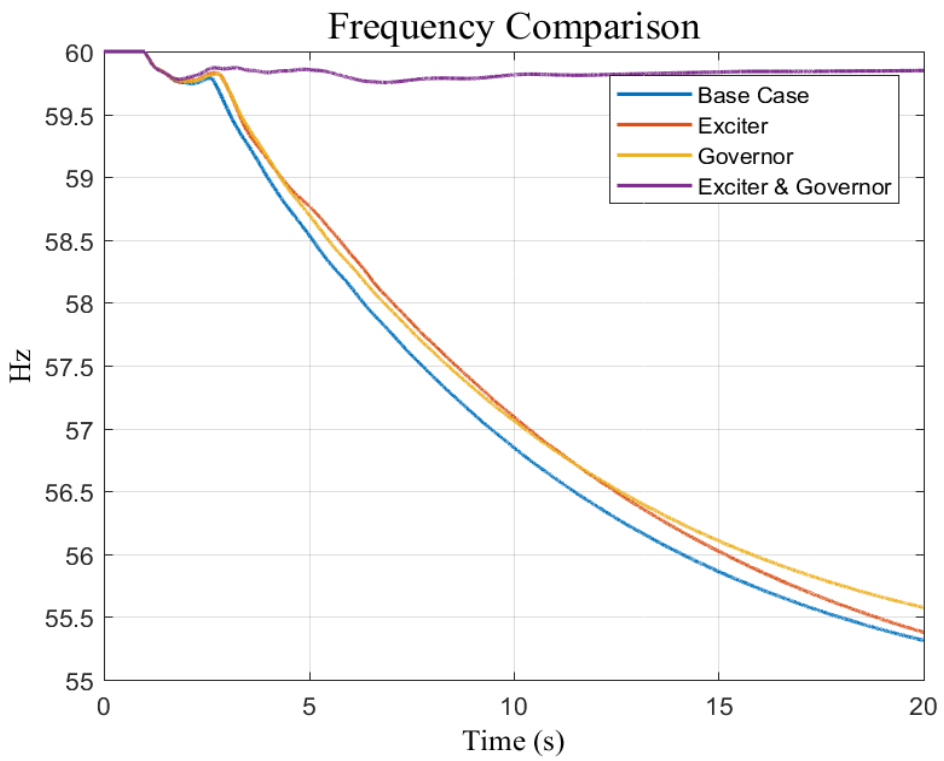


**Figure 4.31:** WADC via multiple actuators frequency response after large generation trip (2040 MW).

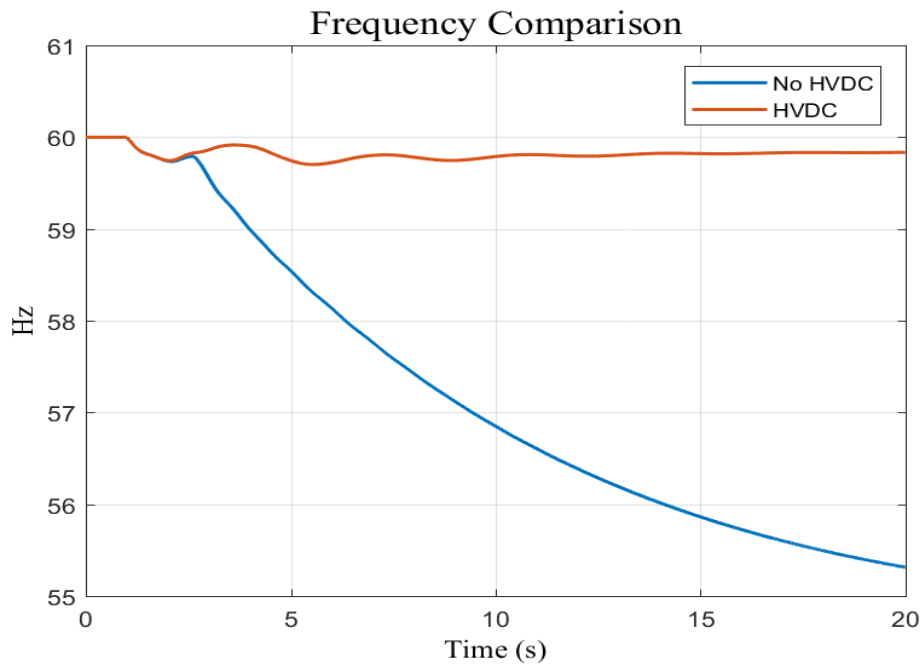


**Figure 4.32:** WADC via HVDC frequency response after large generation trip (2040 MW).

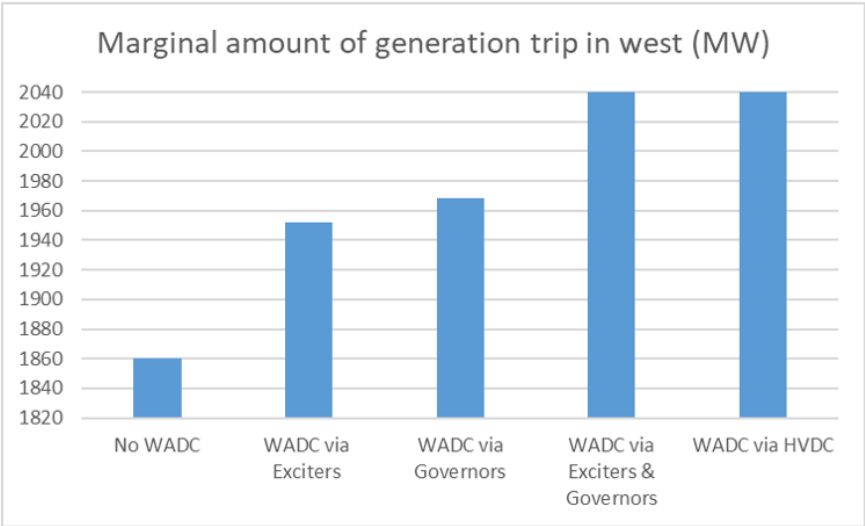


**Figure 4.33:** Marginal generation trip at the western area.

**Table 4.18:** Active power transfer limit With WADCs

| Case | Transfer limit Single-Circuit (MW) | Transfer limit Double-Circuit (MW) |
|---|---|---|
| No WADCs | 1008.5 | 2017 |
| WADC via Exciters | 1014.5 | 2029 |
| WADC via Governors | 1025.6 | 2051.2 |
| WADC via Exciters & Governors | 1029.3 | 2058.6 |
| WADC via HVDC | 1150.2 | 2300.4 |

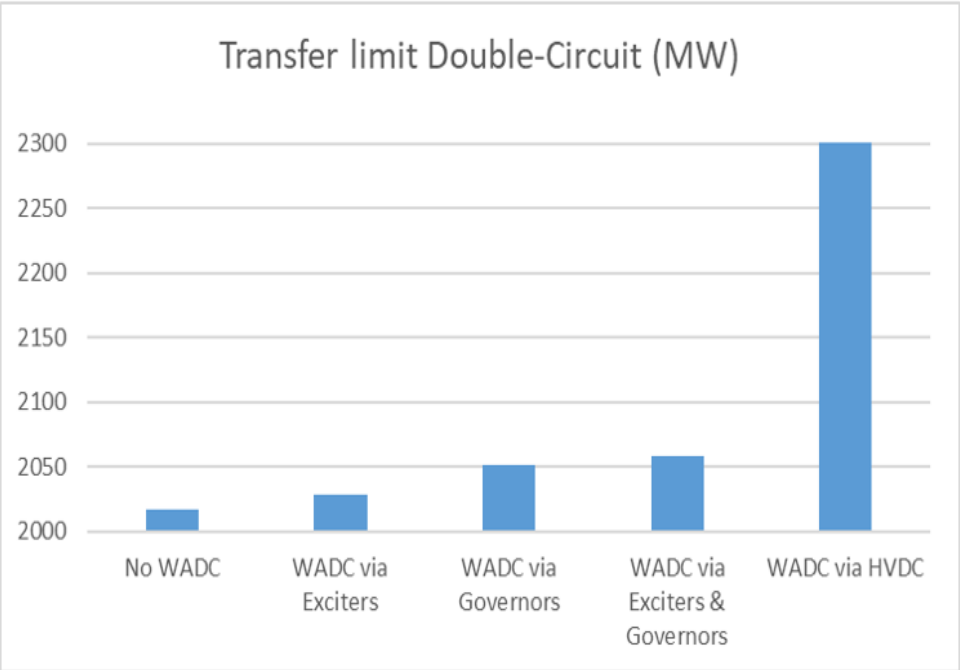


**Figure 4.34:** Transfer limit of the major tieline.

## 4.5 Improving the robustness of the WADC

This section focus on achieving better controller performance. The first is to improve the performance that is used in this dissertation. The other is to design a robust controller using H-infinity. Both approaches are presented briefly in this section.

### 4.5.1 Improving the performance of the used controller

The used WADC is mainly designed to deal with the small-signal stability issue of the system. Although the small-signal stability and the transient stability are two different aspects of power system stability, any measures to enhance the system's small-signal stability can improve the system's transient stability simultaneously. The WADC parameters are determined based on the system identification presented in the first section of this chapter. The gain of the WADC could be described as uncertainty parameters since the disturbance is unknown. The gain setting could improve the robustness of the WADC with multiple contingencies. The performance of the WADC with fixed gain could be limited during severe disturbances. However, the gain increase during a large disturbance to improve the WADC performance will be beneficial for the system. Figure 4.35 shows the implementation of the gain uncertainty function where the function will be fed by the controller input. The results in this part are done with a simple linear function relationship with the input to determine the gain. It is not done using the uncertainty robustness function. The implementation of the uncertainty robustness function could be a start point for future works. The limit of the gain uncertainty function should be determined based on analyzing the studied system. In this case study, the minimum gain used is 100, and the maximum gain is 500.

The results shown in Figures 4.36, 4.37, C.3, and 4.38 are the system response with WADC via four exciters, which are located at the WestJ plant, after multiple disturbances. The results compare different gain settings for the WADC with the gain uncertainty function case. The disturbances that are chosen in this comparison vary in their severity. The impact of low gain during a large disturbance and the impact of high gain during small disturbance can be noticed. It can be concluded that the gain uncertainty function case had better damping for all cases.

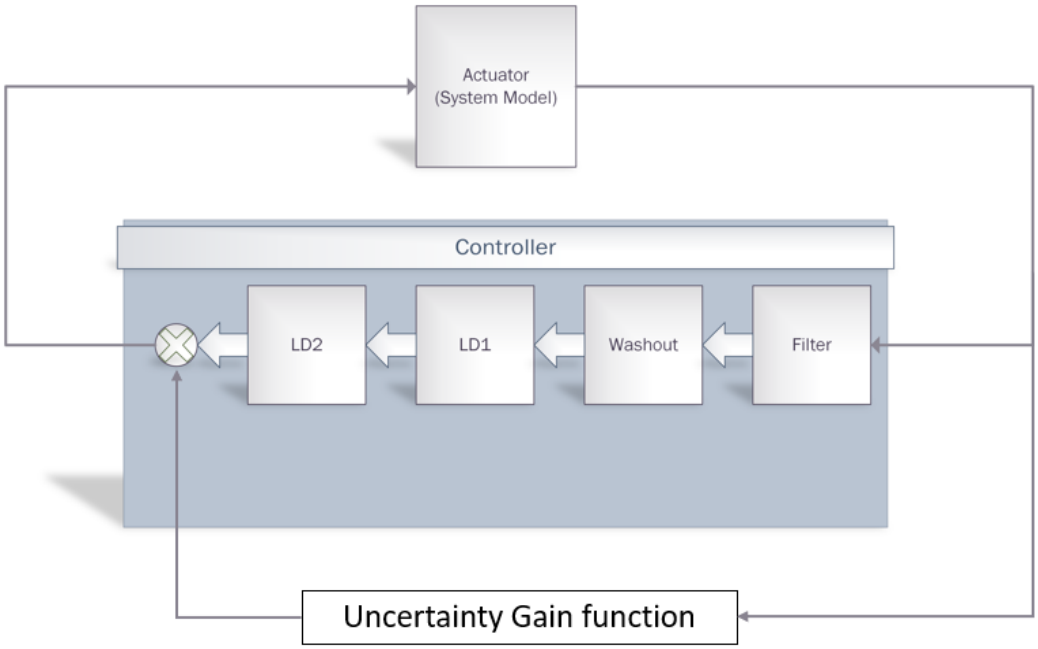


**Figure 4.35:** Gain uncertainty function implementation.

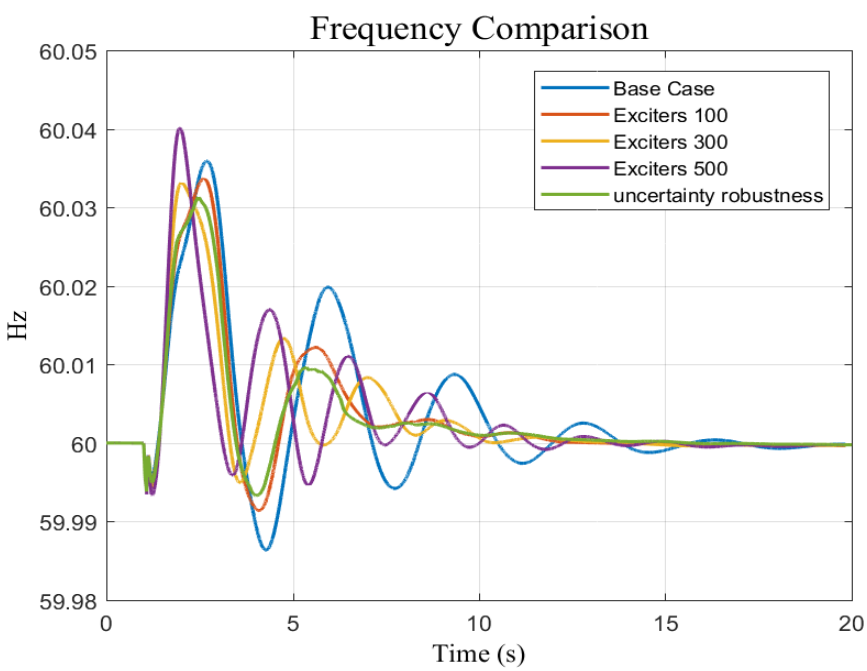


**Figure 4.36:** Frequency response after line fault disturbances with gain robustness function (WADCs via exciters).

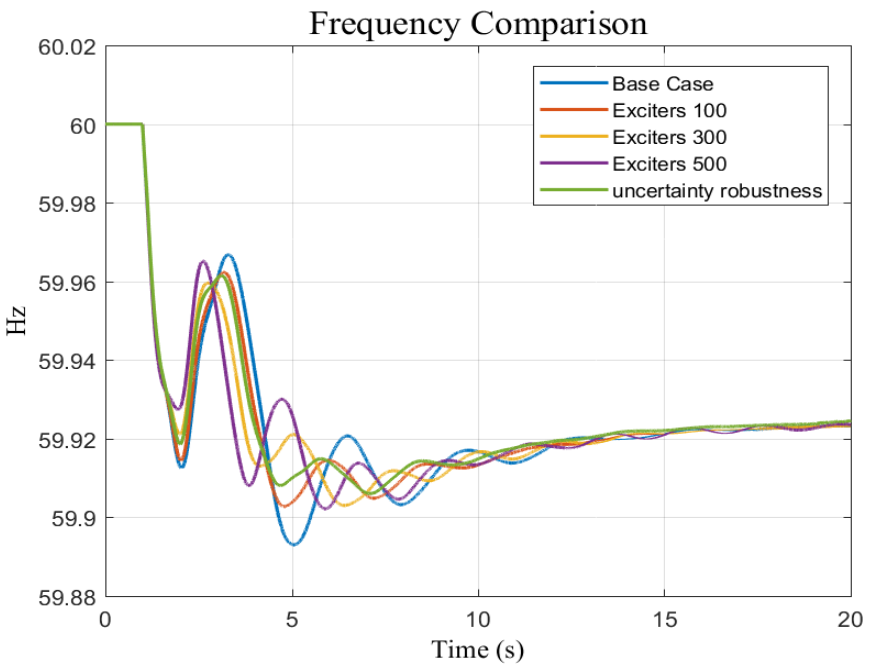


**Figure 4.37:** Frequency response after single generator trip with gain robustness function (WADCs via exciters).

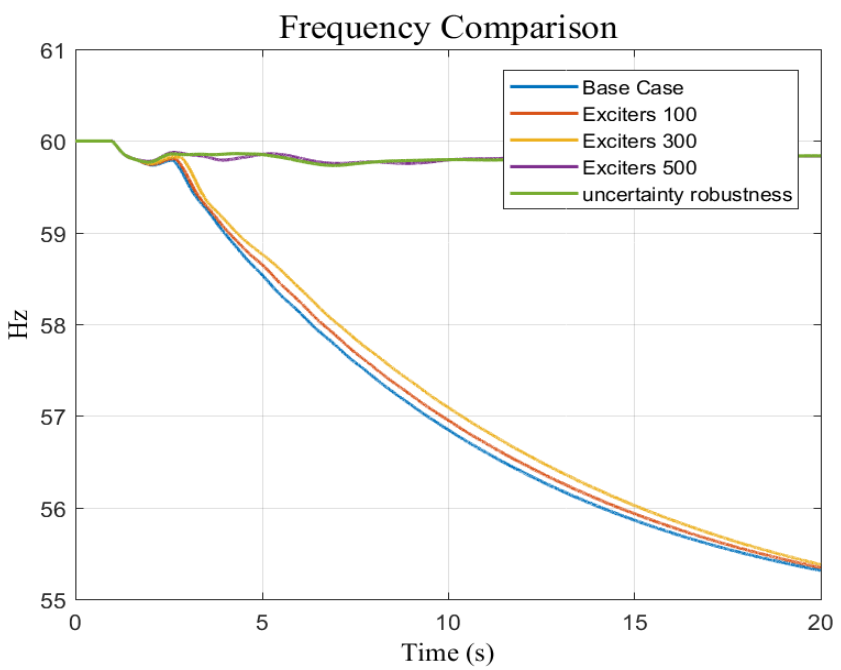


**Figure 4.38:** Frequency response after three generators trip with gain robustness function (WADCs via exciters).

### 4.5.2 Developing a robust controller using H-infinity

Robust control methods aim to achieve robust performance and stability in the presence of bounded modeling errors. There are two main methods for robust controllers, which are H2- and H-infinity. In this part, the controller is designed to damp the dominant oscillation mode using H-infinity controller. H-infinity control has a significant role in robust controller design. Various techniques are available in the literature for the H-infinity controller design, and H-infinity loop shaping is one of the widely accepted among them as the performance requirements can be embedded in the design stage as performance weights [99, 100, 101, 102, 103].

H-infinity control problems' address has been used extensively as a frequency domain loop shaping technique [104]. Minimizing the H-infinity norm of the weighted closed-loop transfer functions minimizes the peak of the system's largest singular value. The selection of weight functions is very important for designing an H-infinity controller to achieve the required loop shaping. For minimum robust performance, the singular value of the loop gain should be high at low frequency, in the presence of disturbances, and the maximum singular value of the loop gain should be small at high frequencies where significant noise is present [99].

The H-infinity controller design is an optimization-based approach to a linear feedback control system that uses H-infinity norms. The H-infinity controller design aims to find a controller K such that it minimizes the cost function $\gamma$ of the closed-loop system [105]. The cost function $\gamma$ for the H-infinity controller is based on the H-infinity norm as

$$\gamma = \|F(G, \gamma)\|_\infty \tag{4.1}$$

The H-infinity controller is designed using the MATLAB command hinfsyn [105]. The arguments that entered the function are the system realization, the input and output dimensions both as 1, the lower bound on $\gamma$ as 0.001, and the upper bound of 50 [105]. The tolerance in the final $\gamma$ values is chosen as 0.001 [105]. In order to design an H-infinity controller for the robust stability of a system, the system transfer function should be identified.

The classical feedback system structure establishes in general that weighing various loop signals in a way is determined by the design specifications. The identified SEC model with different weight functions for designing an H-infinity controller is shown in Figure 4.39. P is indicated for the system model transfer function. The transfer function F is the desired output of the system response with the closed loop. We is the gain of the loop from input to the error y-yf to be of the order 0.001 (tolerance) in the low-frequency range. Wu used to Implement specifications on the controller output, such as limiting the magnitude of the high-frequency component to ensure attenuation of a high-frequency component.

After obtaining the H-infinity controller, the system response with the H-infinity controller and the classical controller, which is designed using Fortran language, is compared. The tested scenario is the WADC via exciters in only WestJ plant, which are 4 machines. The results are shown in Figure 4.40 and Figure 4.41, comparing the two controllers after line fault and 680 MW generation trip, respectively. It can be clearly noticed that the damping of the dominant mode is improved with the classical controller and improved further with the H-infinity controller.

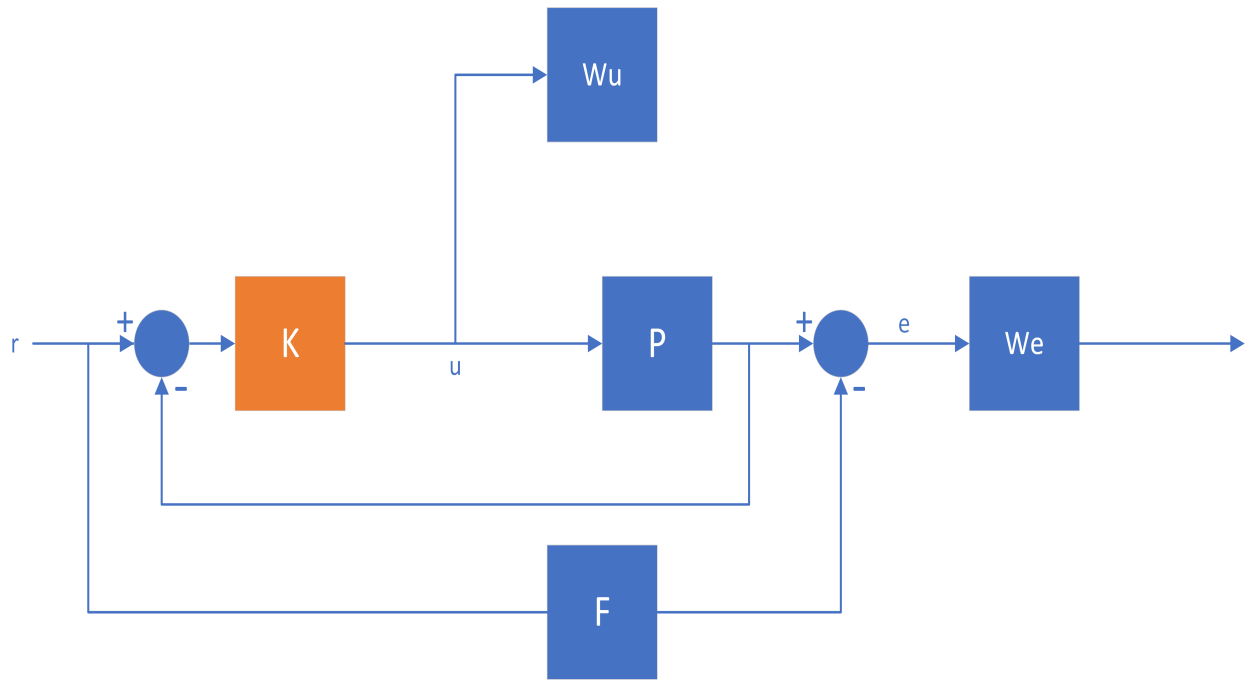


**Figure 4.39:** Hinf Control structure.

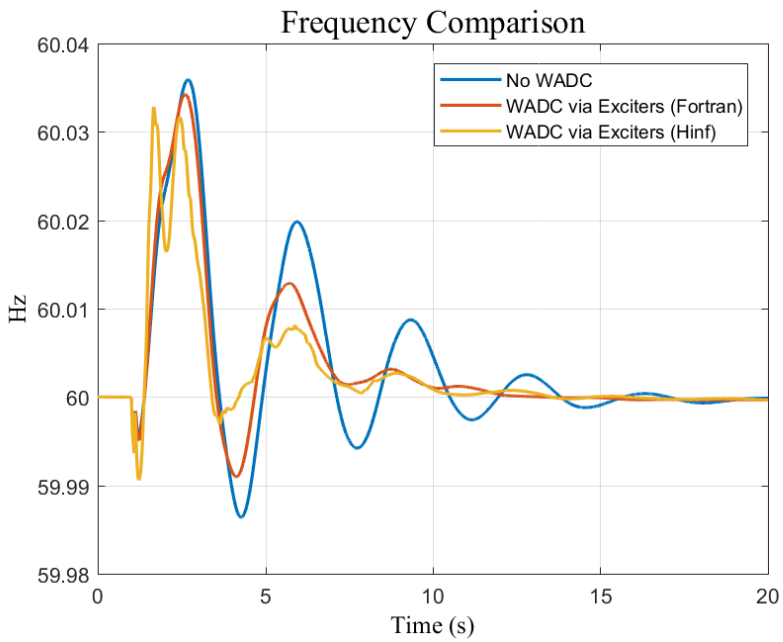


**(a)** Frequency response

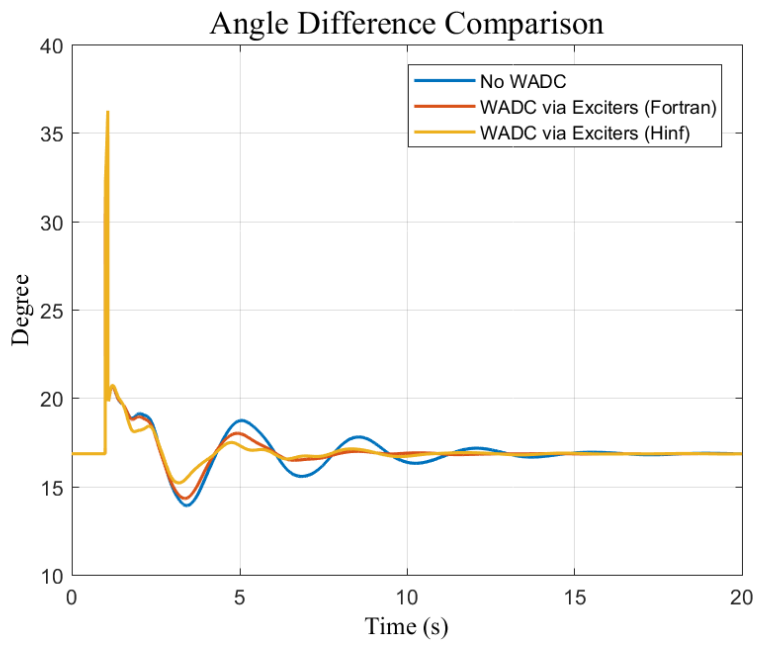


**(b)** Voltage angle difference

**Figure 4.40:** System response with H-infinity controller after line fault.

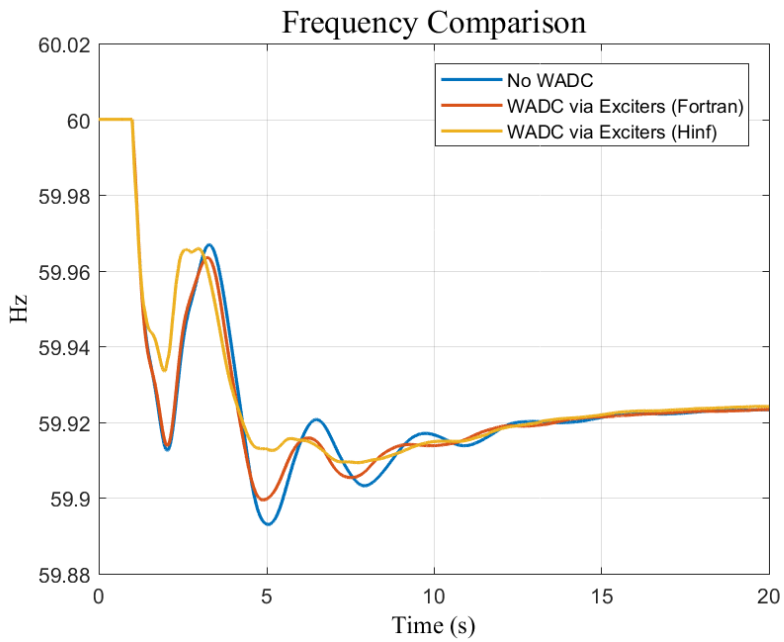


**(a)** Frequency response

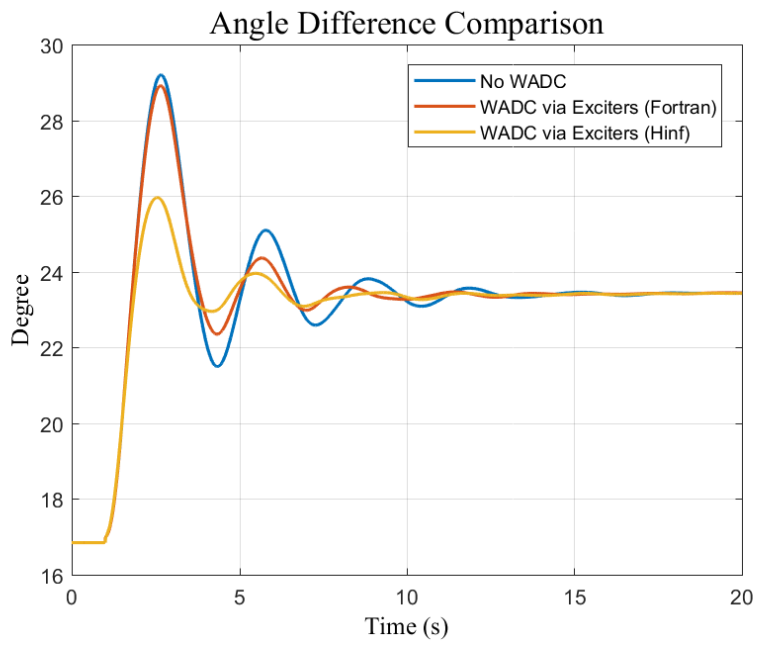


**(b)** Voltage angle difference

**Figure 4.41:** System response with H-infinity controller after generation trip (680 MW).

## 4.6 Summary

This chapter investigated the impact of multiple WADCs using a measurement-driven approach on the SEC grid's stability. Multiple WADCs using a measurement-driven transfer function model were tested to improve SEC's small-signal stability and transient stability by PSSE simulations. The optimal observation signals, as well as actuators, were selected. The frequency difference between the optimal observation buses in the western area and the central area was selected as the WADC input signal for the target oscillation mode. Also, the optimal observation bus in the western area is an alternative since it is the optimal observation bus for the whole SEC system. The WADCs could provide supplementary control via selected generator exciters and governors. The optimal generator exciters and governors to executes WADC control commands were selected using two methods. The first method was based on the frequency response of the optimal observation bus to a down step. A higher magnitude means higher controllability of the corresponding generator exciter or governor. The other method was based on the calculated residue magnitudes from the identified transfer function models. After the transfer function models are identified, the residue magnitudes of the models are compared. The measurement-driven approach was used to design the WADC. WADCs via selected generator exciters and governors can improve the damping ratio of the target oscillation mode. The simulation results validated the effectiveness of the measurement-driven WADC design approach. Meanwhile, multiple WADCs can prevent the system from separating under large-generation trip events and improve the SEC system major tie line transfer limit. The WADC via HVDC was tested. The simulation results validated the effectiveness of the WADC via HVDC to improve the damping ratio of the target oscillation mode. Also, the marginal generation trip in the western area and the transfer limit of the SEC system major tie line are improved when WADC is activated on the HVDC. Finally, two paths are investigated in order to achieve a better controller performance. The first is to improve the used controller's performance, which is the design used in this dissertation. The other is to design a robust controller using H-infinity.

# Chapter 5

# Implementation of the WADC using Real Time Simulator (RTS) and Hardware-In-the-Loop (HIL) testing

## 5.1 Introduction

Real-Time Simulators (RTSs) have been broadly used for testing and validating equipment before installation into real systems [106, 107]. One of the main challenges of these simulations is the limited modeling capacity which presents difficulties in modeling large power systems. The power system models are normally large and must be reduced to be modeled in the RTS. Therefore, reducing the size of the power system model is essential for accurate simulations [108]. One alternative method for simulating a larger power system is to use co-simulation between a RTS and a Transient Stability (TS) software. Consequently, the full size of the system can be simulated while maintaining simulation accuracy. A hybrid simulation using RTS and TS software was introduced in [109, 110].

Aiming at future field implementation and demonstration of the WADC, the work in this chapter focus on testing the WADC for the pure RTDS model and hybrid TSAT-RTDS model.

The chapter comprise of SEC pure RTDS model development for the model reduction of the full SEC model and the development and testing of the WADC with the associated pure RTDS model are presented. Moreover,the full SEC system is modeled using hybrid TSAT-RTDS model due to the difficulty to emulate the full model on RTDS. The implementation of the WADC on a generic-purpose hardware platform is presented. The developed WADC is tested on the HIL test setup under different conditions, including constant/random time delay, random/consecutive data package loss.

## 5.2 SEC pure RTDS model development

The impacts of WADCs on system transient stability are investigated, including system separation prevention under large disturbances and tie-line power transfer limit enhancement with consideration of a three-phase fault on one of the two tie-lines. The full Saudi power grid model in PSS/e is reduced for the real-time simulation on the Real-Time Digital Simulator (RTDS). The RTDS model is validated by comparison with the full PSS/e model and the reduced PSS/e model under different contingencies. The system separation prevention and tie-line power transfer limit by these WADCs are demonstrated by the real-time simulations on the RTDS.

The Saudi power grid model was originally built in the PSS/e tool, which could represent the system operating condition. However, it is difficult to emulate the entire model on the RTDS due to the model size in PSS/e (full model). Therefore, the full model is significantly reduced while preserving its main dynamic features, including the dominant oscillation mode and system separation after a large amount of generation trip. Moreover, the generator units in three selected power plants are preserved to execute WADCs' control commands as the actuators. This section introduces the model reduction using DYNRED, a dynamic reduction tool provided by Powertech Labs Inc [111], and the development and validation of the RTDS model.

The procedure of the model reduction using DYNRED is illustrated in Figure 5.1. The model reduction criteria are determined to preserve the desired features and equipment of the system. Two criteria are used for this model reduction. One is to preserve the dominant oscillation mode of the system, and the other is to preserve the generators chosen as actuators based on the results of the optimal actuation signal selection [112].

The developed reduced PSS/e model can be converted into the RTDS model using the conversion tool in RTDS. The dynamic responses of the full PSS/e model, the reduced PSS/e model, and the RTDS model are compared under a single-generator trip disturbance. Figure 5.2 shows a comparison of the frequency response and the voltage angle difference of the both ends of the tie-lines in the three models after this single-generator trip disturbance. The developed RTDS model can preserve the dominant oscillation mode. Table 5.1 presents the Prony analysis of system frequency response after the single-generator trip disturbance in the three models. The oscillation frequency of the dominant mode in the full model is 0.314 Hz, which is almost the same compared to the reduced model and the RTDS model with 0.31 Hz and 0.308 Hz, respectively. Similarly, the damping ratio of the mode in all three models are close to each other.

Figure 5.3 shows the system response comparison among the three models after a three-generator trip disturbance. When a 2,040 MW generation trip disturbance occurs in the western area at 1 s, the system is separated into two islands in all three models at 2.6 s because of the operation of the out-of-step relays. Figure 5.3a shows the frequency response where the system separation occurred at 2.6 s and that is consistent in all the models. Moreover, the voltage angle difference between the western area and the central area is shown in Figure 5.3b. Please note that the angle difference in PSS/e could keep increasing after the system separation, while that in RTDS bounces between 180° and -180°. Therefore, the system separation after a large amount of generation trip in the western area can be preserved in the RTDS model as well.

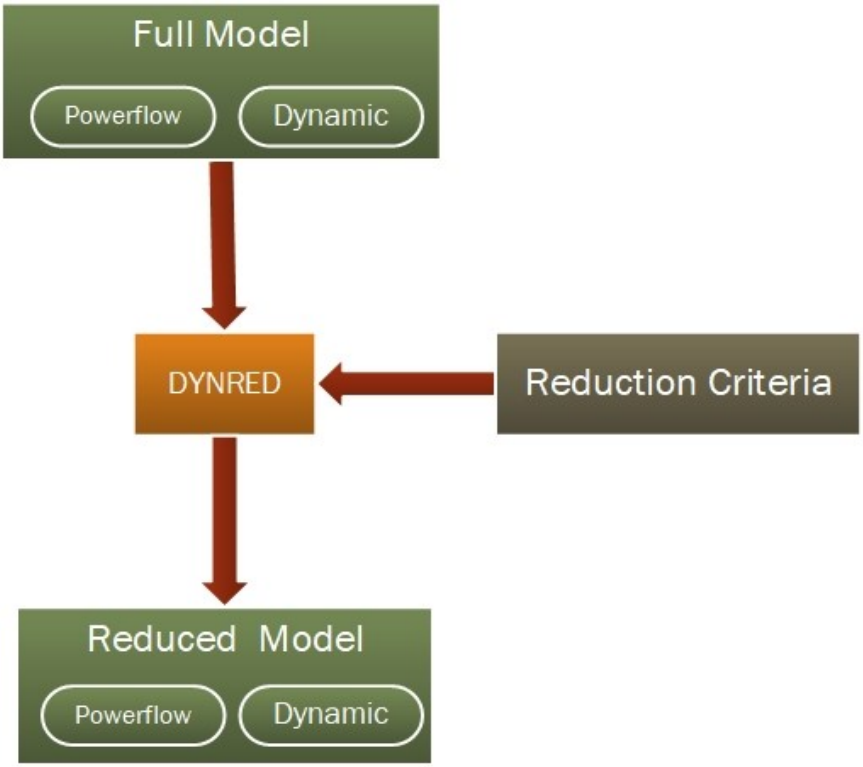


**Figure 5.1:** Model reduction using DYNRED. (Source: Powertech Labs Inc.)

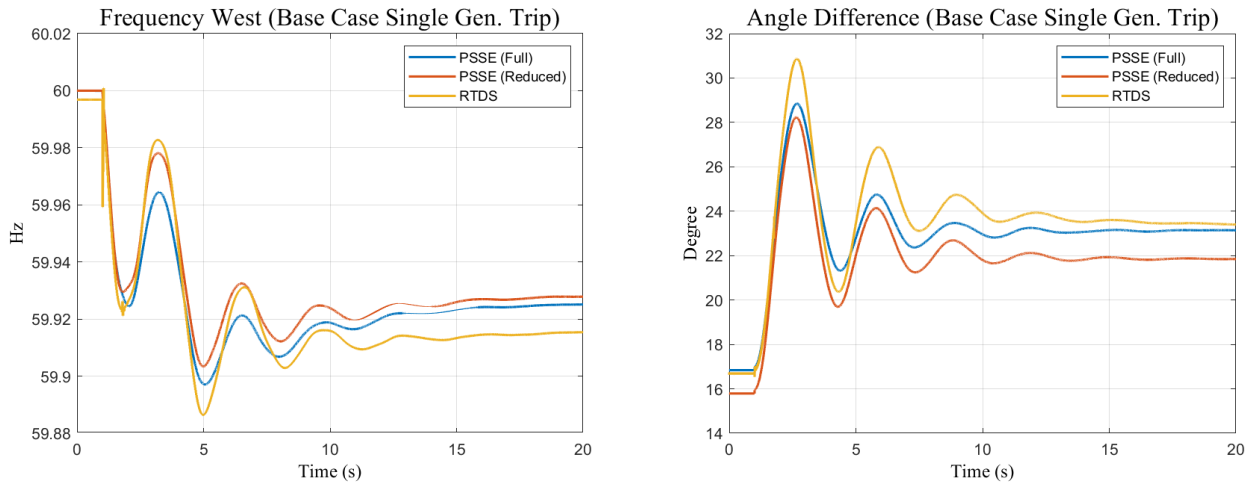


**(a)** Frequency response **(b)** Voltage angle difference

**Figure 5.2:** Models comparison after a single-generator trip (680 MW).

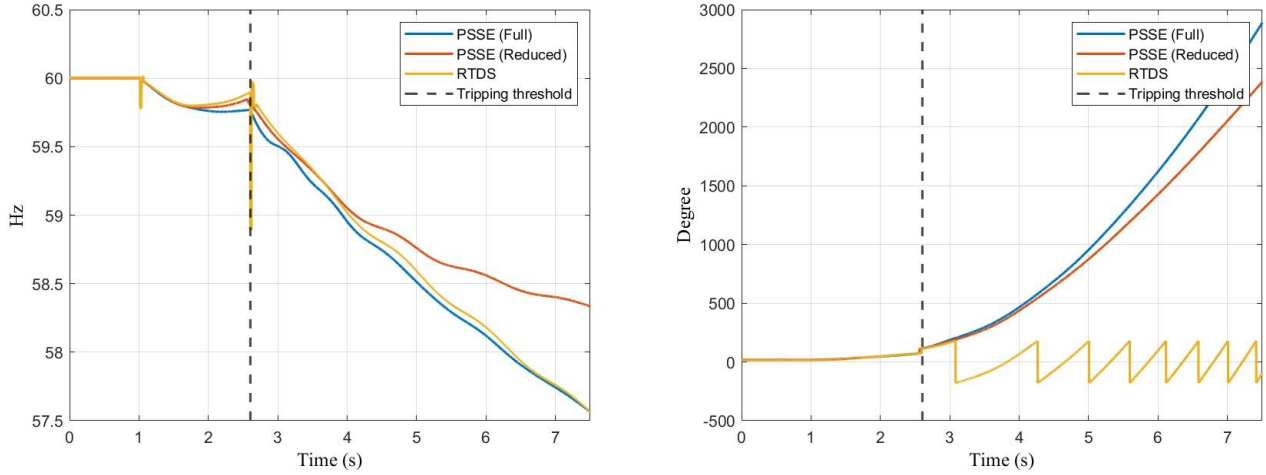


**(a)** Frequency response **(b)** Voltage angle difference

**Figure 5.3:** Models comparison after large generation trip (2,040 MW).

**Table 5.1:** Prony analysis of system responses in three models

| Case | Western & Southern v.s. Central & Eastern | |
|---|---|---|
| | Oscillation Freq. (Hz) | Damping (%) |
| Full PSS/e | 0.314 | 13.79 |
| Reduced PSS/e | 0.310 | 13.23 |
| RTDS | 0.308 | 11.13 |

### 5.2.1 WADC development in the pure RTDS model

The WADC is designed on the RTDS similar as on the PSS/e. Figure 5.4a shows the implementation of the WADC via exciter on the RTDS, which consists of a filter block, washout block, and two lead-lag structures. Similarly, Figure 5.4b shows the implementation of the WADC via governor on the RTDS, which consists of only a filter block and washout block.

Figure 5.5 shows one of the implemented WADCs in the RTDS model. The WADC output (WADC Exciter) is added into the voltage set point of the excitation system, while the WADC output (WADC Governor) is added to mechanical torque (TM) of the synchronous machine. In total, there are 11 WADCs via exciters and another 11 WADCs via governors in this RTDS model.

### 5.2.2 Performance of the WADCs using pure RTDS

The dynamic simulation results of the developed RTDS model with multiple WADCs are presented in this section. Two different contingencies are tested. One is the single-generator trip disturbance where the impact of WADCs on the dominant oscillation mode is studied, and the other one is the large generation trip in the western area to investigate the impact of WADCs on the system separation. Moreover, the impact of the WADC on the transfer limit of the tie-lines between the central area and the western area is studied.

#### Impact of WADCs on the dominant oscillation mode

The control effect of the 11 WADCs is verified in the RTDS model under a single-generator trip (680 MW) event when WADCs via exciters, governors, and exciters & governors are activated. The frequency response is presented in Figure 5.6a and the angle difference between the west and central is shown in Figure 5.6b. It is evident that the damping ratio of the dominant oscillation mode is further improved when the WADCs are activated on the exciters or governors. Also, when the WADCs are activated on both exciters and governors, the best performance is achieved.

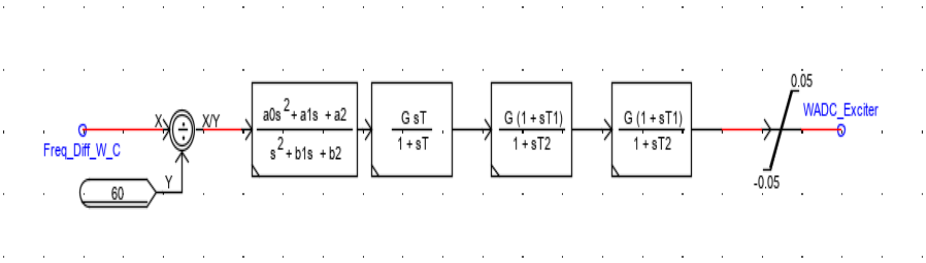


**(a)** WADC via exciters

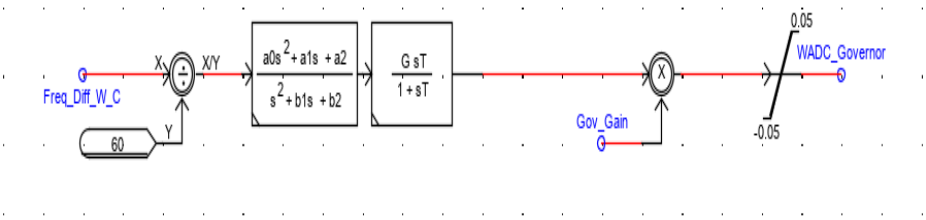


**(b)** WADC via governors

**Figure 5.4:** WADC block diagram.

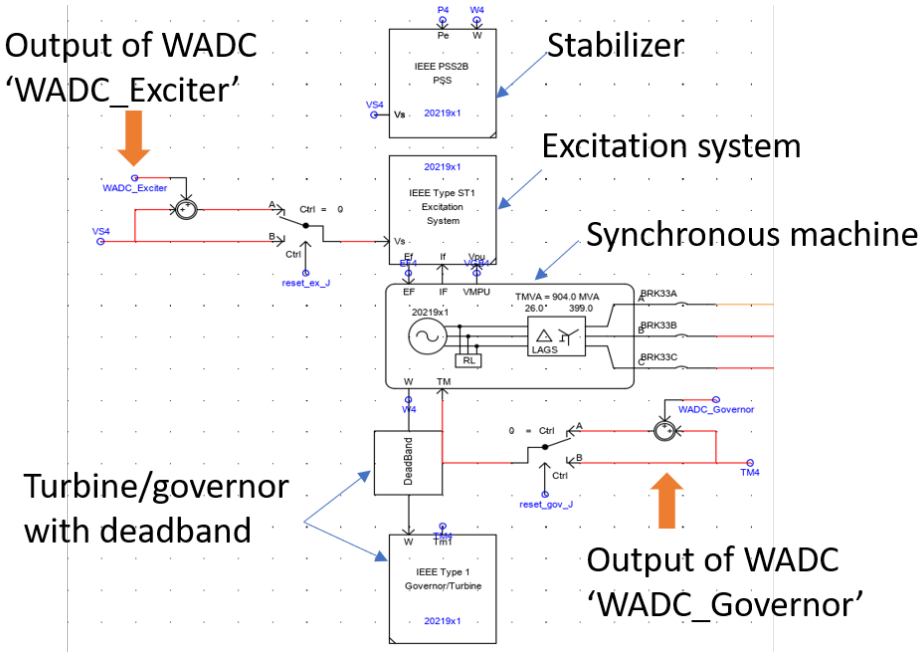


**Figure 5.5:** WADCs via Exciters and Governors on RTDS.

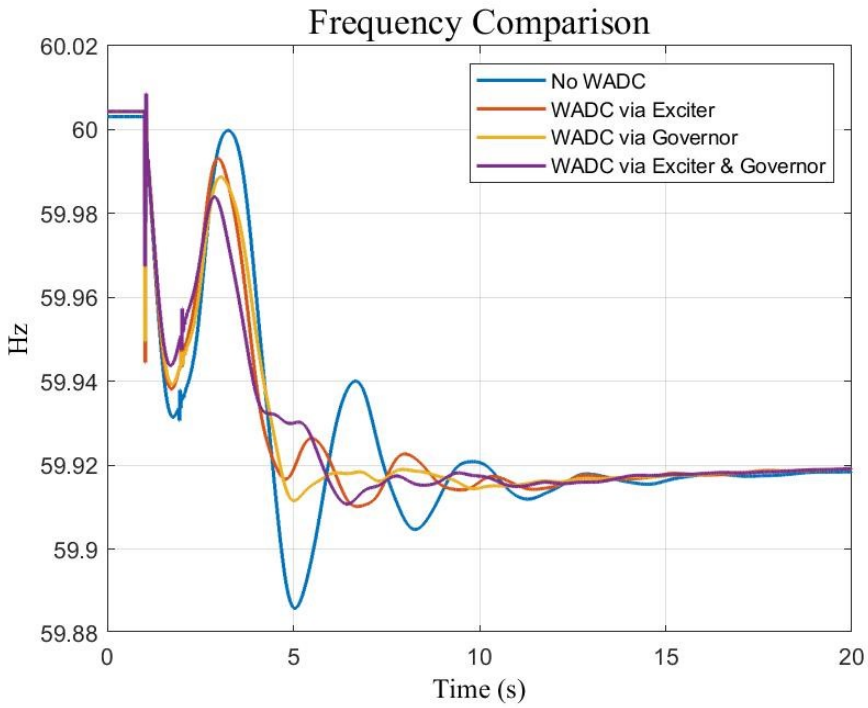


**(a)** Frequency response

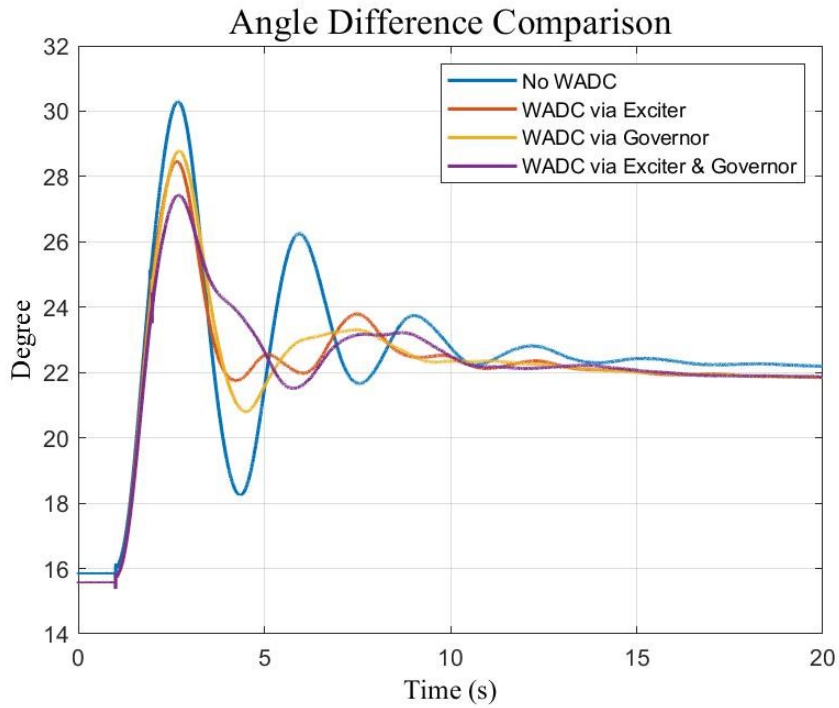


**(b)** Voltage angle difference

**Figure 5.6:** WADC performance after a single-generator trip (pure RTDS).

### Impact of WADCs on system separation

System separation could happen in the Saudi power grid when a large amount of generation trip happens in the western area simultaneously. The designed WADCs can be used to prevent this system separation. In the case of 2,040 MW generation trip in WestJ plant, the system separation can be prevented if eight WADCs via governors and exciters are activated (one unit in WestJ plant, four units in WestR plant, and three units in the Southern plant).

The results in the three models are consistent in the case of three generator trip in WestJ. Figure 5.7b shows the voltage angle difference between two ends of the tie-lines and Figure 5.7a the bus frequency in the western area with and without WADCs after 2,040 MW generation trip in WestJ plant. Without these WADCs, the frequency response of No WADC case and WADC via exciters and governors are compared in Figure 5.7b. From these figures, it is evident that WADCs could prevent system separation after this large generation trip in the studied system.

### Impact of the WADC on tieline transfer limit

The impact of WADCs on the transfer limit of the major tie-lines between the western area and the central area is also studied. The tie-line power flow is increased by increasing one selected load in the western area and decreasing one selected load in the central area. A temporary three-phase fault is applied on one of the tie-lines followed by tripping the faulted tie-line after 80 ms. The tie-line power can be increased step by step.

The transfer limit is determined based on the maximum pre-disturbance power flow for which the system is still connected after the disturbance. Table 5.2 presents the tie-line transfer limit with and without multiple WADCs for the three models. With the 11 WADCs via governors, the tie-line power transfer limit can be increased in all three models. Figure 5.8 visualize the cases that presented in Table 5.2.

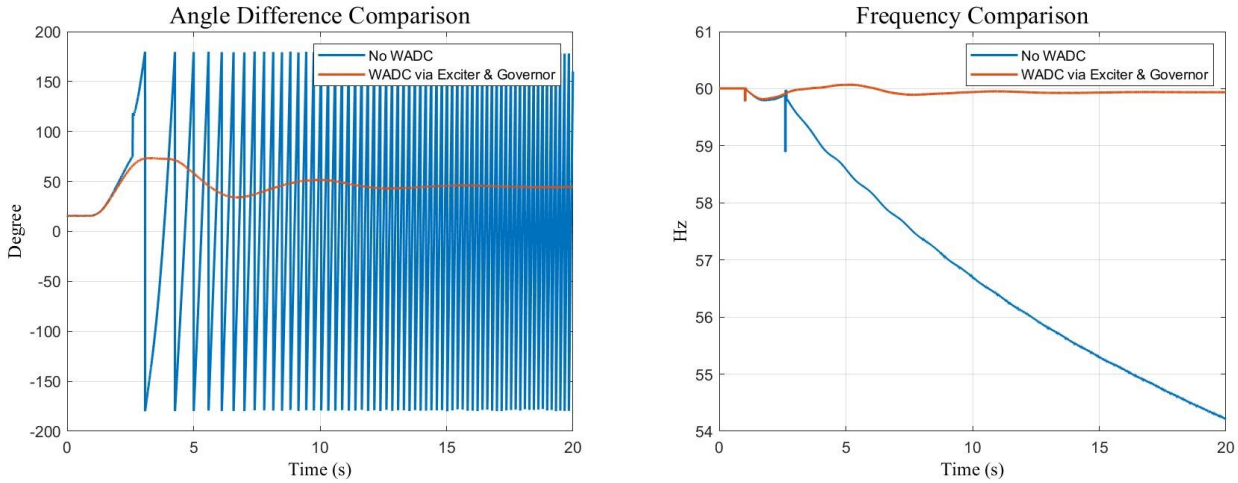


**(a)** Frequency response

**(b)** Voltage angle difference

**Figure 5.7:** System response after large generation trip 2040 MW(pure RTDS).

**Table 5.2:** Active power transfer limit With WADCs For the three models

| Actuator | Model | Transfer limit Single-Circuit (MW) | Transfer limit Double-Circuit (MW) |
|---|---|---|---|
| No WADCs | PSS/e (Full) | 1008.5 | 2017 |
| | PSS/e (Reduced) | 988.3 | 1976.6 |
| | RTDS | 839.2 | 1678.4 |
| 11 Exciters | PSS/e (Full) | 1014.5 | 2029 |
| | PSS/e (Reduced) | 1005.1 | 2010.2 |
| | RTDS | 855.8 | 1711.6 |
| 11 Governors | PSS/e (Full) | 1025.6 | 2051.2 |
| | PSS/e (Reduced) | 1010.7 | 2021.4 |
| | RTDS | 863.5 | 1727 |
| 11 Exciters & Governors | PSS/e (Full) | 1029.3 | 2058.6 |
| | PSS/e (Reduced) | 1012.7 | 2025.4 |
| | RTDS | 870.8 | 1741.6 |

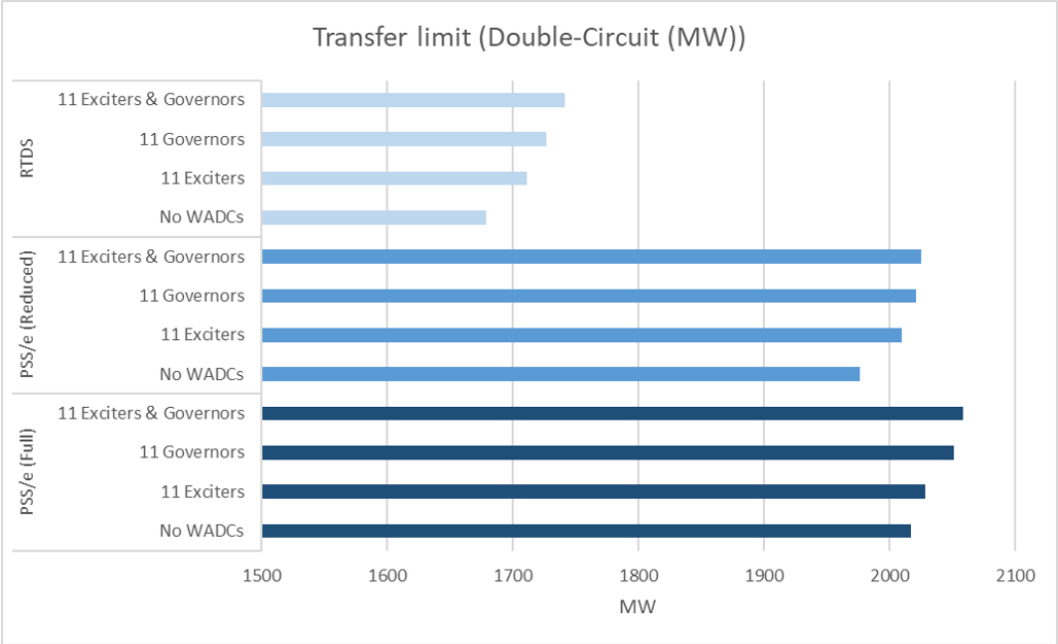


**Figure 5.8:** Transfer limit of the major tieline for the three models.

## 5.3 SEC hybrid TSAT-RTDS model development

Controllers for power systems should be tested adequately in order to verify their applicability and effectiveness before they are installed into the real system [113]. This need introduces the importance of Hardware-In-the-loop testing with a real time simulator to validate the designed controller before installation in the real system. HIL with real-time simulators can be used to test real equipment such as prototypes, protection hardware, power hardware and control devices [106]. The aim is to evaluate the WADC performance under realistic operating conditions including communication uncertainties and measurement error. The CompactRIO system was used to implement the WADC. The CompactRIO system is a general-purpose controller provided by National Instruments (NI) for prototyping [114]. Using the hybrid TSAT-RTDS simulation described before, a HIL testing platform was built to imitate realistic conditions with several communication network uncertainties and impairments. The hardware WADC was tested in the HIL setup, where several auxiliary function modules were implemented within the WADC. The WADC was validated during testing to ensure satisfactory performance under realistic operating conditions.

The hybrid simulation process can be accomplished by dividing the whole system into two subsystems: the internal system, which is the study subsystem, and the external system, which comprises the rest of the system [108]. The study subsystem is the part of the whole system that is the focus of research. The external subsystem is the rest of the whole system, which is usually much larger but demands much fewer modifications during simulations. The efficiency and accuracy of the hybrid simulation depend critically on the performance of the interface between the internal and external subsystems [115, 109, 110]. Therefore, most of the literature about hybrid simulation focuses on designing the interface between RTS and TS subsystems. In this work the TSAT-RTDS hybrid tool has been used that incorporates both the RTDS simulator and the transient simulation program (TSAT) (Powertech Labs) to perform real-time dynamic simulation of a large power system [116].

The studied power system is divided into two regions connected through a set of boundaries known as the TSAT-RTDS Interface (TRI). The overall structure of a TSAT-RTDS hybrid simulation study is shown in Figure 5.9.

The TSAT-RTDS Interface (TRI) component needs to be added to each boundary between internal (RTDS) and external (TSAT) systems [116]. This component exchanges two signals with TSAT through the GTFPGA block, and therefore, two consecutive ports should be reserved for each TRI. TSAT simulates the external system at a time step of 5 ms, and RTDS simulates the internal system at a time step of 50 us. Therefore, the boundary injections are exchanged at the end of every TSAT time-step. In the RTDS model, TRI inputs/outputs are connected to GTFPGA, and the Start Signal is used in the RTDS model to send a start signal to TSAT. This signal should be connected to every TRI as an input.

The Saudi Electricity Company (SEC) grid is developed using TSAT-RTDS hybrid model. SEC system is divided into two subsystems connected through five boundaries known as the TSAT-RTDS Interface (TRI), as shown in Figure 5.10. The studied subsystem consists of three plants used as WADC actuators and the major tie-line of SEC system. Each plant needs one TRI, as shown in Figure 5.10a, while the major tie-line required two TRI, as shown in Figure 5.10b. On the other hand, the rest part of the system, which is the larger part, is modeled and simulated in TSAT software.

The developed TSAT-RTDS hybrid and the full PSS/e model are compared for a single-generator trip event. Figure 5.11 shows a comparison of the frequency response during this single-generation trip event where the deadband models are not added during this comparison. The developed TSAT-RTDS hybrid model result is very close to exhibiting the full model dynamic response.

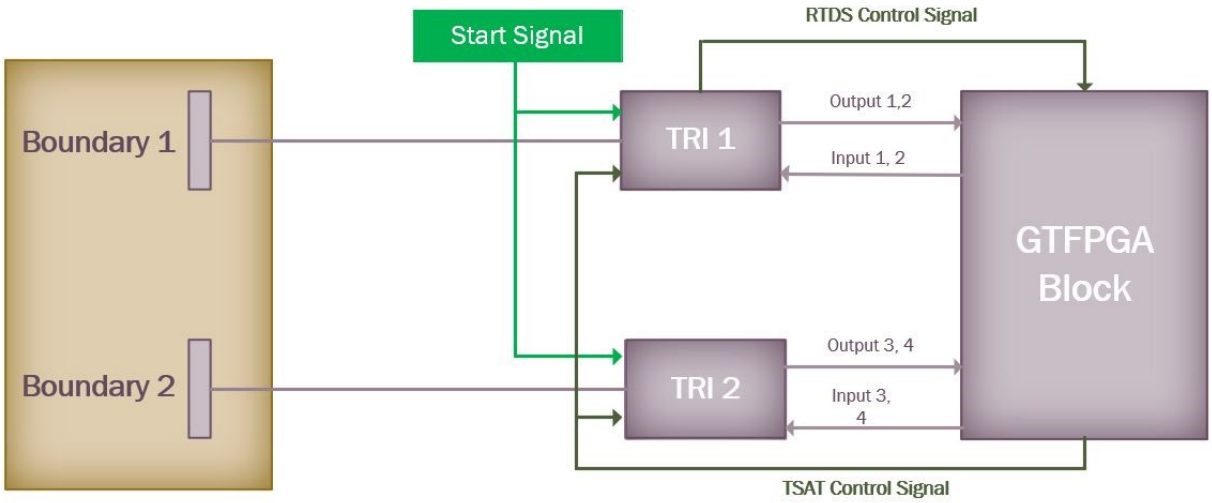


**Figure 5.9:** Hybrid TSAT-RTDS simulation overview. (Source: RTDS).

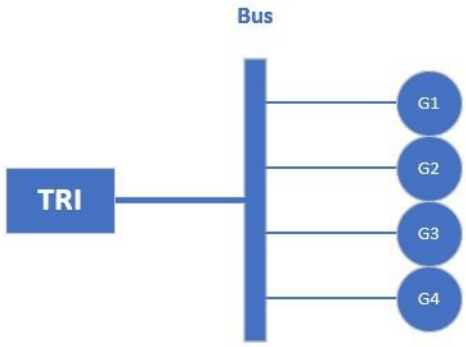


**(a)** Plant model using TRI

**(b)** Tie-line model using TRI

**Figure 5.10:** TRI links for hybrid simulation.

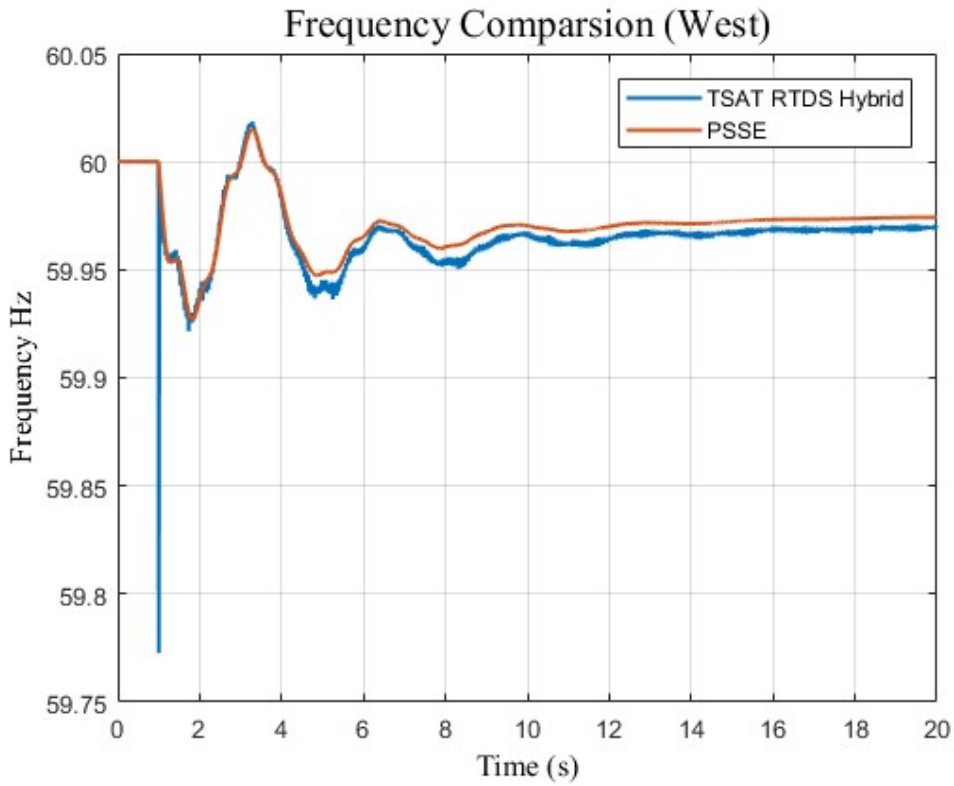


**Figure 5.11:** Frequency response comparison of TSAT-RTDS hybrid and the full PSSE model during a single generation trip.

### 5.3.1 WADC development through Hardware-In-the-Loop

As illustrated in Figure 5.12, the HIL test setup consists of a hybrid TSAT-RTDS real-time simulator, amplifiers, Phasor Measurement Units (PMUs), a network switch, a communication network impairment simulator, and the WADC under test. The Saudi power grid model is emulated in this hybrid TSAT-RTDS real-time simulator. Moreover, the RTDS can generate PMU streaming data using its virtual PMU function. In this work, the hybrid TSAT-RTDS simulation is used as the real-time simulator to validate the controller performance. The hybrid TSAT-RTDS simulation performs co-simulation of electromechanical transient and electromagnetic transient through the TSAT RTDS Interface (TRI) in a real-time manner. Since the vast majority of the system can be modeled in the TSAT for electromechanical transient simulation, the co-simulation can handle the real-time simulation of systems of more than 5000 buses, without model reduction [116].

The power grid model is divided into two subsystems connected through boundary branches. One subsystem is modeled in the RTDS, including the main plants that are used as WADC actuators and the two tie-lines between the western area and the central area. The other subsystem contains the rest of the system, which is modeled in TSAT. The RTDS converts the digital simulation results, e.g., voltage measurements, into analog voltage waveform in real-time using its Giga-Transceiver Analog Output (GTAO) card, as shown in Figure 5.13. The GTAO converts the selected measurements to analog waveforms and then sends them to the amplifiers. The Giga-Transceiver Analog Input (GTAI) card receives the control command from the WADC and converts it to a digital signal, and then injects it into the actuator in the RTDS model. As shown in Figure 5.13, two analog output signals are used, which are the voltage waveform of two selected buses. The analog outputs are connected to amplifiers where the voltage is stepped up from 10 V to 120 V. The two PMUs calculate the frequency of the selected bus voltage measurements and send them to the WADC in the form of data packages compliant with the IEEE C37.118 standard. There is a communication network impairment simulator that processes the data packages before arriving at the controller. This is to emulate communication uncertainties such as random or constant time delay, occasional or consecutive data loss, etc.

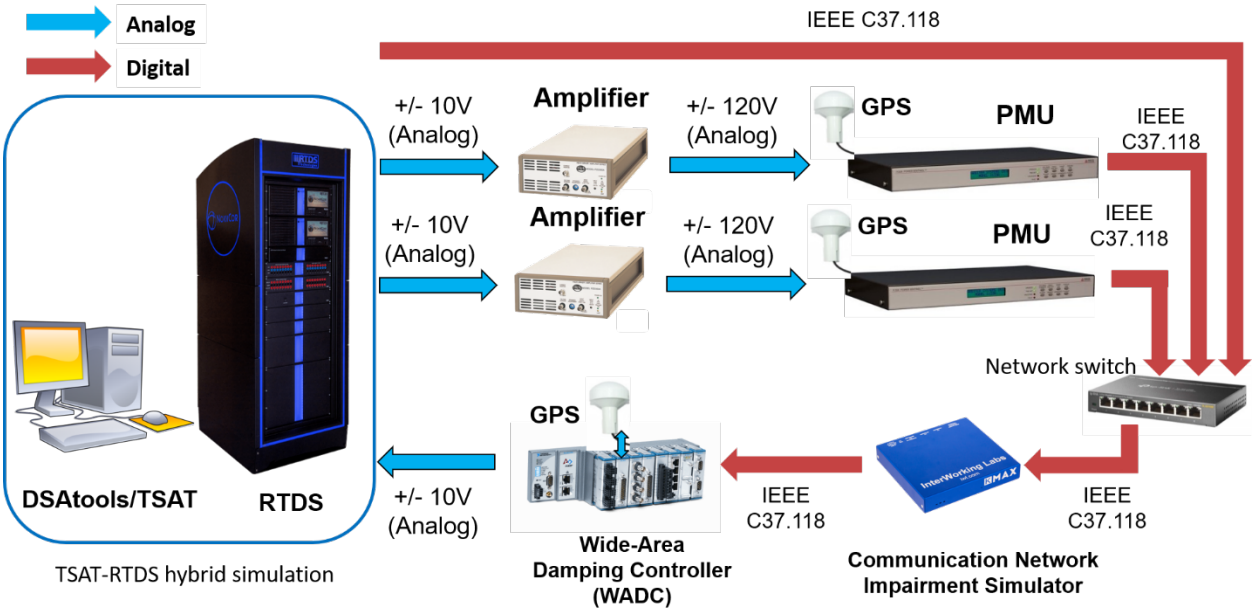


**Figure 5.12:** HIL test setup based on hybrid TSAT-RTDS simulation.

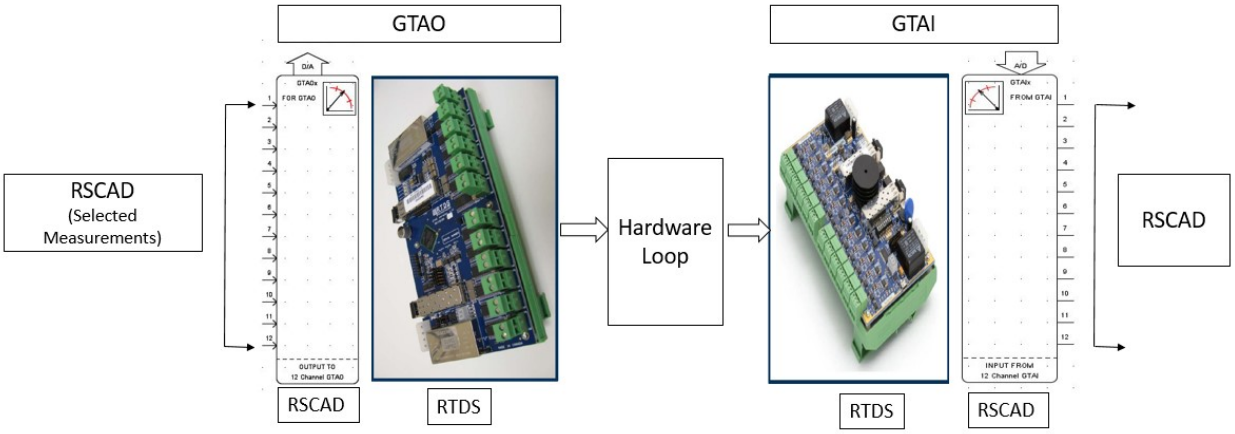


**Figure 5.13:** Analogue Input Output of RTDS (Picture source: RTDS).

The output signals of the WADC are converted to 10 V analog signals that can be accepted by the input ports of the RTDS, where they will be sent to be injected to the actuators in the RTDS model. In this work, the exciter and governor at three plants are selected as the actuators, and the frequency difference between the western area and the central area is used as the feedback signal. Moreover, the RTDS virtual PMU is used as a backup for supervisory control. The Giga-Transceiver Network Communication (GTNET) card is used to generate the virtual PMU streaming data. Figure 5.13 shows the draft component that is used in the RTDS simulations. The PMU firmware option for the GTNET provides synchrophasor output data streams according to the IEEE C37.118 standard.

The WADC is implemented on real-time control platform manufactured by National Instruments, CompactRIO system, where LabVIEW is used as the programming language [117]. This section presents all the blocks that are implemented on CompactRIO 9035 [118]. The overall structure of the WADC is shown in Figure 5.14. The WADC consists of the following: PMU data receiver module, GPS module, delay detector module, lead-lag structure module, supervisory control module, delay compensator module, missing data handling module, oscillation detector module, and D/A conversion module.

**PMU Data Receiver**

The PMU data receiver is a block used to communicate with all the PMUs (both the real PMUs inside the HIL and the virtual PMU in the RTDS) through the phasor measurement communication protocol IEEE C37.118-2011. The PMU data receiver block is based on BabelFish, an open-source real-time data mediator [119]. Some modifications are made to the BabelFish receiver to adapt it for User Datagram Protocol (UDP) since the WADC requires timely measurement updates and is tolerant to occasional data loss. Therefore, the WADC moves on to the latest package available when some packages are lost.

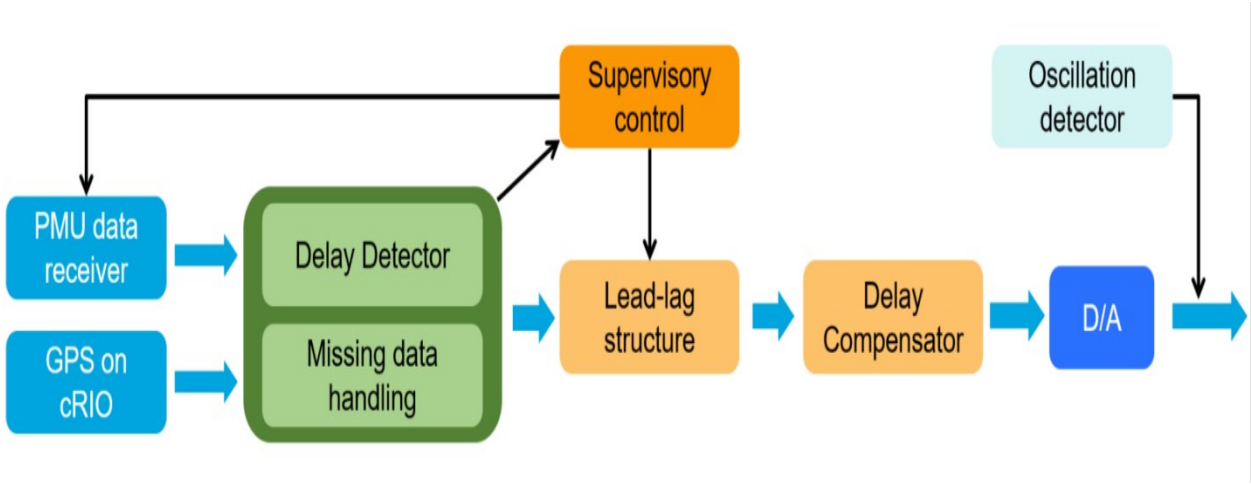


**Figure 5.14:** Overall structure of the controller.

### GPS Module

The GPS module is utilized to obtain the GPS signal with an absolute timestamp. The GPS extension board NI-9467 is used on the CompactRIO to accurately measure the communication delay between the PMUs and the WADC [120]. The WADC requires higher resolution for synchronization than the pulse per second (PPS) signal provided by the NI-9467. Therefore, the FPGA module is used to divide the PPS signal and create accurate timestamps for the WADC.

### Delay Detector

The delay detector is used to obtain the actual delay from the moment the measurement is taken to the moment the controller uses it. This function shares the measured delay with the supervisory control and the delay compensator block for further processing and control. An additional random delay is expected in the communication links in the HIL test environment. If not properly compensated, the delay may cause a phase shift in the WADC output, leading to deterioration in the WADC performance. To compensate for the communication delay, the actual delay of the measurements is used to generate control signals that must first be determined in real-time. Then, by comparing the timestamps at both the PMUs and the WADC, the actual delay can be determined as follows:

$$T_d = t_{PMU} - t_{cRIO} \tag{5.1}$$

### Missing Data Handling

The missing data handling module controls situations when permanent or temporary data loss occurs, resulting from data drops or short-term congestions in the network, respectively. The data packages are stored according to their measurement timestamp inside the module, as shown in Figure D.1 in Appendix A. When data packages are lost or delayed, the module will scan the latest data package in the buffer and engage the delay compensator and detector modules to continuously manage the control commands. Furthermore, the missing data handling module coordinates with the supervisory control module to switch the PMU channels when the data loss continues beyond a specific period.

### Delay Compensation

The delay compensator module monitors the actual delay of the data packages and then determines the optimal parameters to compensate for the delay. The buffer holds all data packages that arrived at the WADC and sorts them based on their delays as calculated by the delay detector, as shown in Figure 5.15. The data packages that are closest to the predefined delay are always used for generating control commands. Therefore, the WADC does not frequently switch among different compensation parameter sets.

### Supervisory Control

The supervisory control module continually monitors all the PMU channels' data and generates control commands to handle the communication links' uncertainties. To minimize the impact of communication delay, the supervisory control module will shift to the backup PMU channel when the primary (default) PMU channel delay is consistently larger than 1 second. When the primary PMU channel returns to regular operation, the controller will wait for a few seconds to guarantee its reliability and then switch back.

### Lead-lag Structure

The lead-lag structure block is used to implement the transfer function of the WADC, which is implement in discrete time.

### Oscillation Detector

The oscillation detector module is designed to continually monitor the system's oscillation and determine when the WADC is activated or not.

### Digital/Analoge Conversion

The D/A module converts the digital output signal of the WADC to an analog signal, which is sent back into the RTDS to be injected into the selected actuator. The D/A extension board installed on the CompactRIO is the NI-9263, which has four analog voltage output channels with a sampling rate of 100 kS/s [121].

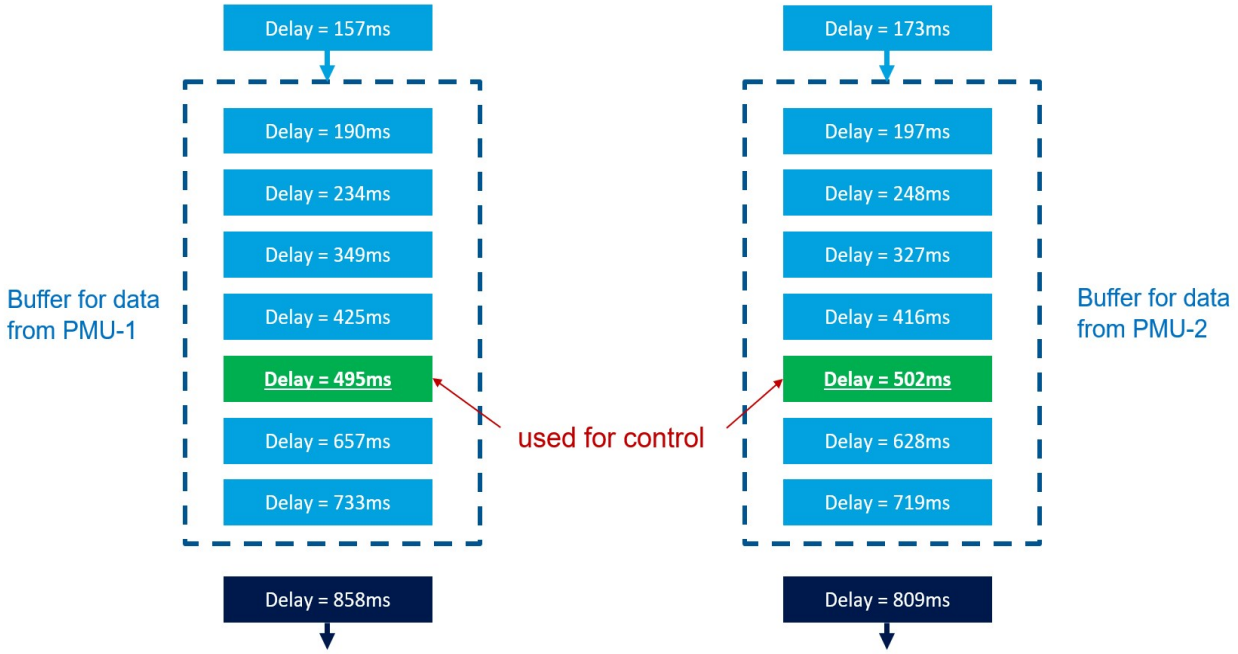


**Figure 5.15:** The delay compensator process.

### 5.3.2 Performance of the WADCs using HIL testing

The frequency difference between the western area and the central area is selected as the input signal of the WADCs. Meanwhile, the exciters and governors of generators in three selected power plants are used as the actuators. Two power plants are in the western area and one power plant in the southern area. Therefore, there are 11 WADCs that implemented on the CompactRIO. The test results of the developed WADCs on the HIL test setup are presented in this section with and without communication impairment.

#### Performance of the WADCs without Communication Impairment

In this section, the HIL test results of the hybrid TSAT-RTDS without communication impairment are presented. The communication network impairment simulator was bypassed to not introduce additional time delays and data drops. A single-generator trip is used as the disturbance to investigate the performance of WADCs via exciters and governors. Also, the system separation condition is studied when the system experiences a large generation trip. The performance of WADCs via exciters was first investigated. The dynamic responses after the single generator trip are shown in 5.16. Three cases are shown in Figure 5.16: no WADCs (blue), WADCs via exciters on RTDS (red), and WADCs via exciters on CompactRIO (yellow). With the WADCs, the damping of the target oscillation mode can be further improved. Also, the control effects are consistent when WADCs are implemented on RTDS (software controller) or CompactRIO (hardware controller). Figure 5.17 shows the control effect of WADCs via governors after the single-generator trip. The WADCs can improve the damping of the target oscillation mode, and the control effects are consistent when WADCs are implemented on RTDS (software controller) and CompactRIO (hardware controller).

The dynamic responses of the hybrid simulation model are evaluated when WADCs via eight exciters and eight governors are activated during a large generation trip of 2,040 MW. The frequency responses of the WADC/No WADC cases are compared in Figure 5.18a. Figure 5.18b shows the comparison of the angle difference between the west and central areas. As demonstrated in Figure 5.18, the WADC case can save the system from separation during a large generation trip.

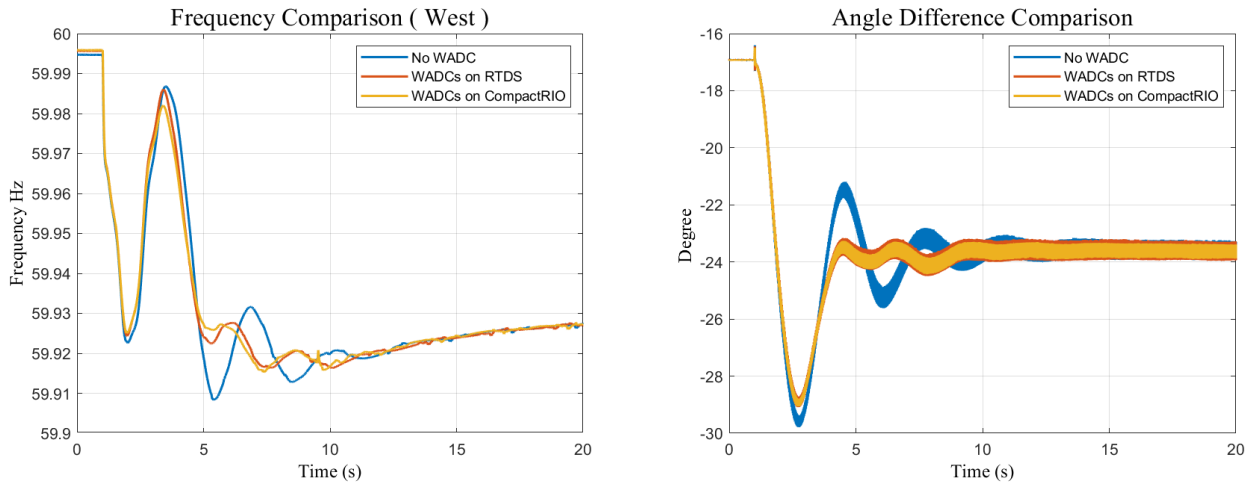


**(a)** Frequency response **(b)** Voltage angle difference

**Figure 5.16:** WADCs via exciters after single-generator trip (TSTA-RTDS Hybrid).

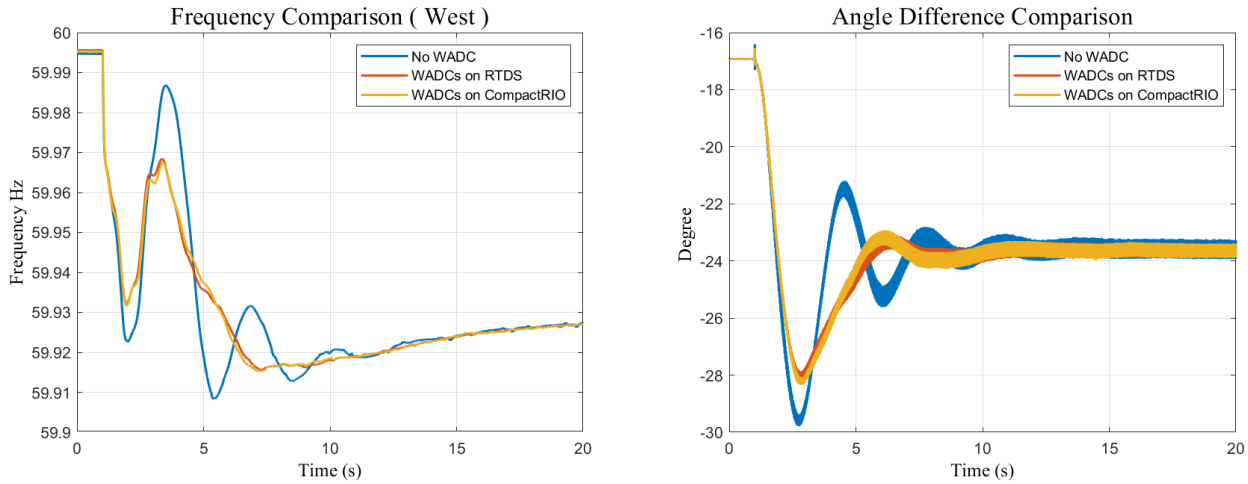


**(a)** Frequency response **(b)** Voltage angle difference

**Figure 5.17:** WADCs via governors after single-generator trip (TSTA-RTDS Hybrid).

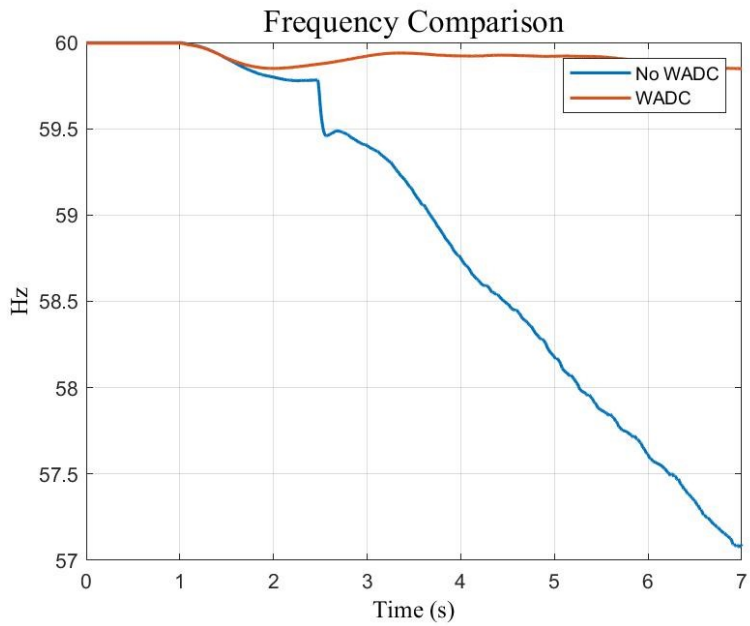


**(a)** Frequency response

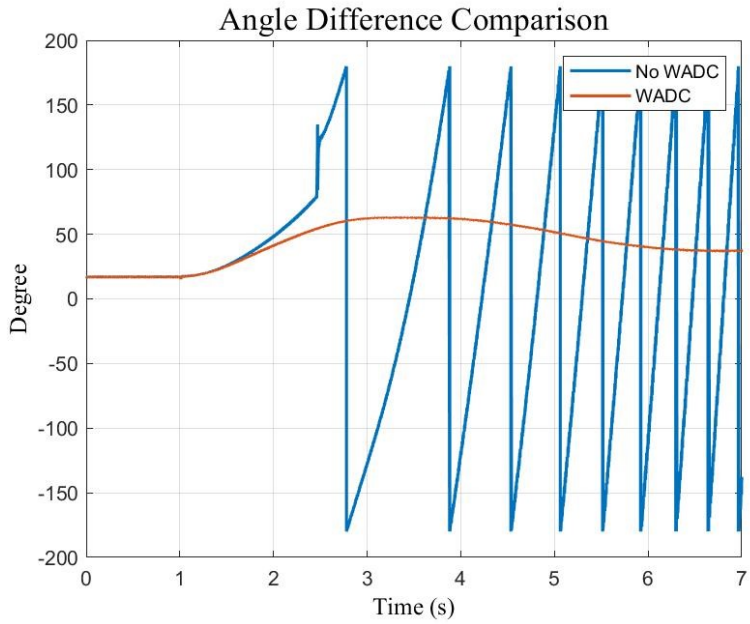


**(b)** Voltage angle difference

**Figure 5.18:** System response during large generation trip of 2040 MW (TSTA-RTDS Hybrid).

### Performance of the WADCs with Communication Impairment

This section presents the results of the WADCs as tested under different communication impairments. All the communication impairment scenarios use the WADCs via exciters during a single-generator trip disturbance.

### Constant Time Delay

The WADCs via exciters during a single-generator trip were tested when a constant time delay is applied to the communication impairment simulator without delay compensation in the controllers. The test results are shown in Figure 5.19a, which compares four cases: No WADCs (blue), WADCs via 10 exciters without delay (red), WADCs via 10 exciters with a 700 ms delay (yellow), and WADCs via 10 exciters with a 1000 ms delay (purple). When the time delay is not compensated, it could reduce the damping and excite the oscillation. However, when the delay compensation is activated, the negative impact of the time delay can be eliminated. Figure 5.19b presents the results after applying the delay compensator and demonstrates that the WADCs can provide sufficient damping. The control effect is similar to the WADCs without a time delay. Note that the parameters of the delay compensators were tuned for 700 ms or 1000 ms.

### Random Time Delay

The WADCs were further tested when a random time delay was introduced. The buffer-based delay compensator (introduced in Section 4) was used, and the buffer size was 500 ms. The mean values are 100 ms, 200 ms, 300 ms , and 700 ms in the four cases, and the standard deviation is 30 ms in all four cases. The test results of the six cases are presented in Figure 5.20. When the mean value of the time delay is less than the buffer size (500 ms), the control effect can be guaranteed under the random time delay. However, the control effect is not as good if the mean value of the time delay is larger than the buffer size of 500 ms.

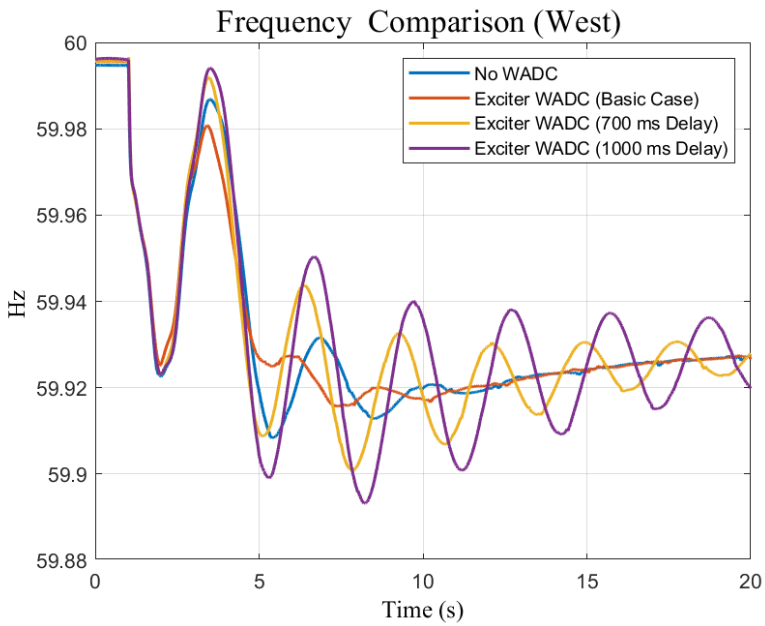


**(a)** Without delay compensation

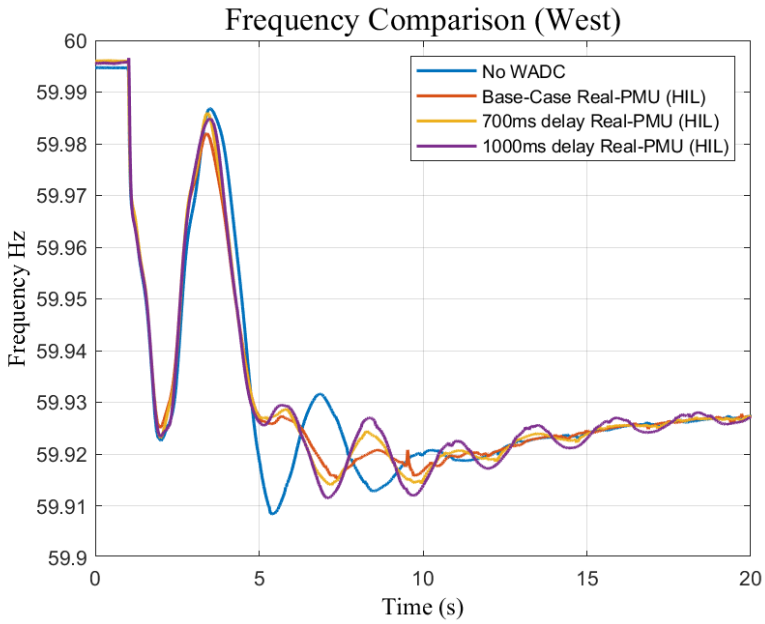


**(b)** With delay compensation

**Figure 5.19:** WADCs via exciters with constant delay during single-generator trip.

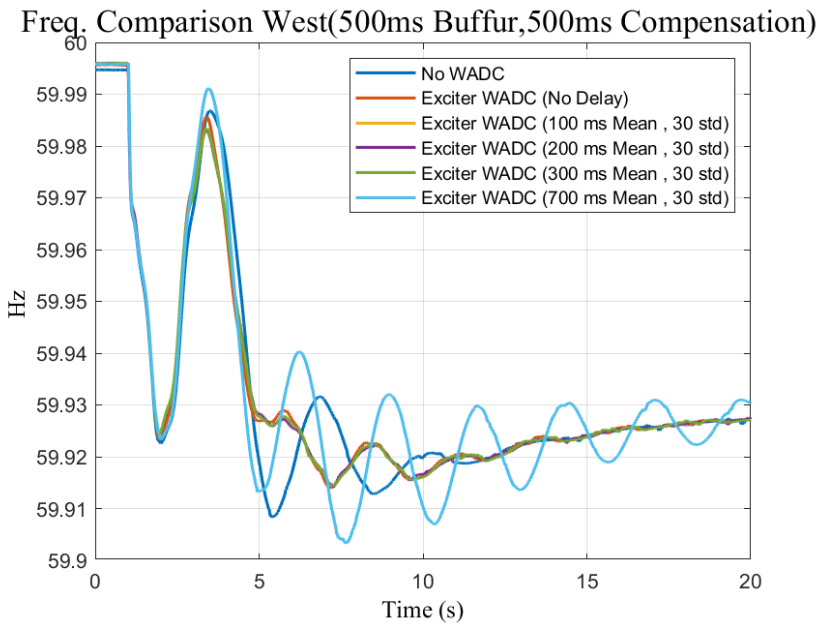


**(a)** Frequency response

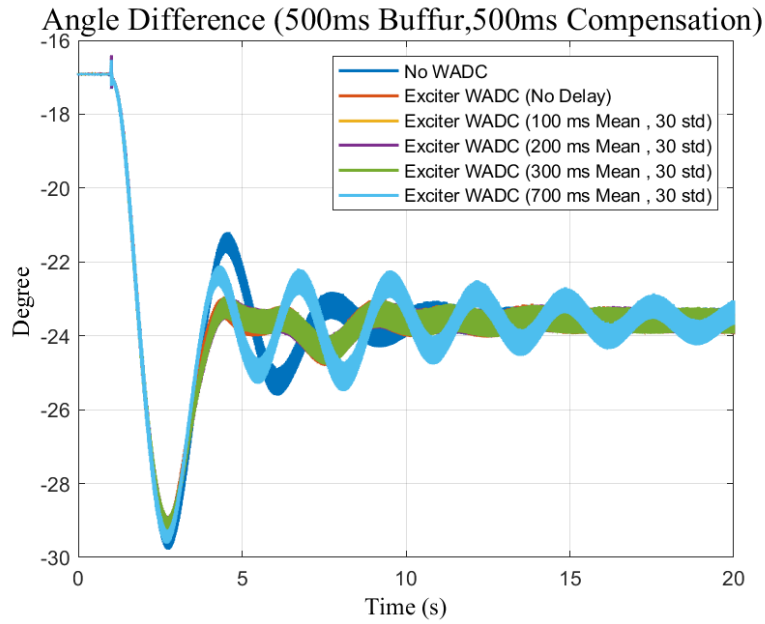


**(b)** Voltage angle difference

**Figure 5.20:** Control effect of WADCs via exciters with random time delay during single-generator trip.

### Random Time Delay and Occasional Data Drop

The WADCs were next tested under random time delay and occasional data drop conditions. The buffer-based delay compensator was used, and the buffer size was 500 ms. The test results are shown in Figure 5.21. When the data drop rate is 5%, 10%, or 50%, the WADCs can still provide sufficient damping. In the last two cases, the WADCs were verified under a random delay (100 ms mean value and 30 ms standard deviation) and data drop rate of 5% or 10%. The WADCs can provide sufficient damping to suppress the oscillation mode.

### Intolerable Time Delay with Supervisory Control

When the time delay is large, i.e., exceeds the buffer size, the controllers could not fully compensate for the time delay, resulting in a bad control effect. In this situation, the supervisory control module can switch the primary PMU to a backup PMU, allowing the controller to generate control commands based on the PMU measurements with better data quality. These test results are given in Figure 5.22. When the time delay is 1000 ms, if there is no supervisory control module, an oscillation with poor damping could appear. However, if the supervisory control module can switch to a backup PMU, the oscillation can be suppressed, and the control effect is similar to the case of no time delay.

### Consecutive Data Drop with Supervisory Control

Similarly, when consecutive data drops occur in the primary PMU, it is necessary to switch to a backup PMU to guarantee the control effect. The test results under consecutive data loss with and without the supervisory control module are compared in Figure 5.23. Again, with the supervisory control module, the control effect is guaranteed.

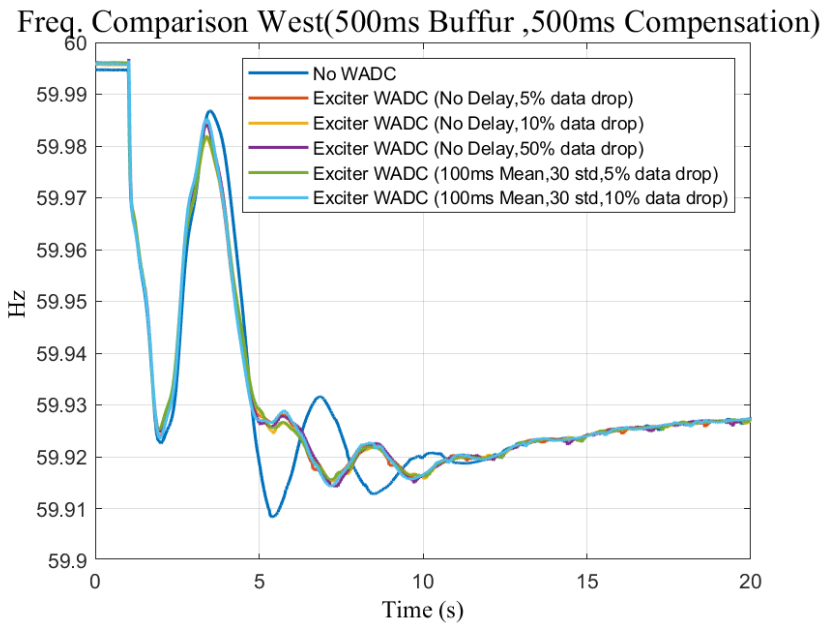


**(a)** Frequency response

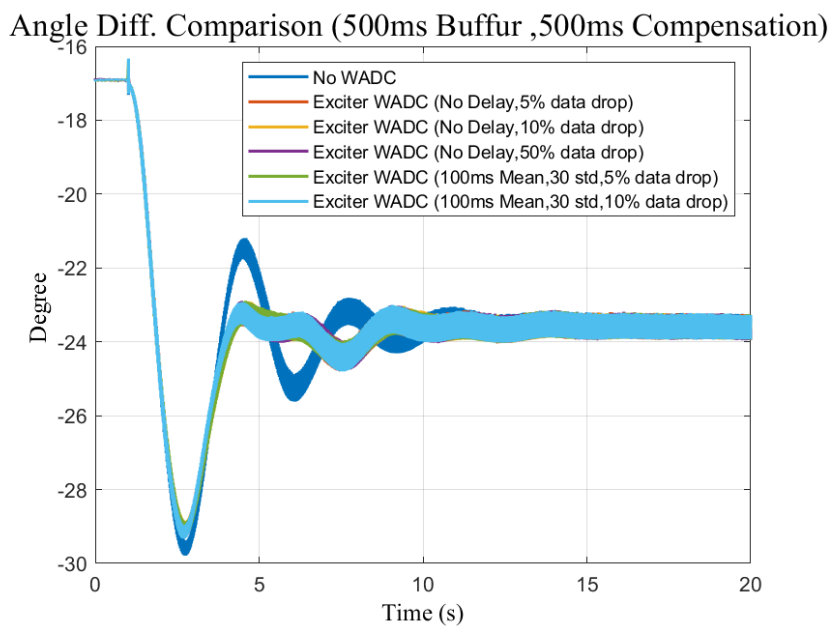


**(b)** Voltage angle difference

**Figure 5.21:** Control effect of WADCs via exciters with random time delay and occasional data drop during single-generator trip.

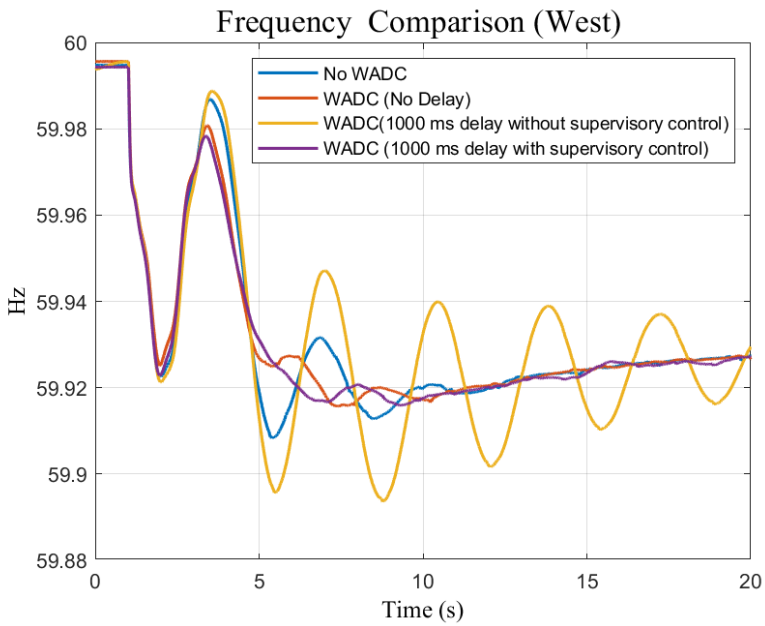


**(a)** Frequency response

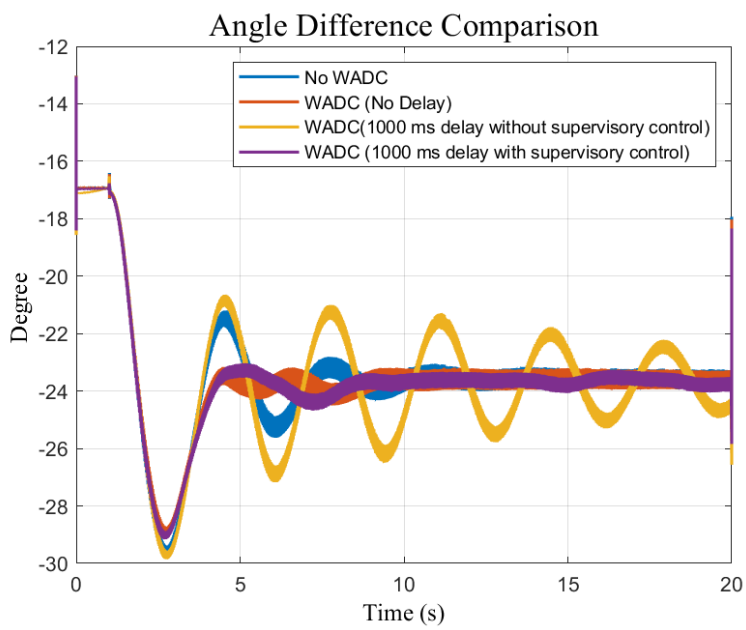


**(b)** Voltage angle difference

**Figure 5.22:** Control effect of WADCs via exciters intolerable time delay with supervisory control during single-generator trip.

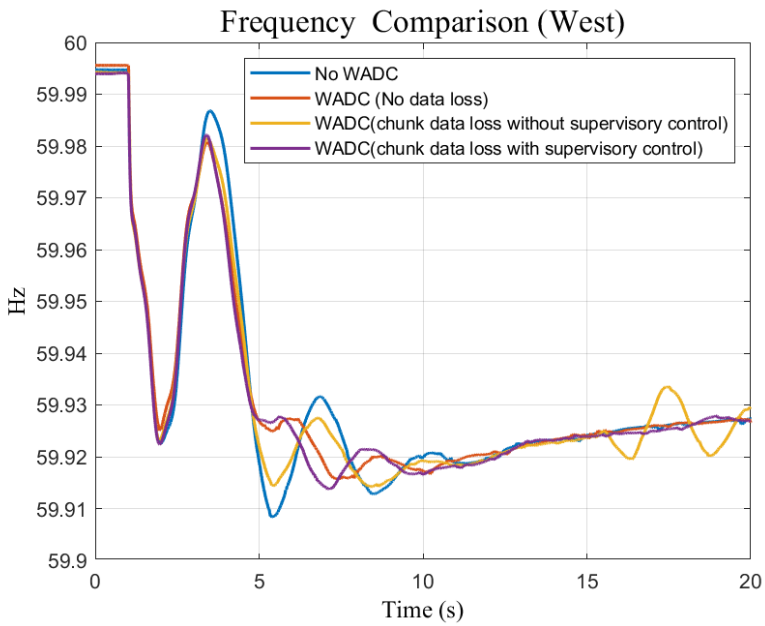


**(a)** Frequency response

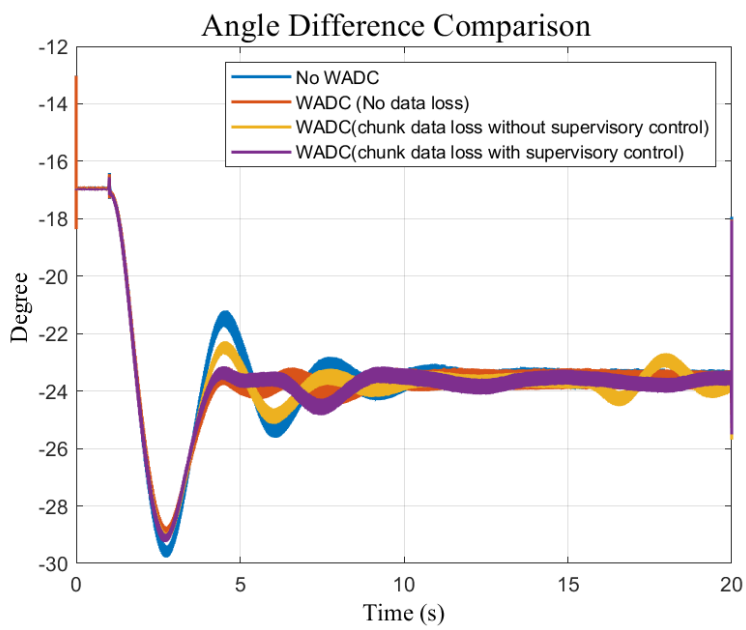


**(b)** Voltage angle difference

**Figure 5.23:** Control effect of WADCs via exciters with data drop with supervisory control during single-generator trip.

## 5.4 Summary

The effective of multiple WADCs is demonstrated in preventing system separation and enhancing tie-line transfer limit by the real-time simulations on RTDS using the Saudi power grid model. The Saudi power grid full model in PSS/e is reduced to a 218-bus equivalent model using DYNRED that preserved the dominant oscillation mode and the selected actuators in three power plants. Also, the reduced model can replicate the system separation after a large amount of generation trip in the full model. The WADCs are designed using a measurement-driven transfer function model and validated to improve both small-signal stability and transient stability of the system. The performance of the WADCs via different actuators is tested and compared. With these WADCs, the system separation after a large amount of generation trip can be prevented. Meanwhile, it is demonstrated that these WADCs can enhance transfer limit of the tie-lines. Moreover,this chapter focuses on WADC implementation and HIL test to validate controller performance in an emulated operational environment considering practical issues including random time delay and data loss. The HIL test setup is built based on a hybrid TSAT-RTDS real-time simulation platform. Power amplifiers, PMU devices, communication network impairment simulators, and WADCs are also included in the loop. The WADC is implemented on the generic-purpose hardware platform Compact-RIO. Besides the basic communication and control function blocks, other critical functions, including a delay compensator and supervisory control block, are also developed to handle realistic conditions such as time delay and data package loss.

# Chapter 6

# Impact of WADC on the system with high PV

## 6.1 Introduction

The increasing penetration of renewable energy will challenge future power system stability. It is known that the converter-based units are different from the synchronous machine counterparts. They do not have any rotating parts, and they are entirely decoupled from grid frequency, which means zero inertia. Thus, its dynamic response is based on the converter dynamics performance, which influences the power system stability. Solar PV generation systems are growing significantly all over the world; they accompany wind energy as a major means of renewable energy generation and are expected to significantly integrate into future power systems. These systems consist of semiconductor cells that convert sunlight directly into Direct Current power, which is then converted into AC through the use of electronic inverters [98]. Solar PV system is conventional synchronous generators, they do not include any rotating parts that could provide the system with inertia [98]. The impact of high solar PV penetration on the power system is a critical issue that should be studied since a high percentage of conventional generators are being replaced with PV units [98]. However, research on the impact of high penetration of solar PV generation on oscillation or small signal stability has not been adequately conducted.

It can be concluded from the literature in the Chapter 2 that solar PV penetration has a significant influence on the characteristics and performance of the power system grid, especially on power system oscillations. This chapter investigates the impact of high renewable penetration on the system oscillation where the case study used is the SEC system. Moreover, the chapter studies the impact of WADC on a system with high renewable penetration. The WADC actuators used in the chapter are the energy storage system, exciter, and governor. The study scope covers transient and small-signal stability.

## 6.2 Impact of high PV on SEC oscillation modes

This section focuses primarily on examining the possible impact of high penetration of PV units on the small-signal oscillation stability of the SEC power grid. It mainly investigates power grid small-signal stability in terms of oscillation frequency and oscillations damping ratio under large solar energy integration. In this chapter, the studied system is tested under temporary line fault of the major tie line to study the impact of high PV penetration on system dominant oscillation. The system's synchronous machines are replaced by PV units with the following penetration percentages: 20%, 40%, and 60%. Since the SEC grid has five major areas, the penetration level of PV is integrated equally in each area. Any extra addition of PV plants more than 75% to the SEC system results in losing the stability of the system. The amount of PV generation for each penetration scenario is listed in Table 6.1.

During multiple levels of PV penetration, the frequency of the optimal observation bus and the angle difference between the tie-line buses under temporary line fault are provided in Figure 6.1 and Figure C.4 respectively, whereas Table 6.2 shows the Prony analysis for the PV scenarios given in Figure 6.1. It can be seen that as the level of PV generation increased, the average oscillation frequency increased. On the other hand, the damping ratio of the dominant oscillation mode decreased as the level of the PV penetration increased.

**Table 6.1:** The generation amount of the solar PV penetration levels

| No. | **Solar PV penetration level** | **PV generation (MW)** |
|---|---|---|
| 1 | 20% PV | 13,077.57 |
| 2 | 40% PV | 27,171.87 |
| 3 | 60% PV | 35,355.92 |

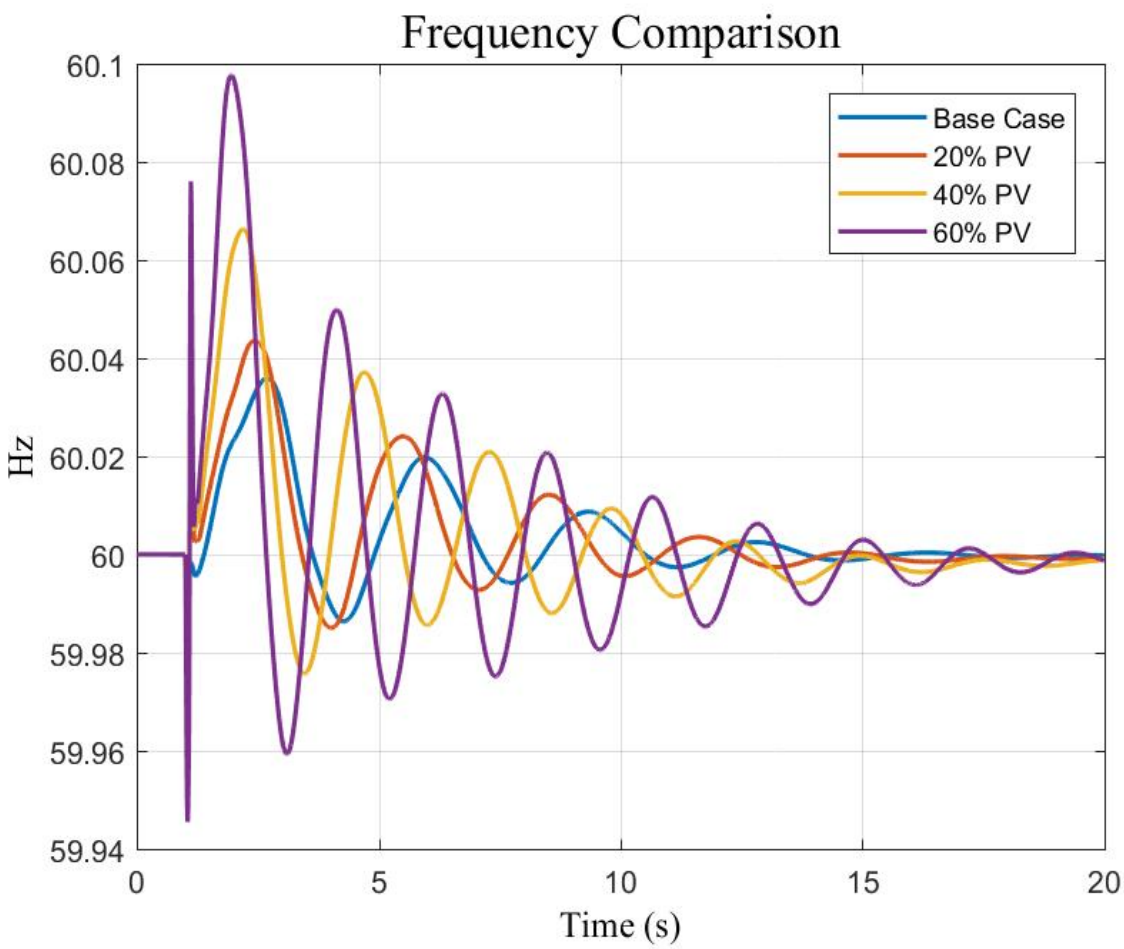


**Figure 6.1:** Frequency response during tie-line fault (PV level comparison).

**Table 6.2:** Prony analysis results of tie-line fault (PV level comparison)

| No. | **Case** | **Oscillation Frequency(Hz)** | **Damping Ratio(%)** |
|---|---|---|---|
| 1 | Base Case | 0.288 | 11.45 |
| 2 | 20% PV | 0.322 | 10.73 |
| 3 | 40% PV | 0.390 | 8.379 |
| 4 | 60% PV | 0.461 | 6.156 |

## 6.3 The Impact of WADC on high PV system oscillation

The WADC is tested under different level of PV penetration. The dominant oscillation mode has deteriorated when the PV penetration is increased. Two methodologies are used in this section to implement the WADC. First, the exciters and governors of the synchronous machines are used as the actuators of the WADC. The other is through using the Battery Energy Storage System (BESS) as the actuator of the WADC. The impact of the designed WADC for three different levels of PV penetration (20%, 40%, and 60%) was studied.

### 6.3.1 Using synchronous machine as WADC actuator

The designed WADC via exciters and governors is tested under different level of PV penetration. Similar to the process that has been done in Chapter 4, the observability and controllability analysis of the WADC design is conducted at each level of PV penetration where the results of the optimal candidates are still consistent with the base case presented in Chapter 4. As shown in Figure 6.2, the controllability index, which is the residue magnitude from the identified transfer function models, increases as the PV penetration level is increased in the selected units for the WADC actuators. This conclusion could vary from one system to another since the same plants of the base case are not replaced with PV.

#### Impact of WADC on 20% PV penetration

The WADC is tested when the PV penetration level is 20%. The frequency of the optimal observation bus and the angle difference between the tie-line buses after temporary line fault are provided in Figure 6.3 and Figure 6.4 respectively. Table 6.3 presents the Prony analysis for the case given in Figure 6.3. It can be clearly seen that the dominant oscillation mode is damped well with the WADC cases. The oscillation frequency increases to 0.486 Hz, 0.501 Hz, and 0.565 Hz for the WADC cases via exciters, governors, and exciters and governors respectfully. Moreover, the damping ratio of the dominant mode is improved to 18.027%, 18.615%, and 20.217% as shown in Table 6.3.

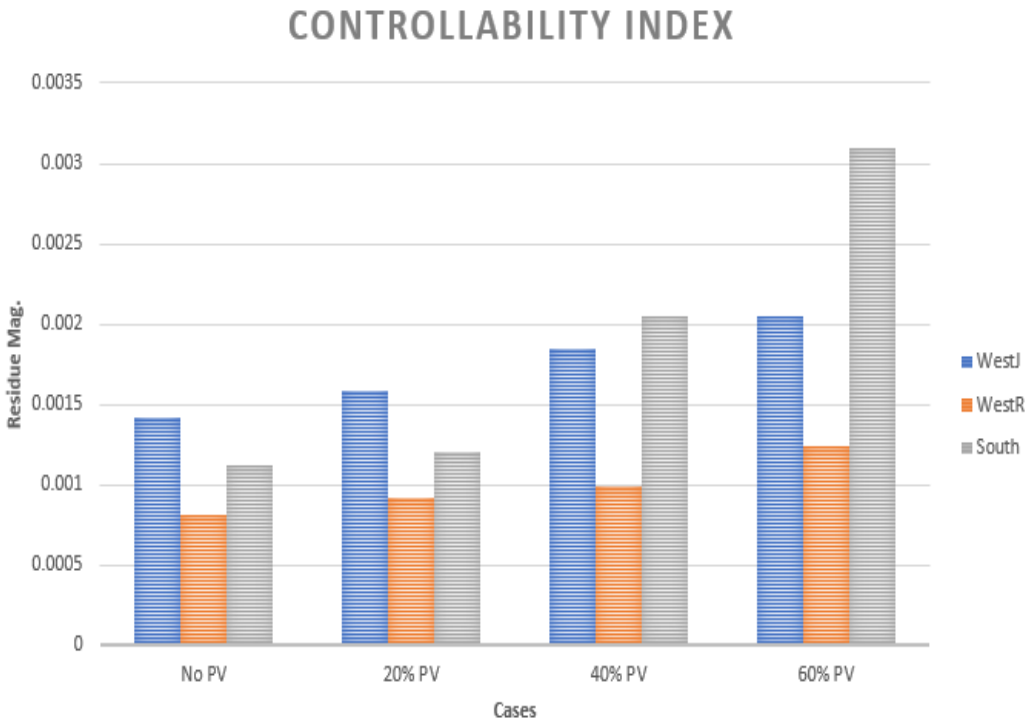


**Figure 6.2:** Residue Mag. of system identification (Exciters case).

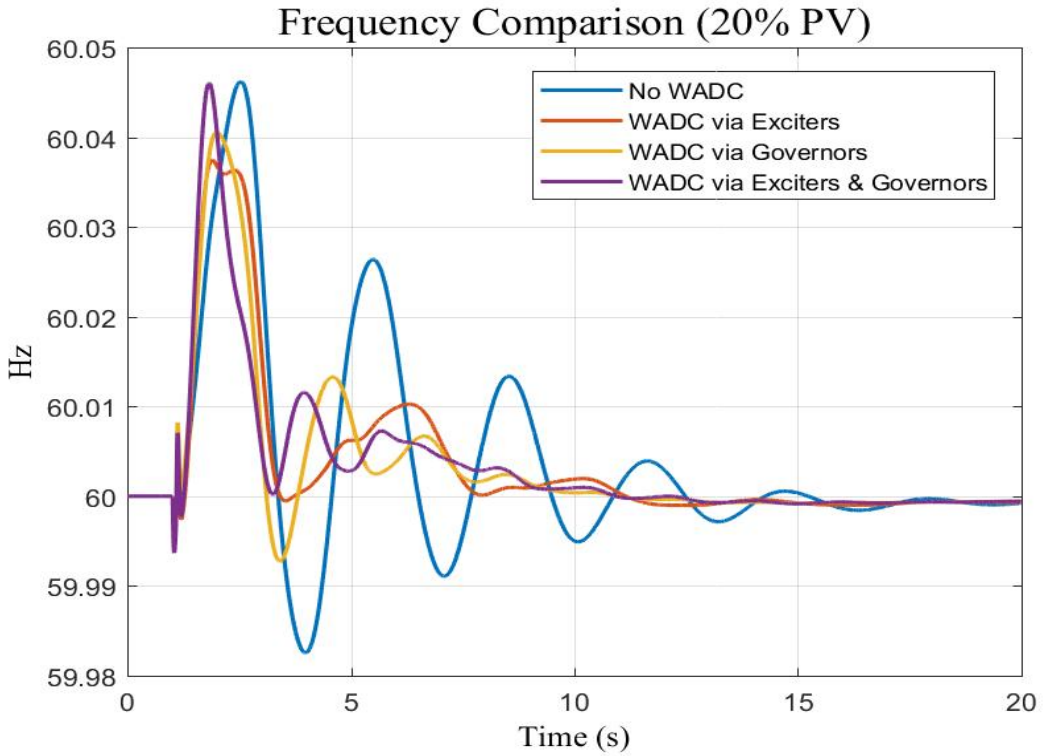


**Figure 6.3:** Frequency response during tie-line fault (20% PV).

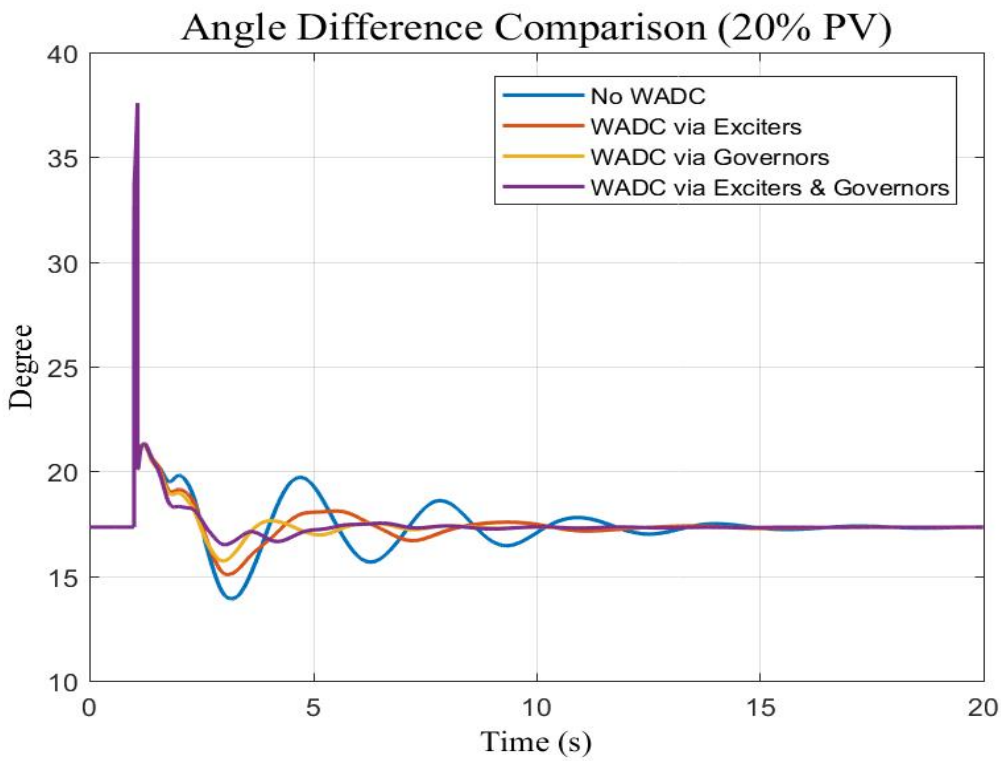


**Figure 6.4:** Angle difference response during tie-line fault (20% PV).

**Table 6.3:** Prony analysis results of tie-line fault (20% PV)

| No. | **Case** | **Oscillation Frequency(Hz)** | **Damping Ratio(%)** |
|---|---|---|---|
| 1 | Base Case (20% PV) | 0.322 | 10.73 |
| 2 | WADC via Exciters | 0.486 | 18.087 |
| 3 | WADC via Governors | 0.501 | 18.615 |
| 4 | WADC via Exciters Governors | 0.565 | 20.217 |

**Impact of WADC on 40% PV penetration**

Similar to the 20% PV case, the impact of WADC with 40% PV after a temporary line fault is tested. The frequency of the optimal observation bus and the angle difference between the tie-line buses are given in Figure 6.5 and Figure C.5 respectively. Table 6.4 provides the Prony analysis for the cases given in Figure 6.5. With all the WADC cases, it is obvious that the dominant oscillation mode is damped well. The oscillation frequency of the dominant mode increases to 0.438 Hz, 0.507 Hz, and 0.557 Hz for the WADC cases via exciters, governors, and exciters and governors respectfully. Furthermore, the damping ratio of the dominant mode is improved to 20.642%, 21.122%, and 21.366% as presented in Table 6.4.

**Impact of WADC on 60% PV penetration**

When the PV penetration level is 60%, the impact of the WADC is studied after temporary line fault. The frequency of the optimal observation bus and the angle difference between the tie-line buses are given in Figure 6.6 and Figure C.6 respectively. Table 6.5 presents the Prony analysis for the cases in Figure 6.6. A similar conclusion of the previous PV cases is observed where the dominant oscillation mode is damped well with the WADC cases. The oscillation frequency of the dominant oscillation mode increases to 0.413 Hz, 0.582 Hz, and 0.644 Hz for the WADC cases via exciters, governors, and exciters and governors respectfully. Moreover, the damping ratio of the dominant mode is improved to 17.849%, 15.35%, and 14.012% as shown in Table 6.5.

**WADC signal output comparison between No PV and PV cases**

The purpose of the comparison is to investigate the designed WADC capability to work perfectly with any modifications. The comparison was done under identical conditions between the base case (No PV penetration) and 60% PV penetration. The WADC (exciter case) signal output is compared for the above-mentioned cases. As shown in Figure 6.7, the WADC signal output changed according to the system dynamic where the dominant oscillation modes are 0.28 Hz and 0.46 Hz for the no PV and 60% PV cases respectively.

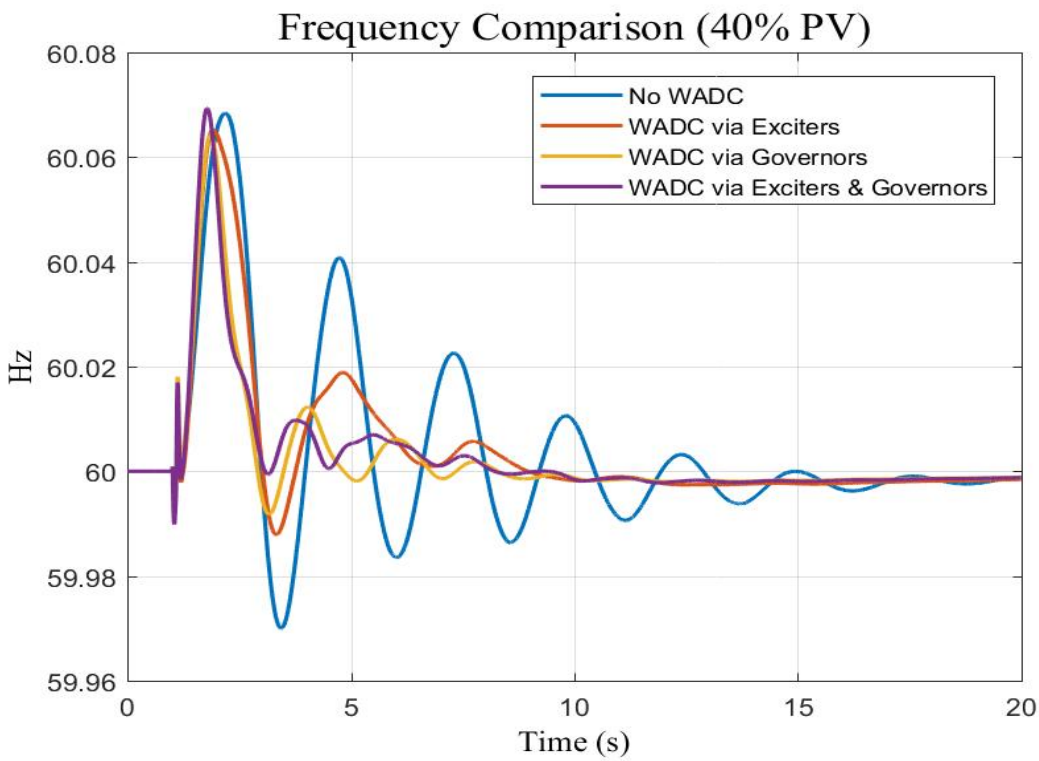


**Figure 6.5:** Frequency response during tie-line fault (40% PV).

**Table 6.4:** Prony analysis results of tie-line fault (40% PV)

| No. | **Case** | **Oscillation Frequency(Hz)** | **Damping Ratio(%)** |
|---|---|---|---|
| 1 | Base Case (40% PV) | 0.390 | 8.379 |
| 2 | WADC via Exciters | 0.4380 | 20.642 |
| 3 | WADC via Governors | 0.507 | 21.122 |
| 4 | WADC via Exciters Governors | 0.557 | 21.366 |

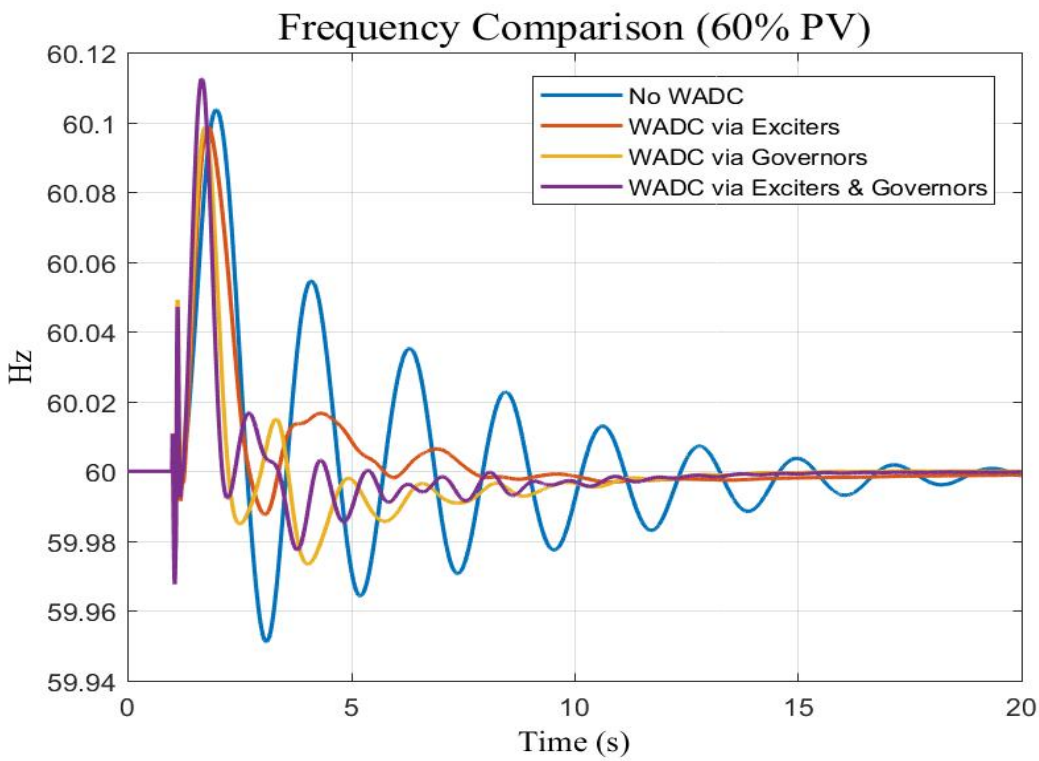


**Figure 6.6:** Frequency response during tie-line fault (60% PV).

**Table 6.5:** Prony analysis results of tie-line fault (60% PV)

| No. | **Case** | **Oscillation Frequency(Hz)** | **Damping Ratio(%)** |
|---|---|---|---|
| 1 | Base Case (60% PV) | 0.461 | 6.156 |
| 2 | WADC via Exciters | 0.413 | 17.849 |
| 3 | WADC via Governors | 0.582 | 15.35 |
| 4 | WADC via Exciters Governors | 0.644 | 14.012 |

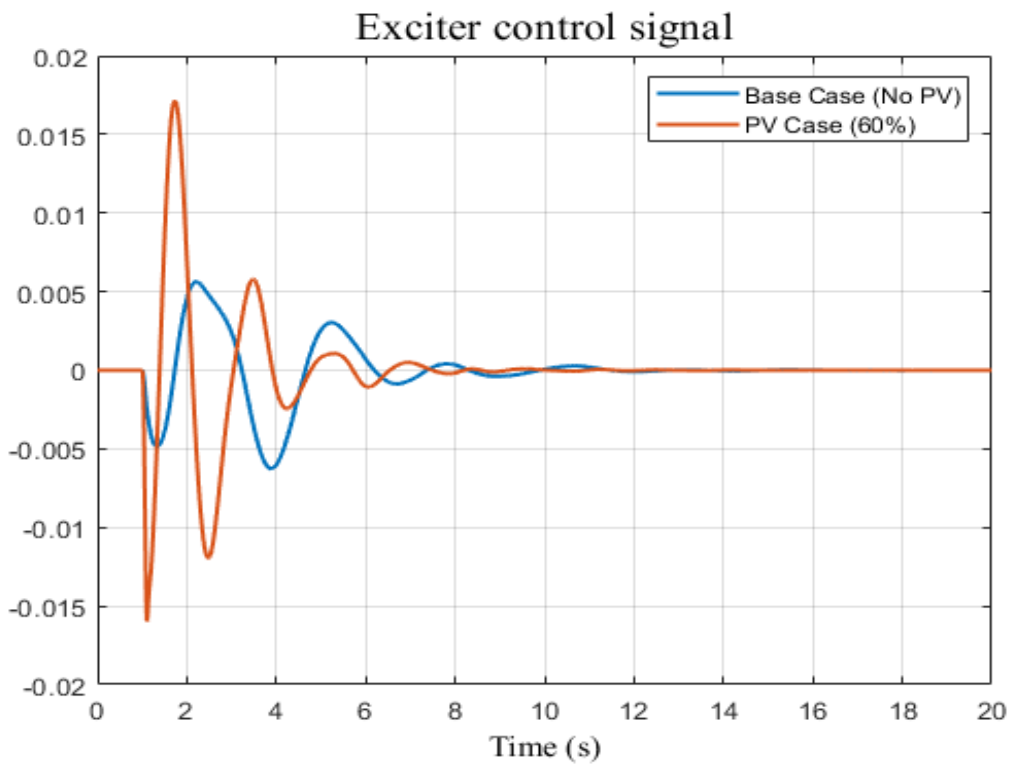


**Figure 6.7:** Exciter Control Signal during line fault (No PV vs 60%PV).

### 6.3.2 Using Battery Electric Storage System (BESS) as WADC actuator

The primary purpose of this section is to study the impact of BESS on the system oscillation under various levels of PV penetration. The economic impact of the BESS is beyond the scope of this research; it is essential to evaluate the proper size of ESS for some of the power system applications. As stated earlier, the power grid operates with low system inertia since the high penetration of renewables is integrated into the grid. Hence, the power system stability, precisely frequency stability, might be deteriorated, leading to grid security and reliability challenges.

The solar PV causes fluctuations in the output power; due to this uncertainty, it is important to assist the system reliability [122]. An energy storage system can help increase system reliability by balancing the active power in a power grid and provide ancillary services [123]. Normally, a storage system is operated in one of two normal conditions, charging or discharging, in which the active and reactive power could be regulated [124]. However, because of its considerable cost, it should not be used just for system balancing but should be further exploited to provide extra damping for the system oscillations [125, 126]. The literature provides fewer investigations on the impact of energy storage on damping power system oscillation [123, 124, 126, 127, 128, 129, 130]. It can be concluded from the available literature that the energy storage system has a beneficial impact on the system stability; however, its cost is a major disadvantage.

Generally, ESS can store and deliver or absorb energy from or to the power grid in a concise time frame to perform useful functions. However, in most system applications, ESS's primary function is the grid frequency regulation. It can quickly control the active power transfer into and from the power grid to regulate system frequency when a disturbance occurs [131]. The response to the first oscillation swing is crucial to maintain grid stability before triggering any protection devices; therefore, restoring the frequency stability in the first seconds after an event requires high-speed ramping storage capability [132].

In this study, three models in PSS/e are used to demonstrate the energy storage system's dynamic characteristics where the BESS capacity is 100 MW. The three models are the Renewable Energy Generator model (REGCAU1), Electrical Control Model for Utility Scale Battery Energy Storage (REECCU1), and Generic Renewable Plant Control Model (REPCAU1). The connection of the BESS battery models is shown in Figure 6.8.

The location of the storage system could have a beneficial influence on the oscillation damping. Most researchers investigate the placement issue from an energy management viewpoint, focusing on economic benefits like minimum operating costs [123]. Few focus on the stability improvement perspective for power system oscillation [133, 134]. In [134], small-signal stability analysis and time-domain simulations are used to categorize the studied system buses based on their controllability using inertia distribution. According to inertia distribution of the studied system, the optimal location of the electric energy storage is determined.

In this dissertation, controllability analysis based on the residue magnitude of the dominant oscillation mode is used to determine the optimal placement of the BESS. Figure 6.9 is mapping the optimal location of the BESS in the SEC grid where Table 6.6 lists the top 10 optimal buses. In order to confirm the analysis results, the system response when the BESS is located at the optimal placement was compared to the worst placement in Figure 6.10. When the BESS is located at the optimal location, the damping of the dominant mode is improved to 19.86% compared to the base case of 11.45%. On the other hand, the damping ratio is slightly improved to 14.46% when the BESS is placed at the worst location.

When the WADC is activated on the BESS, the damping of the dominant oscillation mode can be improved further. As shown in Figure C.7, it can be observed that the damping of the dominant oscillation mode is increased from 19.86%, which is the BESS case without WADC, to 23.23%, which is the case when the BESS is equipped with WADC. Therefore, in all the cases in the following sections, the WADC is used with BESS during the comparison with the impact of the WADC on the conventional machines.

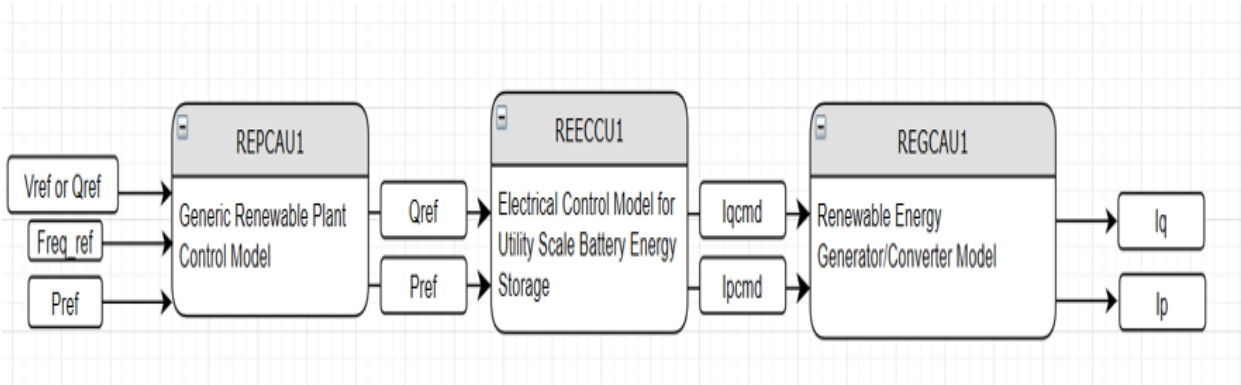


**Figure 6.8:** BESS Model in the PSSE.

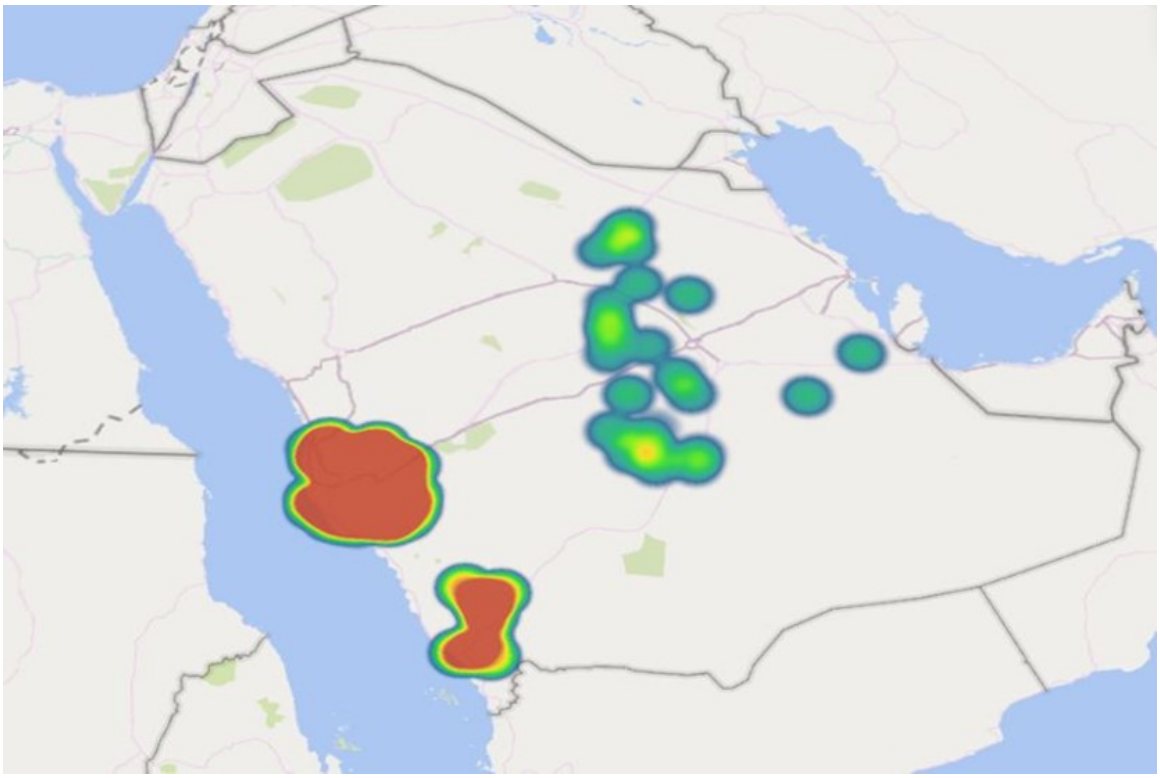

**Figure 6.9:** Controllability comparison of the BESS based on residue analysis.

**Table 6.6:** Top 10 buses based on residue magnitude of the BESS placement

| No. | Bus NO. | Residue Magnitude(Normalized) |
|---|---|---|
| 1 | West45 | 1.0000 |
| 2 | West70 | 0.959283 |
| 3 | West02 | 0.958595 |
| 4 | West55 | 0.939933 |
| 5 | South800 | 0.907734 |
| 6 | West62 | 0.903147 |
| 7 | West 50 | 0.881815 |
| 8 | South90 | 0.874837 |
| 9 | South15 | 0.873236 |
| 10 | West32 | 0.8598 |

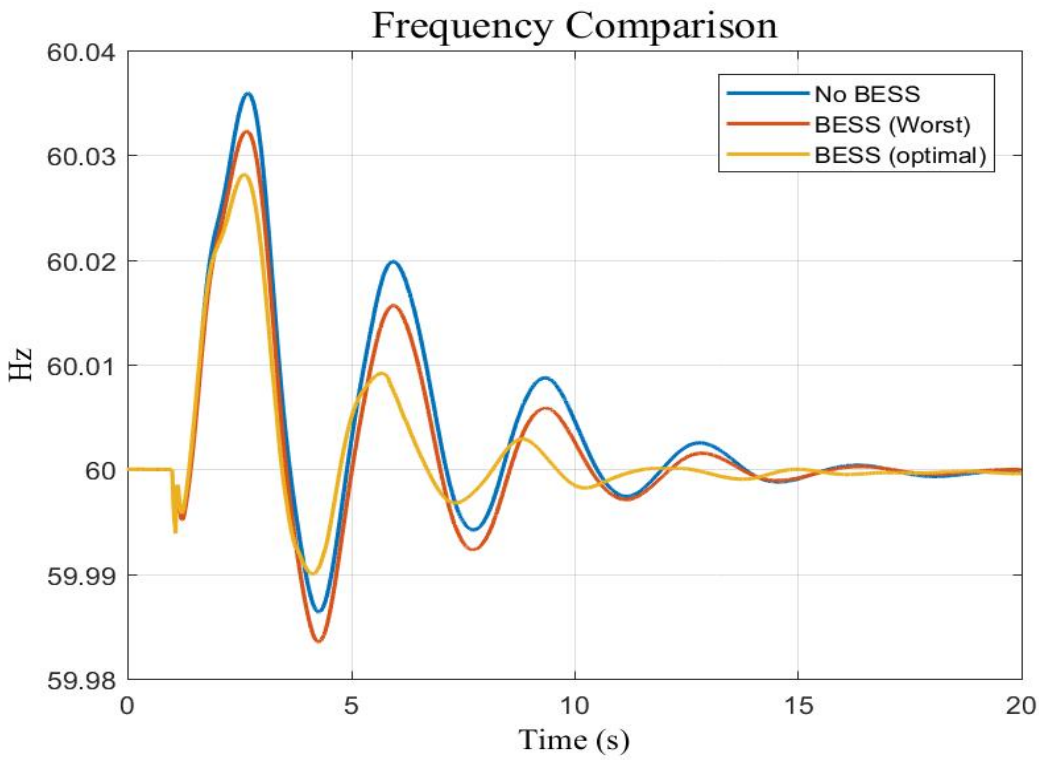


**Figure 6.10:** Frequency response during line fault for BESS optimal placement.

**Impact of WADC on 20% PV penetration**

The WADC via BESS is tested when the PV penetration level is 20% and then compared to the WADC via exciters & governors. The frequency of the optimal observation bus and the angle difference between the tie-line buses after temporary line fault are provided in Figure 6.11 and Figure C.8 respectively. It can be seen obviously that the dominant oscillation mode is damped well with the WADC via BESS compared to the no WADC case. The oscillation frequency is slightly increased to 0.342 Hz, and the damping ratio of the dominant mode is improved to 38.80% as presented in Table 6.7.

**Impact of WADC on 40% PV penetration**

Similar to the 20% PV case, the impact of WADC via BESS with 40% PV after a temporary line fault is tested. The frequency of the optimal observation bus and the angle difference between the tie-line buses are presented in Figure 6.12 and Figure C.9 respectively. The WADC via BESS is compared to the WADC via exciters and governors. It is clear that the dominant oscillation mode is damped well with the WADC via BESS. The oscillation frequency slightly increased to 0.468 Hz, and the damping ratio of the dominant mode is well improved to 25.433% as shown in Table 6.7.

**Impact of WADC on 60% PV penetration**

When the PV penetration level is 60%, the impact of the WADC via BESS is studied after temporary line fault. The frequency of the optimal observation bus and the angle difference between the tie-line buses are given in Figure 6.13 and Figure C.11 respectively. A similar conclusion of the previous PV cases is observed; the dominant oscillation mode is well damped with the WADC via BESS. The oscillation frequency slightly increased to 0.567 Hz, and the damping ratio of the dominant mode is well improved to 17.19% as shown in Table 6.7.

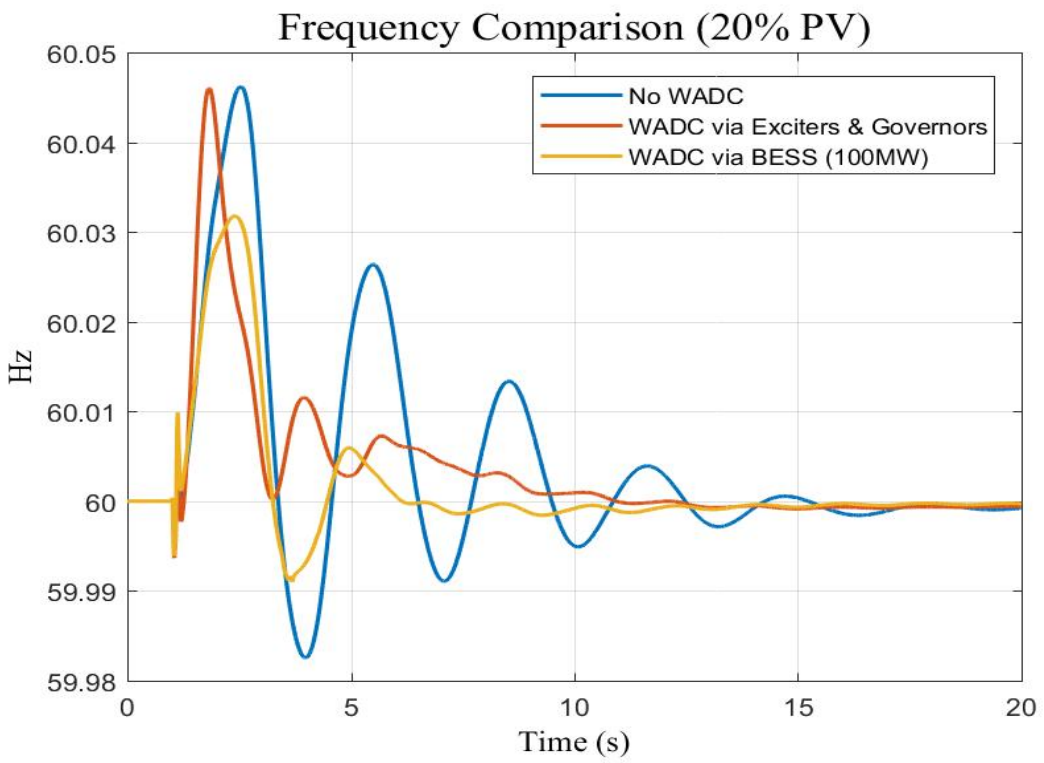


**Figure 6.11:** Frequency response during tie-line fault (20% PV with BESS).

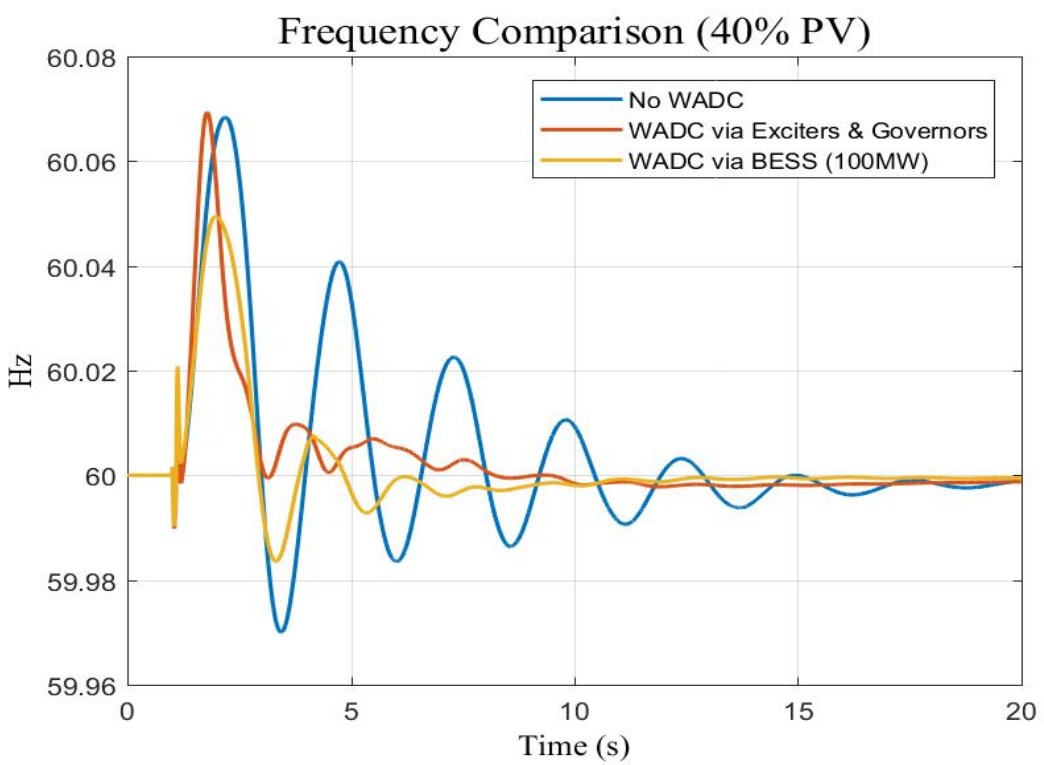


**Figure 6.12:** Frequency response during tie-line fault (40% PV with BESS).

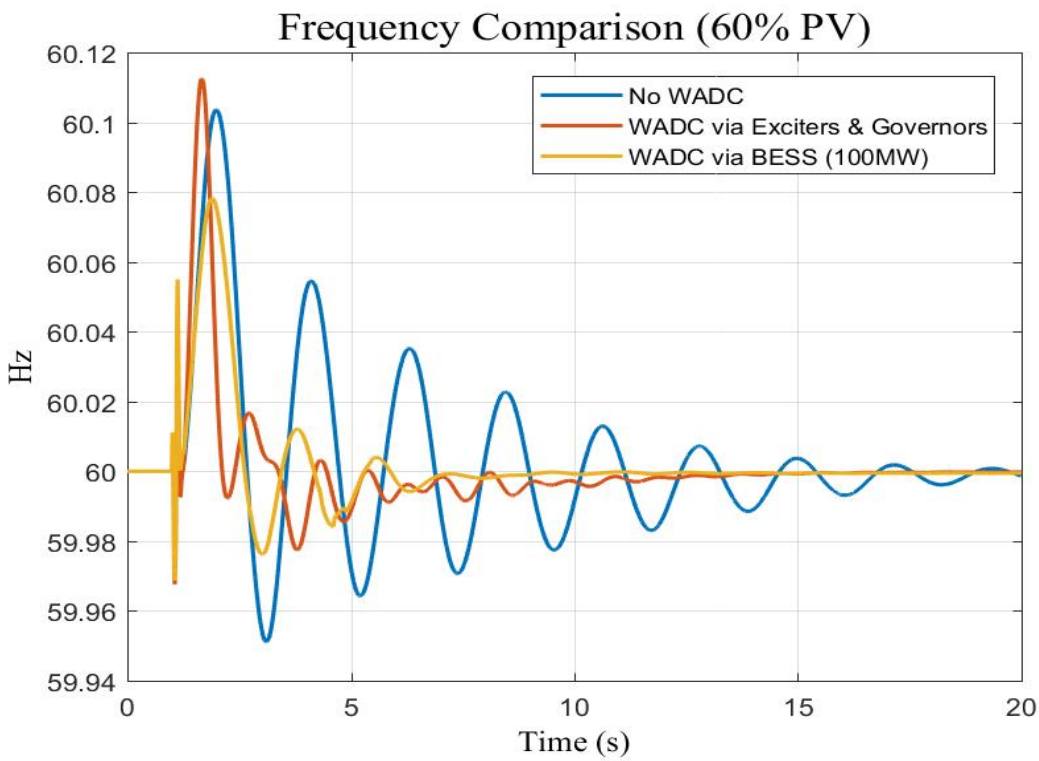


**Figure 6.13:** Frequency response during tie-line fault (60% PV with BESS).

**Table 6.7:** Prony analysis results of tie-line fault (BESS cases)

| Case | Oscillation Freq. (Hz) | Damping Ratio (%) |
|---|---|---|
| 20% PV | 0.342 | 38.8 |
| 40% PV | 0.468 | 25.433 |
| 60% PV | 0.567 | 17.19 |

**Dynamic response comparison between WADC via BESS and WADC via exciter & governor**

The purpose of the comparison is to investigate how fast the converter-based actuator responds to the disturbance compared to the synchronous machine actuator (exciter and governor). The comparison was performed during line fault where the faults occurred at 1s and cleared at 1.08s. The active power deviation output of the BESS and WestJ generator are compared in this study. As shown in Figure 6.14, there are four compared signals which are the active power output of the WestJ generator (No WADC), the WestJ generator (WADC via exciter and governor), BESS (No WADC), and BESS (WADC). It can be concluded that the impact of the WADC via BESS can be noticed right after the fault was cleared. However, the impact of the WADC via exciter and governor took longer time to respond than WADC BESS since the time constant of the converted-based actuators (BESS) is small compared to the exciter and governor.

## 6.4 Transient stability improvement with the designed WADC

This section introduces the benefit of the designed WADCs in improving the SEC's transient stability during multiple PV penetrations. The impact of designed WADCs on the marginal generation trip and transfer limit is presented in the following.

### 6.4.1 Impact of WADC on system marginal generation trip

This section presents the cases where the WADC could improve the marginal generation trip that causes the system separation. System separation could happen in the Saudi power grid when a large amount of generation trip happens in the western area simultaneously.

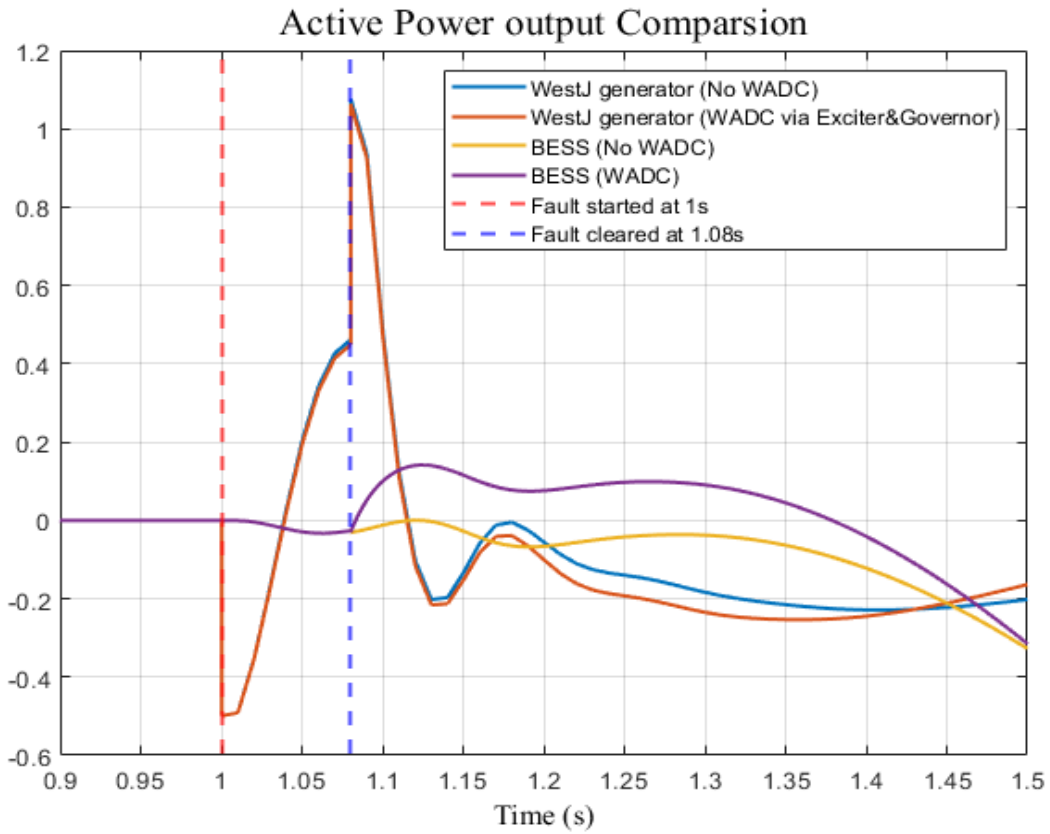


**Figure 6.14:** Actuator output Active Power comparison.

The designed WADCs can be used to improve the marginal generation trip. Table 6.8 shows the marginal amount of generation trip for different WADC configurations for all PV cases. For example, when there is no WADC, the system will be separated by the out-of-step relay if the generation trip amount is larger than 1536 MW, 1394 MW, and 1196 MW for the PV cases 20%, 40%, and 60%, respectively.

In all the cases that are listed in Table 6.8, the marginal generation trip decreased as the PV penetration increased. The maximum marginal generation trip for each individual PV case can be achieved with WADC via BESS, WADC via exciters and governors, WADC via governors, and WADC via exciters. It can be concluded that the marginal amount of generation trip to the western area is reduced as the PV penetration percentage is increased. Figure 6.15 visualize the data presented in Table 6.8.

### 6.4.2 Impact on the tie-line active power transfer limit

The impact of WADCs on the transfer limit of the major tie lines between the western area and the central area is also studied for the PV cases. Similar to the process that is used in Chapter 4, the transfer limit is determined based on the pre-disturbance power flow when the system is still connected after a temporary three-phase fault is applied on one of the tie lines followed by tripping the faulted tie line after 80 ms.

Table 6.9 presents the tie-line transfer limit with and without multiple WADCs for all the PV cases when the WADCs are equipped with exciters, governors, exciters and governors, and BESS. In general, the transfer limit of the major tie line is decreased as the PV penetration is increased. It can be seen from Figure Figure 6.16 that the WADC via BESS has a higher impact on the transfer limit for all the PV cases. Figure 6.16 visualize the data presented in Table 6.9.

**Table 6.8:** Marginal amount of generation trip With WADCs (PV cases)

| Case | Marginal amount of generation trip in west (MW) | | |
|---|---|---|---|
| | 20% PV | 40% PV | 60% PV |
| No WADC | 1536 | 1394 | 1196 |
| WADC via Exciters | 1591 | 1421 | 1224 |
| WADC via Governors | 1645 | 1498 | 1285 |
| WADC via Exciters & Governors | 1686 | 1530 | 1312 |
| WADC via BESS | 1768 | 1618 | 1414 |

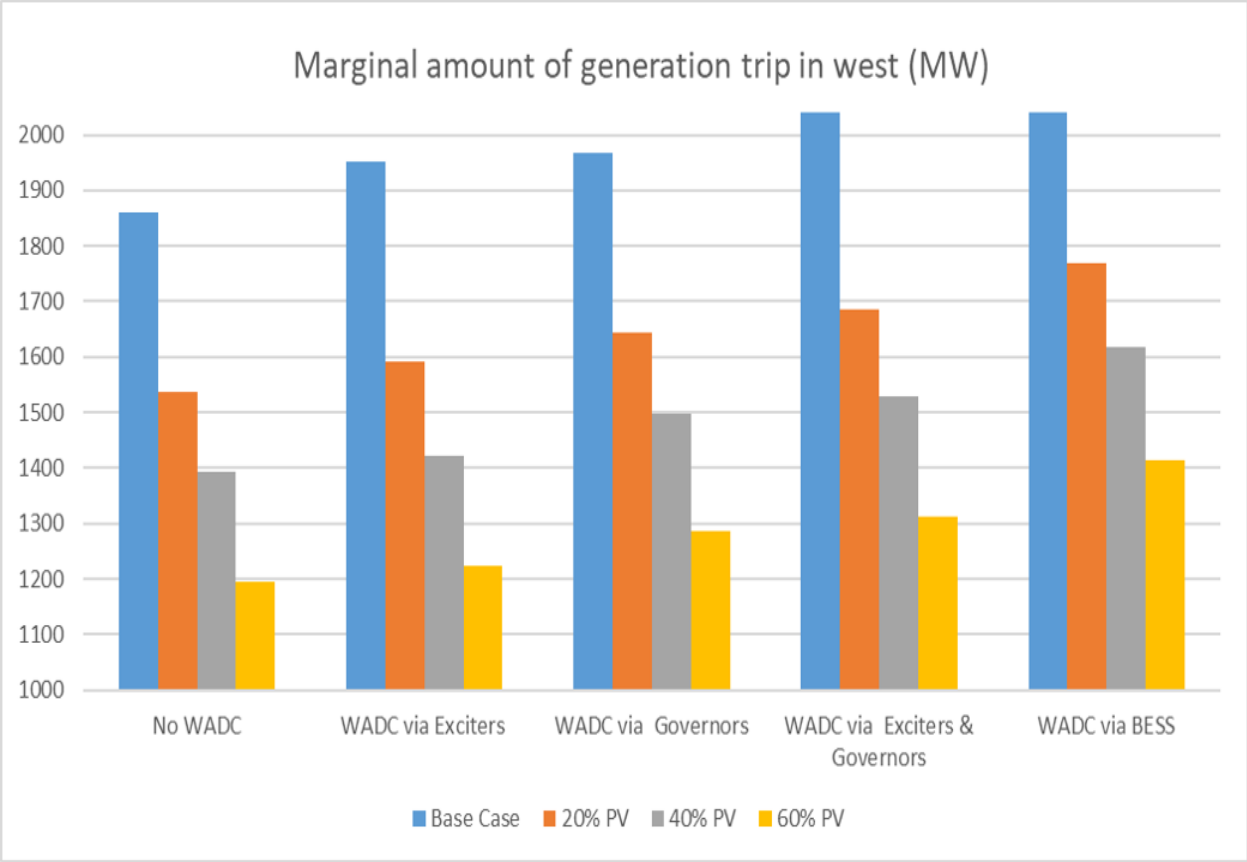


**Figure 6.15:** Marginal generation trip at the western area with PV.

**Table 6.9:** Active power transfer limit With WADCs (PV cases)

| Case | Tie-line transfer limit (MW) | | |
|---|---|---|---|
| | 20% PV | 40% PV | 60% PV |
| No WADC | 890.9 | 886.9 | 864.8 |
| WADC via Exciters | 900.9 | 891.9 | 882.9 |
| WADC via Governors | 930.9 | 929.3 | 910.9 |
| WADC via Exciters & Governors | 933.2 | 931.9 | 920.01 |
| WADC via BESS | 990.1 | 992.2 | 981.7 |

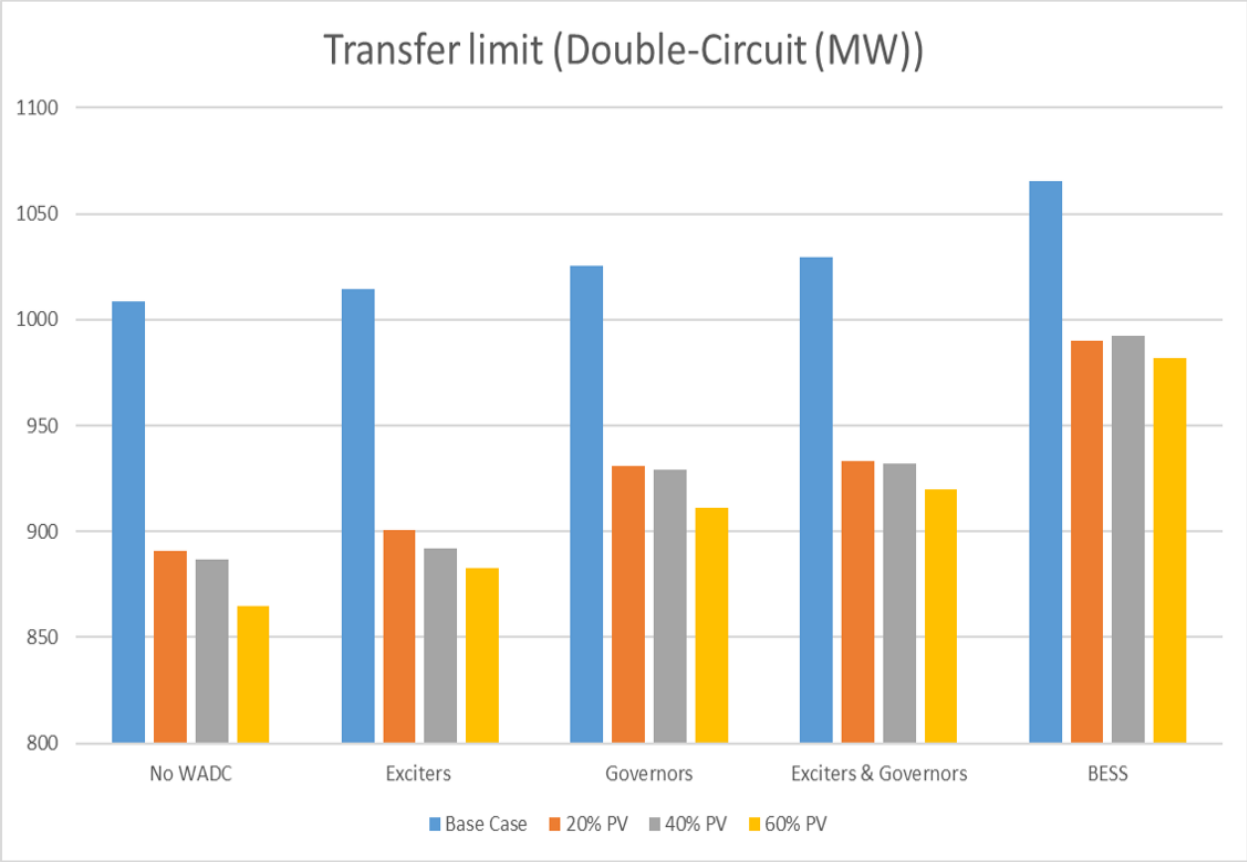


**Figure 6.16:** Transfer limit of the major tieline with PV.

## 6.5 Summary

The impacts of the higher PV penetration on the interarea oscillations are investigated. It has been concluded that the dominant oscillation modes of the system are highly affected by the penetration level of solar generation. The oscillation frequency is increased, whereas the oscillation damping is reduced as the PV penetration is increased in the SEC grid. This pinpoints the fact that the reduced system inertia resulting from displacing conventional generation units is one of the causes of deteriorated rotor angle stability. Consequently, keeping critical conventional machines online can help alleviate the adverse impact on the rotor angle stability and interarea oscillations resulting from the contribution of the solar PV units. Then, the WADC was tested when the SEC system has high PV penetration levels. The simulation results validated the effectiveness of the WADC in improving the damping ratio of the target oscillation mode. Also, the marginal generation trip in the western area and the transfer limit of the SEC system's major tie line are improved when multiple WADCs are activated for all PV penetrating levels. The WADC via 100 MW BESS was tested with different levels of PV penetration. The simulation results validated the effectiveness of the WADC via BESS in improving the damping ratio of the target oscillation mode. Also, the marginal generation trip in the western area and the transfer limit of the SEC system's major tie line are improved when WADC is activated on the BESS.

# Chapter 7

# Conclusion

In general, this dissertation investigates the impact of multiple WADCs using a measurement-driven approach on the SEC grid's stability. Multiple WADCs using a measurement-driven transfer function model were designed and validated to improve SEC's small-signal stability and transient stability by computer simulations. A summary of the tasks performed in this project are listed below:

- The optimal observation signals, as well as actuators, were selected. The frequency difference between the optimal observation buses in the western area and the central area was selected as the WADC input signal for the target oscillation mode. Also, the optimal observation bus in the western area is an alternative since it is the optimal observation bus for the whole SEC system. The WADCs could provide supplementary control via selected generator exciters and governors. The optimal generator exciters and governors to executes WADC control commands were selected using two methods. The first method was based on the frequency response of the optimal observation bus to a down step. A higher magnitude means higher controllability of the corresponding generator exciter or governor. The other method was based on the calculated residue magnitudes from the identified transfer function models. After the transfer function models are identified, the residue magnitudes of the models are compared.

- The measurement-driven approach was used to design the WADC. WADCs via selected generator exciters and governors can improve the damping ratio of the target oscillation

mode. The simulation results validated the effectiveness of the measurement-driven WADC design approach. Meanwhile, multiple WADCs can prevent the system from separating under large-generation trip events and improve the SEC system major tie line transfer limit.

- The WADC via HVDC was tested. The simulation results validated the effectiveness of the WADC via HVDC to improve the damping ratio of the target oscillation mode. Also, the marginal generation trip in the western area and the transfer limit of the SEC system major tie line are improved when WADC is activated on the HVDC.

- The impacts of the higher PV penetration on the inter-area oscillations are investigated. It has been concluded that the dominant oscillation modes of the system are highly affected by the penetration level of solar generation. The oscillation frequency is increased, whereas the oscillation damping is reduced as the PV penetration is increased in the SEC grid. This pinpoints the fact that the reduced system inertia resulted from displacing conventional generation units is one of the causes of deteriorated rotor angle stability. Consequently, keeping critical conventional machines online can help alleviate the adverse impact on the rotor angle stability and inter-area oscillations resulting from the contribution of the solar PV units. Then, the WADC was tested when the SEC system has high PV penetration levels. The simulation results validated the effectiveness of the WADC to improve the damping ratio of the target oscillation mode. Also, the marginal generation trip in the western area and the transfer limit of the SEC system's major tie-line are improved when multiple WADCs are activated for all PV penetrating level.

- The WADC via 100 MW BESS was tested with different levels of PV penetration. The simulation results validated the effectiveness of the WADC via BESS to improve the damping ratio of the target oscillation mode. Also, the marginal generation trip in the western area and the transfer limit of the SEC system's major tie-line are improved when WADC is activated on the BESS.

The WADC was implemented using real-time simulator, and then the performance validation is proven. The implementation and HIL test is further validate the controller

performance in an emulated operational environment with consideration of more realistic issues, e.g. random time delay and data loss. A summary of the tasks performed in this project are listed below:

- The SEC power grid full model in PSS/e was reduced to a 218-bus equivalent model by using DYNRED. The reduced model preserved the dominant oscillation mode, the selected actuators in three power plants, and SVC buses. The reduced model can also replicate the system separation after a large amount of generation trip in the full model.

- The WADCs (software) were added to the RTDS model, and the performances of the WADCs via different actuators were tested and compared. With these WADCs, system separation after a large amount of generation trip can be prevented. The detailed headroom requirements were also investigated. Additionally, it is demonstrated that the WADCs can enhance the transfer limit of the tie-lines.

- The HIL test setup was built based on the hybrid RTDS-TSAT real-time simulation platform. Power amplifiers, PMU devices, communication network impairment simulator, and WADC were also included in the loop.

- The WADC was implemented on a generic-purpose hardware platform - CompactRIO. Besides the basic communication and control function blocks, a few critical function blocks, e.g., delay compensator and supervisory control, were also developed to handle time delay, data package loss, and other realistic scenarios. The delay compensator was used to compensate for the angle shift that is caused by communication latency. The supervisory control block was implemented to switch the primary PMU to backup ones when long-time abnormal PMU measurements are detected in the primary PMU. An oscillation detector was also added in the WADC prototype to disable the controller when no oscillation is detected.

# Bibliography

[1] G. Bridge, B. Özkaynak, and E. Turhan, "Energy infrastructure and the fate of the nation: Introduction to special issue," *Energy Research and Social Science*, 2018. 1

[2] P. Kundur, *Power system stability and control*, 1993. 1, 7, 22, 23, 25

[3] L. L. Grigsby, *Power system stability and control*, 2017. 2

[4] Graham Rogers, *Power System Oscillations*, Boston, London, 2000. 2

[5] P. M. Anderson and A. A. Fouad, *Power system control and stability, second edition*, 2002. 2, 25

[6] X. Zhang, C. Lu, S. Liu, and X. Wang, "A review on wide-area damping control to restrain inter-area low frequency oscillation for large-scale power systems with increasing renewable generation," 2016. 2, 8, 9, 11

[7] Y. Zhang and A. Bose, "Design of wide-area damping controllers for interarea oscillations," *IEEE Transactions on Power Systems*, 2008. 2, 8

[8] J. Zhang, C. Y. Chung, C. Lu, K. Men, and L. Tu, "A Novel Adaptive Wide Area PSS Based on Output-Only Modal Analysis," *IEEE Transactions on Power Systems*, 2015. 2

[9] J. Zhang, C. Y. Chung, S. Zhang, and Y. Han, "Practical wide area damping controller design based on ambient signal analysis," *IEEE Transactions on Power Systems*, 2013. 2

[10] W. Yao, L. Jiang, J. Wen, Q. Wu, and S. Cheng, "Wide-area damping controller for power system interarea oscillations: A networked predictive control approach," *IEEE Transactions on Control Systems Technology*, 2015. 2, 11, 16

[11] P. Li, X. Wu, C. Lu, J. Shi, J. Hu, J. He, Y. Zhao, and A. Xu, "Implementation of CSG's wide-area damping control system: Overview and experience," in *2009 IEEE/PES Power Systems Conference and Exposition, PSCE 2009*, 2009. 2, 8

[12] R. Preece, A. M. Almutairi, O. Marjanovic, and J. V. Milanović, "Damping of electromechanical oscillations by VSC-HVDC active power modulation with supplementary wams based modal LQG controller," in *IEEE Power and Energy Society General Meeting*, 2011. 2

[13] D. Trudnowski, D. Kosterev, and J. Undrill, "PDCI damping control analysis for the western North American power system," in *IEEE Power and Energy Society General Meeting*, 2013. 2

[14] W. Yao, L. Jiang, J. Wen, Q. H. Wu, and S. Cheng, "Wide-area damping controller of Facts devices for inter-area oscillations considering communication time delays," *IEEE Transactions on Power Systems*, 2014. 2

[15] J. Deng, C. Li, and X. P. Zhang, "Coordinated Design of Multiple Robust FACTS Damping Controllers: A BMI-Based Sequential Approach with Multi-Model Systems," *IEEE Transactions on Power Systems*, 2015. 2

[16] L. P. Kunjumuhammed, R. Singh, and B. C. Pal, "Robust signal selection for damping of inter-area oscillations," *IET Generation, Transmission and Distribution*, 2012. 2

[17] Y. Li, C. Rehtanz, S. Ruberg, L. Luo, and Y. Cao, "Assessment and choice of input signals for multiple HVDC and FACTS wide-area damping controllers," *IEEE Transactions on Power Systems*, 2012. 2

[18] H. Nguyen-Duc, L. A. Dessaint, A. F. Okou, and I. Kamwa, "Selection of input/output signals for wide area control loops," in *IEEE PES General Meeting, PES 2010*, 2010. 2

[19] Y. Zhao, C. Lu, Y. Liu, and Y. Han, "Residue and identification based wide-area damping controller design in large-scale power system," in *2012 IEEE PES Innovative Smart Grid Technologies, ISGT 2012*, 2012. 2

[20] N. R. Chaudhuri, A. Domahidi, R. Majumder, B. Chaudhuri, P. Korba, S. Ray, and K. Uhlen, "Wide-area power oscillation damping control in Nordic equivalent system," *IET Generation, Transmission and Distribution*, 2010. 2, 11

[21] C. Lu, X. Zhang, X. Wang, and Y. Han, "Mathematical Expectation Modeling of Wide-Area Controlled Power Systems with Stochastic Time Delay," *IEEE Transactions on Smart Grid*, 2015. 2

[22] H. Wu, K. S. Tsakalis, and G. T. Heydt, "Evaluation of time delay effects to wide area power system stabilizer design," *IEEE Transactions on Power Systems*, 2004. 2

[23] N. T. Anh, L. Vanfretti, J. Driesen, and D. Van Hertem, "A Quantitative Method to Determine ICT Delay Requirements for Wide-Area Power System Damping Controllers," *IEEE Transactions on Power Systems*, 2015. 2

[24] S. You, J. Guo, G. Kou, Y. Liu, and Y. Liu, "Oscillation mode identification based on wide-area ambient measurements using multivariate empirical mode decomposition," *Electric Power Systems Research*, 2016. 3

[25] P. Kundur, J. Paserba, V. Ajjarapu, G. Andersson, A. Bose, C. Canizares, N. Hatziargyriou, D. Hill, A. Stankovic, C. Taylor, T. Van Cursem, and V. Vittal, "Definition and classification of power system stability," *IEEE Transactions on Power Systems*, 2004. 6

[26] Z. Huang, N. Zhou, F. Tuffner, Y. Chen, D. Trudnowski, W. Mittelstadt, J. Hauer, and J. Dagle, "Improving small signal stability through operating point adjustment," in *IEEE PES General Meeting, PES 2010*, 2010. 6

[27] D. N. Kosterev, C. W. Taylor, and W. A. Mittelstadt, "Model validation for the august 10,1996 wscc system outage," *IEEE Transactions on Power Systems*, 1999. 6, 7, 9

[28] J. Hauer, "Preliminary examination of the alberta trip on august 4, 2000," *Working Note for the WECC Modeling and Validation Work Group*, 2002. 6

[29] R. Hauer, J., Lee, H., Burns, J., and Baker, "Preliminary analysis of western system oscillation event on june 4, 2003: Bpa and canada," *Working Note for the WECC Disturbance Monitoring Work Group*, 2003. 6

[30] R. Jenatton, J. Mairal, G. Obozinski, and F. Bach, "Proximal methods for hierarchical sparse coding," *Journal of Machine Learning Research*, 2011. 6

[31] P. Kundur, D. C. Lee, and H. M. El-Din, "Power system stabilizers for thermal units: Analytical techniques and on-site validation," *IEEE Transactions on Power Apparatus and Systems*, 1981. 6

[32] P. Kundur, M. Klein, G. J. Rogers, and M. S. Zywno, "Application of power system stabilizers for enhancement of overall system stability," *IEEE Transactions on Power Systems*, 1989. 7

[33] B. Keyvani, M. Karbalaye Zadeh, and H. Lesani, "Stability enhancement of multi-machine systems using adaptive reclosing of transmission lines," *International Journal of Electrical Power and Energy Systems*, 2014. 7

[34] M. E. Aboul-Ela, A. A. Sallam, J. D. McCalley, and A. A. Fouad, "Damping controller design for power system oscillations using global signals," *IEEE Transactions on Power Systems*, 1996. 7

[35] Z. Wang, C. Y. Chung, K. P. Wong, and C. T. Tse, "Robust power system stabiliser design under multi-operating conditions using differential evolution," *IET Generation, Transmission and Distribution*, 2008. 7

[36] J. Dagle, "The North American SynchroPhasor Initiative (NASPI)," in *IEEE PES General Meeting, PES 2010*, 2010. 8

[37] A. Chakrabortty, "Wide-area damping control of power systems using dynamic clustering and TCSC-based redesigns," *IEEE Transactions on Smart Grid*, 2012. 8

[38] D. Dotta, A. S. e Silva, and I. C. Decker, "Wide-area measurements-based two-level control design considering signal transmission delay," *IEEE Transactions on Power Systems*, 2009. 8

[39] H. Ni, G. T. Heydt, and L. Mili, "Power system stability agents using robust wide area control," *IEEE Transactions on Power Systems*, 2002. 8

[40] I. Kamwa, R. Grondin, and Y. Hébert, "Wide-area measurement based stabilizing control of large power systems - A decentralized/hierarchical approach," *IEEE Transactions on Power Systems*, 2001. 8

[41] R. Yousefian and S. Kamalasadan, "Design and real-time implementation of optimal power system wide-area system-centric controller based on temporal difference learning," *IEEE Transactions on Industry Applications*, 2016. 8

[42] R. Yousefian, A. Sahami, and S. Kamalasadan, "Hybrid Transient Energy Function-Based Real-Time Optimal Wide-Area Damping Controller," *IEEE Transactions on Industry Applications*, 2017. 8

[43] M. Mahmoudi, J. Dong, K. Tomsovic, and S. Djouadi, "Application of distributed control to mitigate disturbance propagations in large power networks," in *2015 North American Power Symposium, NAPS 2015*, 2015. 9, 10

[44] F. Hu, K. Sun, A. Del Rosso, E. Farantatos, and N. Bhatt, "Measurement-Based Real-Time Voltage Stability Monitoring for Load Areas," *IEEE Transactions on Power Systems*, 2016. 9

[45] H. Liu, L. Zhu, Z. Pan, F. Bai, Y. Liu, Y. Liu, M. Patel, E. Farantatos, and N. Bhatt, "ARMAX-based transfer function model identification using wide-area measurement for adaptive and coordinated damping control," *IEEE Transactions on Smart Grid*, 2017. 9, 11, 15

[46] M. Begovic, "Inter-Area Oscillations in Power Systems: A Nonlinear and Nonstationary Perspective (Messina, A.R.) [Book Reviews]," *IEEE Power and Energy Magazine*, 2011. 9, 10

[47] L. Vanfretti, R. García-Valle, K. Uhlen, E. Johansson, D. Trudnowski, J. W. Pierre, J. H. Chow, O. Samuelsson, J. Østergaard, and K. E. Martin, "Estimation of eastern Denmark's electromechanical modes from ambient phasor measurement data," in *IEEE PES General Meeting, PES 2010*, 2010. 9

[48] N. Zhou, J. W. Pierre, and J. F. Hauer, "Initial results in power system identification from injected probing signals using a subspace method," *IEEE Transactions on Power Systems*, 2006. 9, 10, 15

[49] D. J. Trudnowski, "Estimating electromechanical mode shape from synchrophasor measurements," *IEEE Transactions on Power Systems*, 2008. 10

[50] J. Zhang, C. Lu, and Y. Han, "MIMO identification of power system with low level probing tests: Applicability comparison of subspace methods," *IEEE Transactions on Power Systems*, 2013. 10

[51] D. J. Trudnowski, "Order reduction of large-scale linear oscillatory system models," *IEEE Transactions on Power Systems*, 1994. 10

[52] J. J. Sanchez-Gasca, "Performance comparison of three identification methods for the analysis of electromechanical oscillations," *IEEE Transactions on Power Systems*, 1999. 10

[53] R. Doraiswami and W. Liu, "Real-Time Estimation of the Parameters of Power System Small Signal Oscillations," *IEEE Transactions on Power Systems*, 1993. 10

[54] A. Hasanović, A. Feliachi, A. Hasanović, N. B. Bhatt, and A. G. DeGroff, "Practical robust PSS design through identification of low-order transfer functions," *IEEE Transactions on Power Systems*, 2004. 10

[55] H. Ghasemi, C. A. Cañizares, and A. Moshref, "Oscillatory stability limit prediction using stochastic subspace identification," *IEEE Transactions on Power Systems*, 2006. 10

[56] S. A. Nezam Sarmadi and V. Venkatasubramanian, "Electromechanical mode estimation using recursive adaptive stochastic subspace identification," *IEEE Transactions on Power Systems*, 2014. 10, 11

[57] R. Eriksson and L. Soder, "Wide-area measurement system-based subspace identification for obtaining linear models to centrally coordinate controllable devices," *IEEE Transactions on Power Delivery*, 2011. 10, 19

[58] I. Kamwa and L. Gérin-Lajoie, "State-space system identification-toward MIMO models for modal analysis and optimization of bulk power systems," *IEEE Transactions on Power Systems*, 2000. 10

[59] P. Van Overschee and B. De Moor, *Subspace Identification for Linear Systems*, 1996. 10

[60] W. Favoreel, B. De Moor, and P. Van Overschee, "Subspace state space system identification for industrial processes," *Journal of Process Control*, 2000. 10

[61] J. Turunen, M. Larsson, P. Korba, J. Jyrinsalo, and L. Haarla, "Experiences and future plans in monitoring the inter-area power oscillation damping," in *IEEE Power and Energy Society 2008 General Meeting: Conversion and Delivery of Electrical Energy in the 21st Century, PES*, 2008. 10

[62] R. W. Wies, J. W. Pierre, and D. J. Trudnowski, "Use of ARMA block processing for estimating stationary low-frequency electromechanical modes of power systems," *IEEE Transactions on Power Systems*, 2003. 11

[63] L. Dosiek and J. W. Pierre, "Estimating electromechanical modes and mode shapes using the multichannel ARMAX model," *IEEE Transactions on Power Systems*, 2013. 11, 15

[64] S. You, G. Kou, Y. Liu, X. Zhang, Y. Cui, M. J. Till, W. Yao, and Y. Liu, "Impact of High PV Penetration on the Inter-Area Oscillations in the U.S. Eastern Interconnection," *IEEE Access*, vol. 5, pp. 4361–4369, 2017. 11, 12, 14

[65] R. Shah, N. Mithulananthan, and K. Y. Lee, "Large-scale PV plant with a robust controller considering power oscillation damping," *IEEE Transactions on Energy Conversion*, vol. 28, no. 1, pp. 106–116, 2013. 11, 12, 14

[66] S. Eftekharnejad, V. Vittal, G. T. Heydt, B. Keel, and J. Loehr, "Impact of increased penetration of photovoltaic generation on power systems," *IEEE Transactions on Power Systems*, vol. 28, no. 2, pp. 893–901, 2013. 12

[67] Y. Liu, S. You, J. Tan, Y. Zhang, and Y. Liu, "Frequency Response Assessment and Enhancement of the U.S. Power Grids Toward Extra-High Photovoltaic Generation Penetrations-An Industry Perspective," *IEEE Transactions on Power Systems*, vol. 33, no. 3, pp. 3438–3449, 2018. 12

[68] S. Eftekharnejad, V. Vittal, G. T. Heydt, B. Keel, and J. Loehr, "Small signal stability assessment of power systems with increased penetration of photovoltaic generation: A case study," *IEEE Transactions on Sustainable Energy*, vol. 4, no. 4, pp. 960–967, 2013. 12, 13

[69] M. H. Nguyen, T. K. Saha, and M. Eghbal, "Impact of high level of renewable energy penetration on inter-area oscillation," *2011 21st Australasian Universities Power Engineering Conference, AUPEC 2011*, 2011. 12

[70] R. Shah, N. Mithulananthan, and R. C. Bansal, "Oscillatory stability analysis with high penetrations of large-scale photovoltaic generation," *Energy Conversion and Management*, vol. 65, pp. 420–429, 2013. [Online]. Available: http://dx.doi.org/10.1016/j.enconman.2012.08.004 12, 13, 14

[71] R. Elliott, R. Byrne, A. Ellis, and L. Grant, "Impact of increased photovoltaic generation on inter-area oscillations in the Western North American power system," *IEEE Power and Energy Society General Meeting*, vol. 2014-Octob, no. October, pp. 1–5, 2014. 12

[72] A. Golshani, S. M. Bathaee, and S. M. Moghaddas-Tafreshi, "Small signal stability analysis of photovoltaic array based on averaged switch modeling technique," *Journal of Renewable and Sustainable Energy*, 2012. 12

[73] J. Quintero, V. Vittal, G. T. Heydt, and H. Zhang, "The impact of increased penetration of converter control-based generators on power system modes of oscillation," *IEEE Transactions on Power Systems*, vol. 29, no. 5, pp. 2248–2256, 2014. 12, 13, 14

[74] R. Shah, N. Mithulananthan, A. Sode-Yome, and K. Y. Lee, "Impact of large-scale PV penetration on power system oscillatory stability," in *IEEE PES General Meeting, PES 2010*, 2010. 13

[75] B. Tamimi, C. Canizares, and K. Bhattacharya, "Modeling and performance analysis of large solar photo-voltaic generation on voltage stability and inter-area oscillations," *IEEE Power and Energy Society General Meeting*, pp. 1–6, 2011. 13

[76] R. Shah, N. Mithulananthan, and R. C. Bansal, "Damping performance analysis of battery energy storage system, ultracapacitor and shunt capacitor with large-scale photovoltaic plants," *Applied Energy*, 2012. 13

[77] W. Du, H. F. Wang, and R. Dunn, "Power system small-signal oscillation stability as affected by large-scale PV penetration," *1st International Conference on Sustainable Power Generation and Supply, SUPERGEN '09*, no. 1, pp. 1–6, 2009. 13

[78] M. Yagami, S. Ishikawa, Y. Ichinohe, K. Misawa, and J. Tamura, "Power system transient stability analysis in the case of high-penetration photovoltaics (part 2)," *2015 IEEE Eindhoven PowerTech, PowerTech 2015*, 2015. 13

[79] Z. Tashman, H. Khalilinia, and V. Venkatasubramanian, "Multi-dimensional fourier ringdown analysis for power systems using synchrophasors," *IEEE Transactions on Power Systems*, 2014. 15

[80] V. S. Peric and L. Vanfretti, "Power-system ambient-mode estimation considering spectral load properties," *IEEE Transactions on Power Systems*, 2014. 16

[81] L. Ljung, "System identification toolbox," *The Matlab user's guide*, 2011. 16

[82] K. Ogata, *Modern Control Engineering Fifth Edition*, 2009. 16, 22

[83] MATLAB, "Output-Error polynomial model in MATLAB." [Online]. Available: https://www.mathworks.com/help/ident/ref/oe.html 18

[84] C. Van Loan, *Computational Frameworks for the Fast Fourier Transform*, 1992. 20

[85] L. Zhu, Y. Zhao, Y. Liu, E. Farantatos, M. Patel, P. Dattaray, D. Ramasubramanian, L. Michi, E. Carlini, G. Giannuzzi, and R. Zaottini, "Oscillation damping controller design using ringdown measurements for the Italian power grid," *2019 IEEE Milan PowerTech, PowerTech 2019*, no. 1509624, 2019. 21, 26, 27

[86] X. Yang and A. Fellachi, "Stabilization of inter area oscillation modes through excitation systems," *IEEE Transactions on Power Systems*, 1994. 22

[87] Y. Zhao, C. Lu, Y. Liu, and Y. Han, "Residue and Identification based Wide-area Damping Controller Design in Large-scale Power System," pp. 1–7, 2011. 23, 25

[88] J. Zhang, C. Y. Chung, and Y. Han, "A novel modal decomposition control and its application to PSS design for damping interarea oscillations in power systems," *IEEE Transactions on Power Systems*, 2012. 27

[89] OPEC, "OPEC : OPEC Share of World Crude Oil Reserves," 2018. 29

[90] SEC, "Annual Report 2017," Tech. Rep., 2017. [Online]. Available: https://www.se.com.sa/enus/Lists/NGReports/Attachments/3/NG{_}2017{_}AR.pdf 29

[91] Y. Zhang, P. Markham, T. Xia, L. Chen, Y. Ye, Z. Wu, Z. Yuan, L. Wang, J. Bank, J. Burgett, R. W. Conners, and Y. Liu, "Wide-area frequency monitoring network (FNET) architecture and applications," *IEEE Transactions on Smart Grid*, 2010. 31

[92] I. P. E. Society, E. D. Committee, P. Generation, I. o. E. Engineers, Electronics, and I.-S. S. Board, "IEEE Standard for High-Potential Test Requirements for Excitation Systems for Synchronous Machines," *IEEE Std 421.3-1997*, 1998. 37

[93] G. Zhang, "EPRI Power Systems Dynamics Tutorial," EPRI, Tech. Rep., 2009. 37

[94] A. Almubarak, Alkadhem Motaz, A. Agustoni, A. Ardito, A. Danelli, S. Malgarotti, and I. Valadè, "Saudi Arabia Central-West HVDC Project: 3500 MW ±600 kV 770km High Performance embedded link crossing a desert area." Paris, France: CIGRE, 2016, p. 10. 61

[95] Siemens, *PSSe Manual*. 61

[96] N. K. Rajalwal and D. Ghosh, "Recent trends in integrity protection of power system: A literature review," *International Transactions on Electrical Energy Systems*, vol. 30, no. 10, pp. 1–43, 2020. 65

[97] R. Moreno and A. Torres, "Security of the power system based on the separation into islands," *2011 IEEE PES Conference on Innovative Smart Grid Technologies Latin America SGT LA 2011 - Conference Proceedings*, pp. 1–5, 2011. 65

[98] J. O'Brien, E. Barrett, X. Fan, R. Diao, R. Huang, and Q. Huang, "Adaptive RAS/SPS System Settings for Improving Grid Reliability and Asset Utilization through Predictive Simulation and Controls," PACIFIC NORTHWEST NATIONAL LABORATORY, Tech. Rep., 2017. [Online]. Available: https://www.osti.gov/servlets/purl/1580707 65, 113

[99] P. Apkarian, M. N. Dao, and D. Noll, "Parametric Robust Structured Control Design," *IEEE Transactions on Automatic Control*, 2015. 73

[100] P. Apkarian and D. Noll, "The H Control Problem is Solved," *Control*, 2006. 73

[101] L. C. G. De Souza and X. C. Méndez Cubillos, "Using of H-infinity control method in attitude control system of rigid-flexible satellite," *Mathematical Problems in Engineering*, 2009. 73

[102] P. Lundstrom, S. Skogestad, and Z. Q. Wang, "Uncertainty weight selection for H-infinity and mu-control methods," in *Proceedings of the IEEE Conference on Decision and Control*, 1991. 73

[103] J. Gadewadikar, F. L. Lewis, K. Subbarao, and B. M. Chen, "Structured H command and control-loop design for unmanned helicopters," *Journal of Guidance, Control, and Dynamics*, 2008. 73

[104] A. Akrami, M. Doostizadeh, and F. Aminifar, "Power system flexibility: an overview of emergence to evolution," 2019. 73

[105] K. Zhou, "Essentials of robust control," *Automatica*, 1999. 73, 74

[106] M. O. Faruque, T. Strasser, G. Lauss, V. Jalili-Marandi, P. Forsyth, C. Dufour, V. Dinavahi, A. Monti, P. Kotsampopoulos, J. A. Martinez, K. Strunz, M. Saeedifard, X. Wang, D. Shearer, M. Paolone, R. Brandl, M. Matar, A. Davoudi, and R. Iravani, "Real-Time Simulation Technologies for Power Systems Design, Testing, and Analysis," *IEEE Power and Energy Technology Systems Journal*, 2015. 79, 91

[107] P. M. Menghal and A. J. Laxmi, "Real time simulation: Recent progress & challenges," *2012 International Conference on Power, Signals, Controls and Computation, EPSCICON 2012*, pp. 1–6, 2012. 79

[108] C. Yang, Y. Xue, X. P. Zhang, Y. Zhang, and Y. Chen, "Real-time FPGA-RTDS co-simulator for power systems," *IEEE Access*, vol. 6, pp. 44 917–44 926, 2018. 79, 91

[109] F. Tian, C. Yue, Z. Wu, and X. Zhou, "Realization of electromechanical transient and electromagnetic transient real time hybrid simulation in power system," in *Proceedings of the IEEE Power Engineering Society Transmission and Distribution Conference*, 2005. 79, 91

[110] D. Shu, X. Xie, Q. Jiang, Q. Huang, and C. Zhang, "A Novel Interfacing Technique for Distributed Hybrid Simulations Combining EMT and Transient Stability Models," *IEEE Transactions on Power Delivery*, 2018. 79, 91

[111] Powertech Labs Inc., "TSAT-RTDS Interface." [Online]. Available: https://www.dsatools.com/wp-content/uploads/2020/01/TRI{_}brochure.pdf 80

[112] I. Altarjami, L. Zhu, D. Lu, X. Deng, Y. Liu, E. Farantatos, D. Ramasubramanian, M. Patel, M. Ijaz, A. AlMubarak, and S. Bashraheel, "Impact of Wide-Area Oscillation Damping Control on System Separation - Saudi Grid Case Study," in *IEEE PES T&D 2020*. Chicago: IEEE PES T&D 2020, 2020. 81

[113] X. Guillaud, M. O. Faruque, A. Teninge, A. H. Hariri, L. Vanfretti, M. Paolone, V. Dinavahi, P. Mitra, G. Lauss, C. Dufour, P. Forsyth, A. K. Srivastava, K. Strunz, T. Strasser, and A. Davoudi, "Applications of Real-Time Simulation Technologies in

Power and Energy Systems," *IEEE Power and Energy Technology Systems Journal*, 2015. 91

[114] "CompactRIO Controller." [Online]. Available: http://www.ni.com/en-us/shop/select/compactrio-controller?modelId=119752 91

[115] V. Jalili-Marandi, V. Dinavahi, K. Strunz, J. A. Martinez, and A. Ramirez, "Interfacing techniques for transient stability and electromagnetic transient programs: IEEE task force on interfacing techniques for simulation tools," *IEEE Transactions on Power Delivery*, 2009. 91

[116] "TSAT-RTDS™ INTERFACE (TRI)." [Online]. Available: https://www.dsatools.com/tsat-rtds-interface-tri/ 91, 92, 95

[117] NationalInstruments, "LabVIEW for CompactRIO Developer's Guide," Austin,TX, Tech. Rep. 97

[118] "National Instruments - 9035." [Online]. Available: https://www.ni.com/en-us/support/model.crio-9035.html 97

[119] M. S. Almas, L. Vanfretti, and M. Baudette, "BabelFish—Tools for IEEE C37.118.2-compliant real-time synchrophasor data mediation," *SoftwareX*, 2017. 97

[120] "National Instruments - 9467." [Online]. Available: https://www.ni.com/en-us/support/model.ni-9467.html 99

[121] "National Instruments - 9263." [Online]. Available: https://www.ni.com/en-us/support/model.ni-9263.html 100

[122] S. Gurung, S. Naetiladdanon, and A. Sangswang, "Impact of photovoltaic penetration on small signal stability considering uncertainties," in *2017 IEEE Innovative Smart Grid Technologies - Asia: Smart Grid for Smart Community, ISGT-Asia 2017*, 2018. 124

[123] C. S. Lai, Y. Jia, L. L. Lai, Z. Xu, M. D. McCulloch, and K. P. Wong, "A comprehensive review on large-scale photovoltaic system with applications of electrical energy storage," 2017. 124, 125

[124] S. Adhikari and F. Li, "Coordinated V-f and P-Q control of solar photovoltaic generators with MPPT and battery storage in microgrids," *IEEE Transactions on Smart Grid*, 2014. 124

[125] M. Dreidy, H. Mokhlis, and S. Mekhilef, "Inertia response and frequency control techniques for renewable energy sources: A review," 2017. 124

[126] H. Setiadi, A. U. Krismanto, and N. Mithulananthan, "Influence of BES system on local and inter-Area oscillation of power system with high penetration of PV plants," in *Proceedings of the 2017 IEEE International Conference on Applied System Innovation: Applied System Innovation for Modern Technology, ICASI 2017*, 2017. 124

[127] J. C. Neely, R. H. Byrne, R. T. Elliott, C. A. Silva-Monroy, D. A. Schoenwald, D. J. Trudnowski, and M. K. Donnelly, "Damping of inter-area oscillations using energy storage," in *IEEE Power and Energy Society General Meeting*, 2013. 124

[128] X. Sui, Y. Tang, H. He, and J. Wen, "Energy-storage-based low-frequency oscillation damping control using particle swarm optimization and heuristic dynamic programming," *IEEE Transactions on Power Systems*, 2014. 124

[129] M. Beza and M. Bongiorno, "An adaptive power oscillation damping controller by STATCOM with energy storage," *IEEE Transactions on Power Systems*, 2015. 124

[130] L. Shi, K. Y. Lee, and F. Wu, "Robust ESS-Based Stabilizer Design for Damping Inter-Area Oscillations in Multimachine Power Systems," *IEEE Transactions on Power Systems*, 2016. 124

[131] I. Serban and C. Marinescu, "Control strategy of three-phase battery energy storage systems for frequency support in microgrids and with uninterrupted supply of local loads," *IEEE Transactions on Power Electronics*, 2014. 124

[132] M. A. Torres L., L. A. Lopes, L. A. Morán T., and J. R. Espinoza C., "Self-tuning virtual synchronous machine: A control strategy for energy storage systems to support dynamic frequency control," *IEEE Transactions on Energy Conversion*, 2014. 124

[133] Y. Zhu, C. Liu, B. Wang, and K. Sun, "Damping control for a target oscillation mode using battery energy storage," *Journal of Modern Power Systems and Clean Energy*, 2018. 125

[134] H. Silva-Saravia, H. Pulgar-Painemal, and J. M. Mauricio, "Flywheel Energy Storage Model, Control and Location for Improving Stability: The Chilean Case," *IEEE Transactions on Power Systems*, 2017. 125

# Appendices

# A SEC Coherent groups

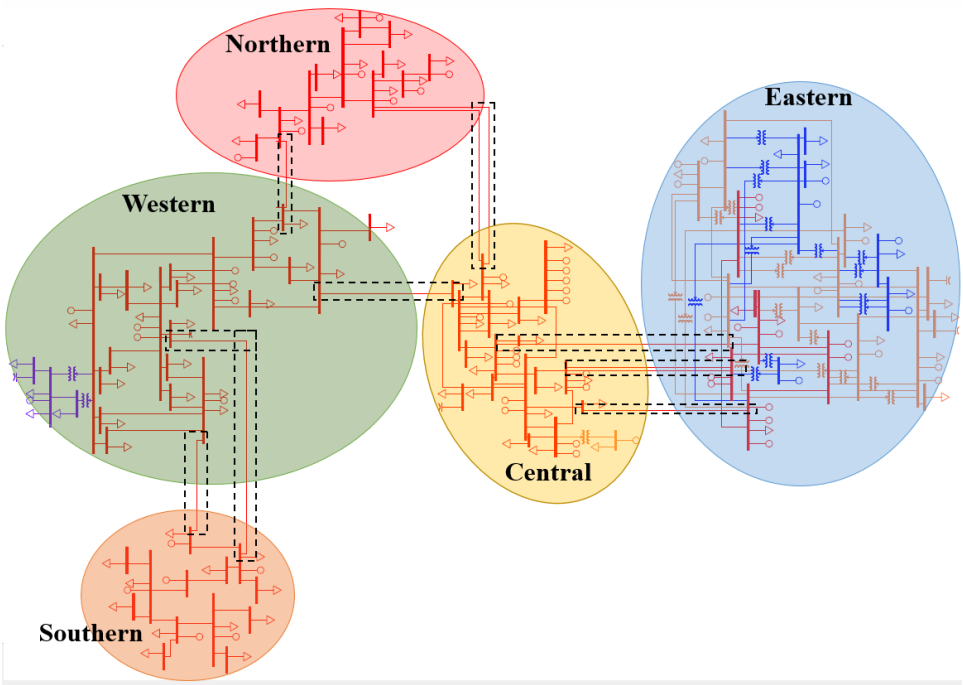


**Figure A.1:** SEC Coherent groups

# B Addition Results for Impact of the WADC (Base Case)

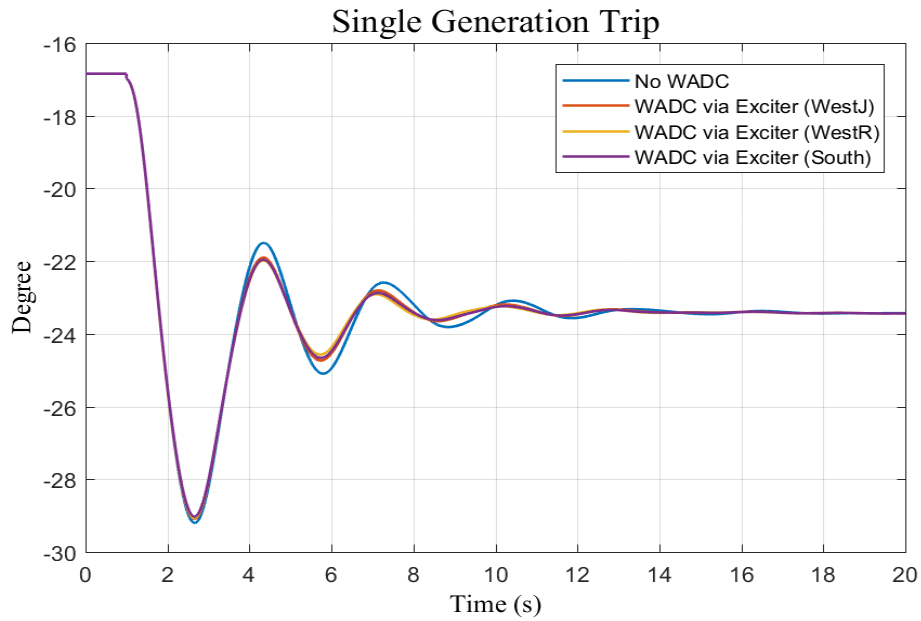


**Figure B.2:** Angle difference response during single generation trip (WADCs via single plant exciters).

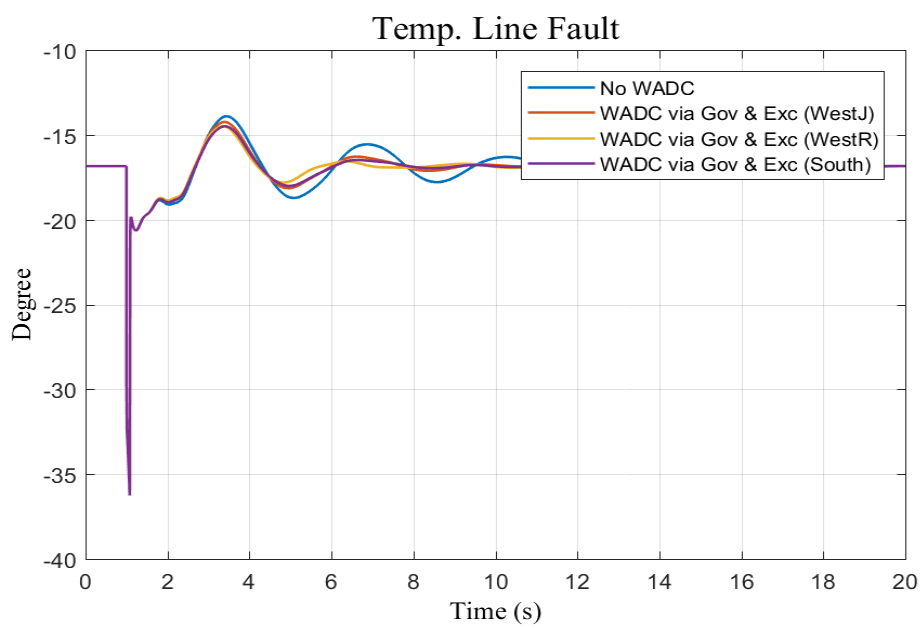


**Figure B.3:** Angle difference response during tie-line fault (WADCs via governor and exciter).

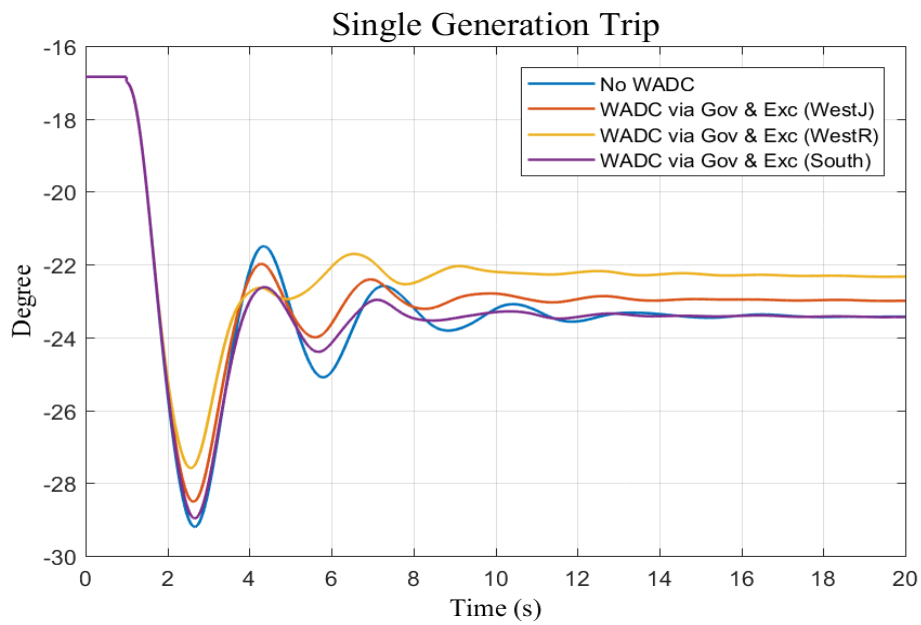


**Figure B.4:** Angle difference response during single generation trip (WADCs via governor and exciter).

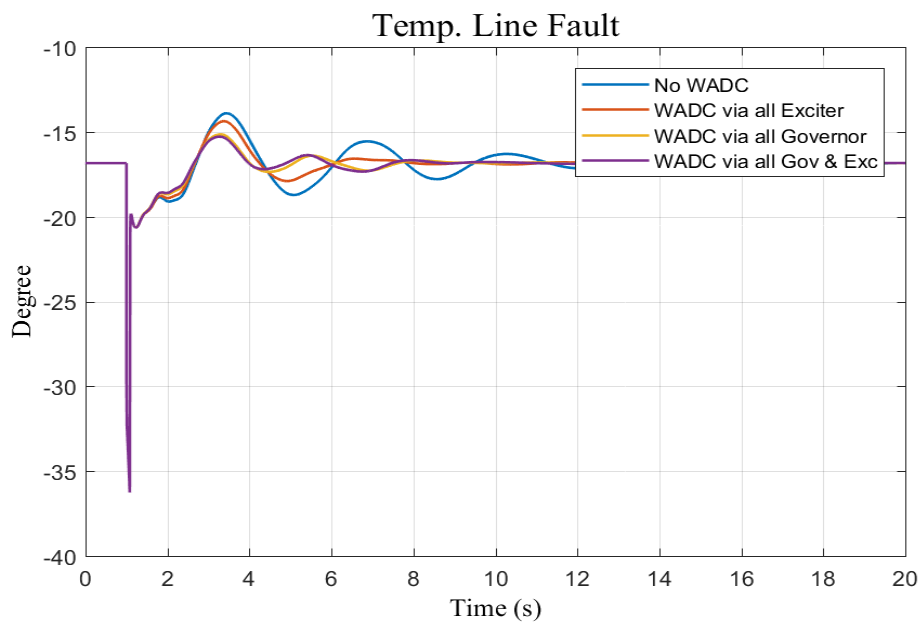


**Figure B.5:** Angle difference response during tie-line fault (WADCs via multiple actuators).

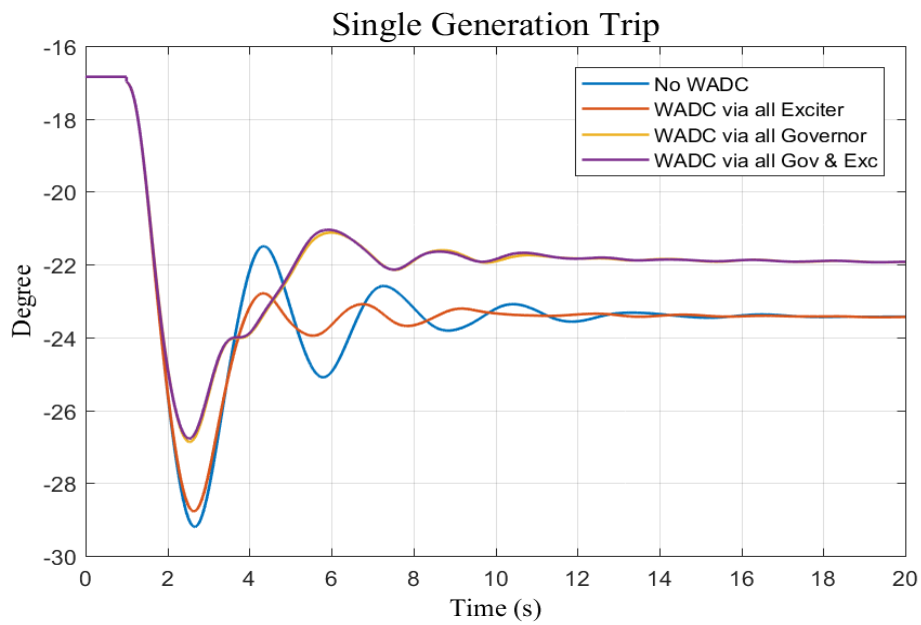


**Figure B.6:** Angle difference response during single generation trip (WADCs via multiple actuators).

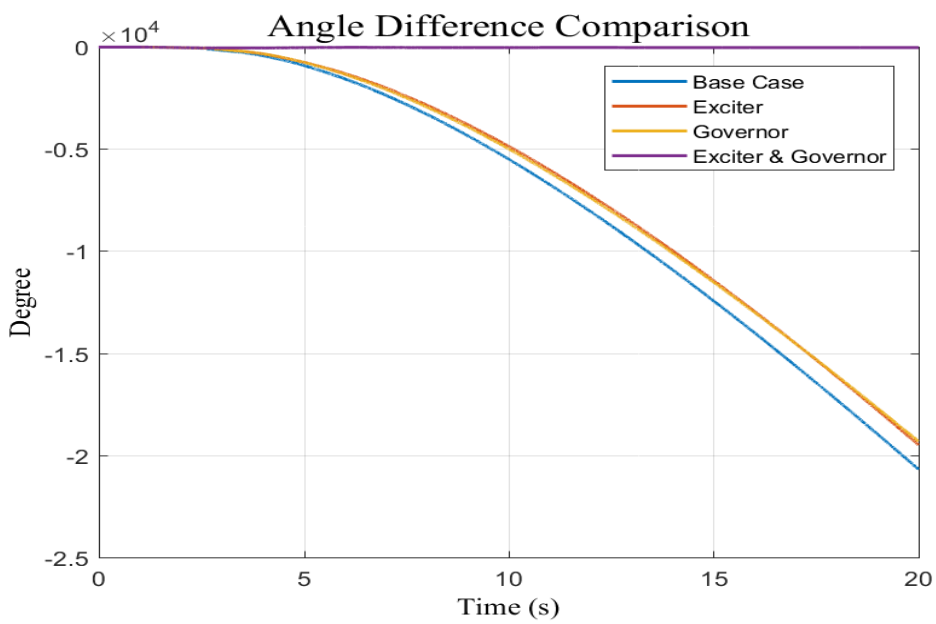


**Figure B.7:** WADC via multiple actuators angle difference after large generation trip (2040 MW).

**Table B.1:** Transfer function model for each selected generator exciter actuator

| **Bus No.** | **Order** | **Fitness Index (%)** | **Residue Angle (deg.)** | **Residue Mag. (Normalized)** | **Oscillation frequency (Hz)** | **Damping ratio (%)** |
|---|---|---|---|---|---|---|
| South57 | 6 | 84.08 | 156.13 | 1.000 | 0.2855 | 20.18 |
| West17 | 6 | 80.88 | 135.2 | 0.928 | 0.2916 | 16.88 |
| East44 | 6 | 85.25 | -108.70 | 0.825 | 0.2890 | 18.91 |
| West80 | 8 | 83.32 | 43.94 | 0.784 | 0.2909 | 16.25 |
| West94 | 8 | 83.29 | 43.90 | 0.761 | 0.2806 | 15.96 |
| East181 | 6 | 87.72 | -108.63 | 0.436 | 0.2827 | 14.50 |
| West69 | 10 | 85.56 | 87.04 | 0.667 | 0.2627 | 22.66 |
| South11 | 8 | 83.47 | 87.04 | 0.667 | 0.2630 | 22.66 |
| South07 | 8 | 85.12 | 87.04 | 0.667 | 0.2630 | 22.66 |
| East88 | 5 | 89.52 | 12.93 | 0.422 | 0.2818 | 17.49 |
| East481 | 10 | 85.21 | -111.09 | 0.297 | 0.2827 | 11.04 |
| East37 | 5 | 89.04 | -6.65 | 0.278 | 0.2791 | 16.01 |
| West15 | 7 | 75.01 | 125.17 | 0.201 | 0.2943 | 15.31 |

**Table B.2:** Transfer function model for each selected generator governor actuator

| **Bus No.** | **Order** | **Fitness Index (%)** | **Residue Angle (deg.)** | **Residue Mag. (Normalized)** | **Oscillation frequency (Hz)** | **Damping ratio (%)** |
|---|---|---|---|---|---|---|
| South57 | 6 | 75.97 | -85.44 | 1.000 | 0.275 | 14.67 |
| West17 | 6 | 85.76 | -31 | 0.981 | 0.287 | 19.05 |
| East88 | 6 | 88.81 | 127.98 | 0.875 | 0.305 | 17.98 |
| West55 | 7 | 83.51 | -65.78 | 0.872 | 0.294 | 18.36 |
| West94 | 6 | 84.89 | -66.37 | 0.855 | 0.309 | 17.68 |
| West80 | 6 | 82.95 | -64.98 | 0.824 | 0.301 | 15.48 |
| South11 | 5 | 87.92 | -62.10 | 0.814 | 0.293 | 16.93 |
| West20 | 5 | 87.91 | -68.39 | 0.801 | 0.304 | 17.76 |
| West69 | 5 | 81.93 | -71.95 | 0.800 | 0.316 | 15.58 |
| West15 | 6 | 85.43 | -79.91 | 0.759 | 0.311 | 16.28 |
| East181 | 6 | 86.80 | 120.14 | 0.715 | 0.313 | 16.95 |
| East37 | 7 | 87.31 | 143.35 | 0.702 | 0.299 | 15.45 |

**Table B.3:** WADC parameters

| WADC location | Actuator | Filter block | | | | | Washout block | | Lead-lag block | | |
|---|---|---|---|---|---|---|---|---|---|---|---|
| | | a0 | a1 | a2 | b1 | b2 | G | T | G | T1 | T2 |
| WestJ | exciter | 0 | 1.788 | 0 | 1.788 | 3.162 | 10 | 10 | 10 | 0.6733 | 0.4670 |
| WestR | exciter | 0 | 1.788 | 0 | 1.788 | 3.162 | 10 | 10 | 10 | 0.7466 | 0.4269 |
| South | exciter | 0 | 1.788 | 0 | 1.788 | 3.162 | 10 | 10 | 10 | 0.6178 | 0.5107 |
| WestJ | governor | 0 | 1.788 | 0 | 1.788 | 3.162 | 10 | 10 | 20 | N/A | N/A |
| WestR | governor | 0 | 1.788 | 0 | 1.788 | 3.162 | 10 | 10 | 20 | N/A | N/A |
| South | governor | 0 | 1.788 | 0 | 1.788 | 3.162 | 10 | 10 | 20 | N/A | N/A |

# C Addition Results of impact for the WADC (HVDC, PV cases, and BESS)

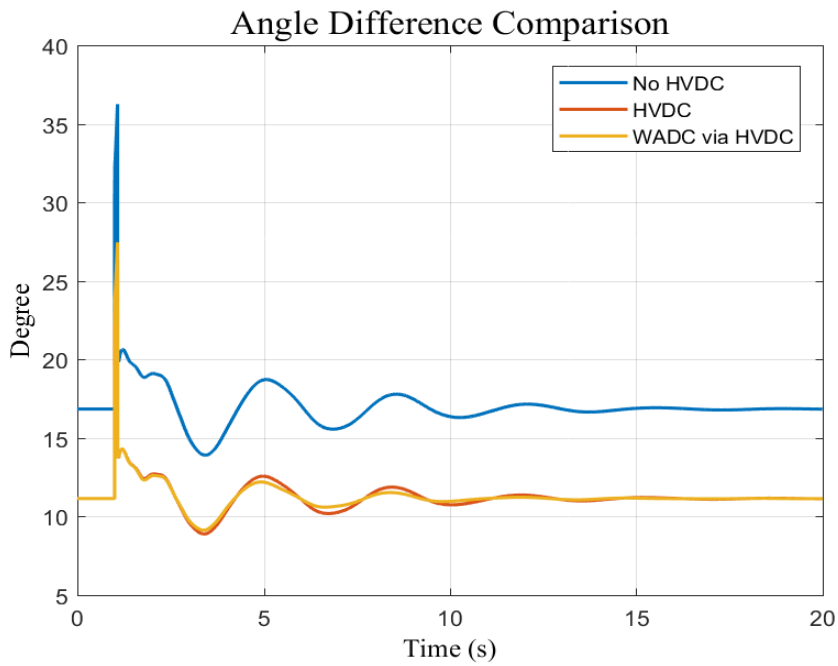


**Figure C.1:** Angle difference comparison response during line fault (HVDC case).

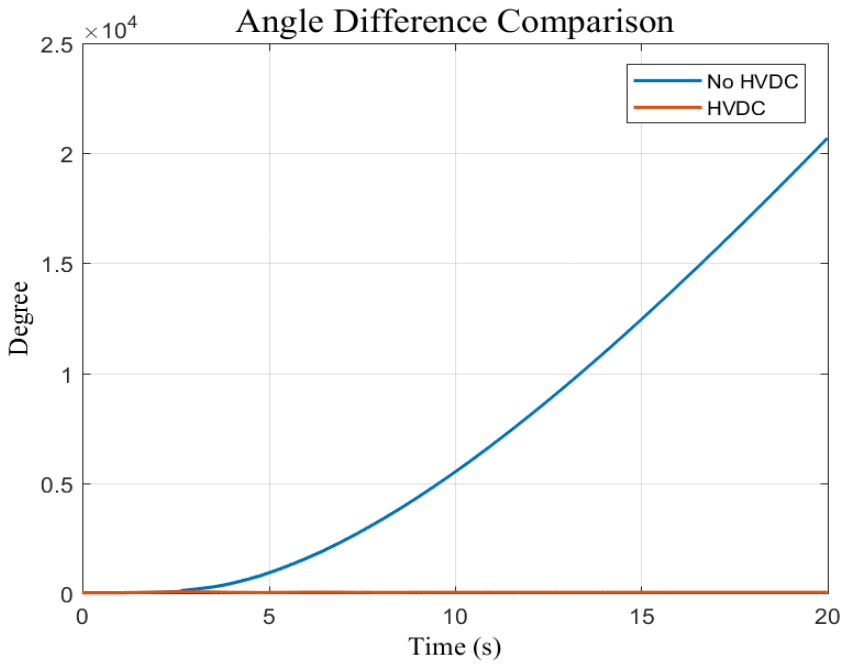


**Figure C.2:** WADC via HVDC angle difference after large generation trip (2040 MW).

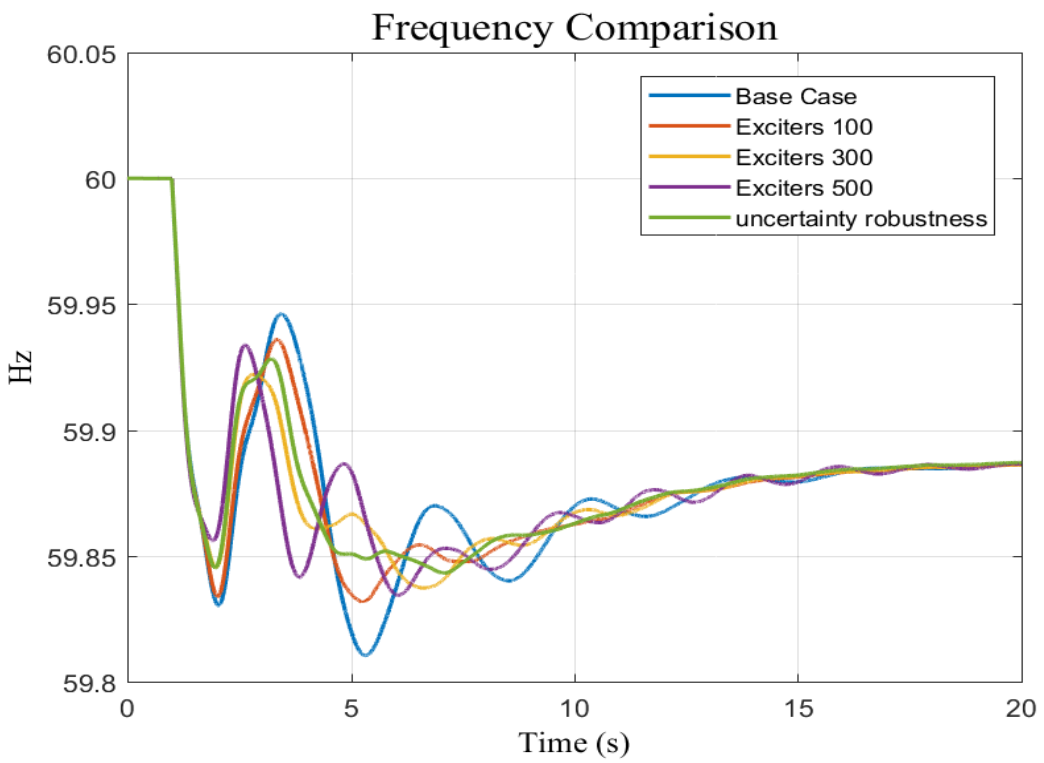


**Figure C.3:** Frequency response after two generators trip with gain robustness function (WADCs via exciters).

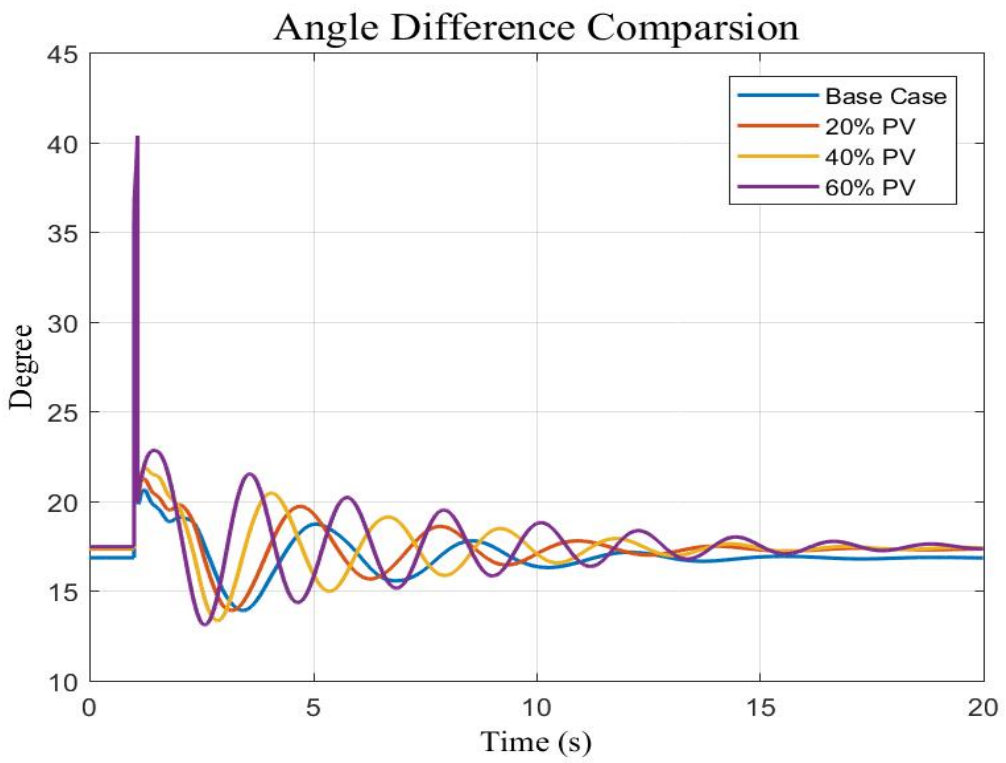


**Figure C.4:** Tie-line angle difference response during tie-line fault (PV level comparison).

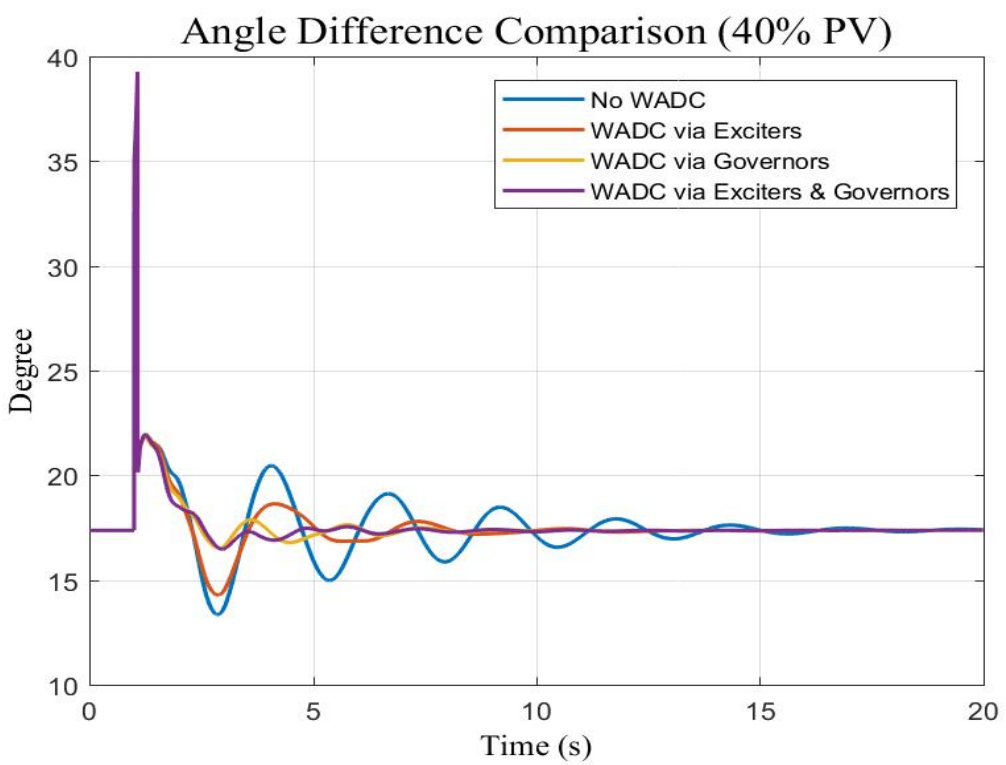


**Figure C.5:** Angle difference response during tie-line fault (40% PV).

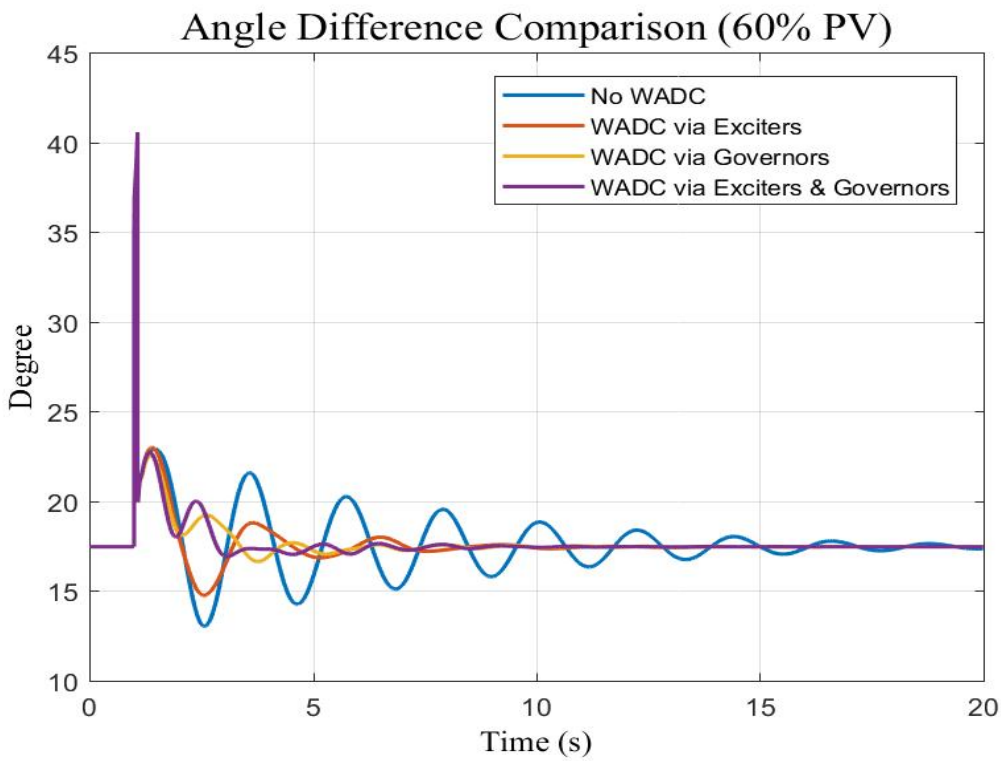


**Figure C.6:** Angle difference response during tie-line fault (60% PV).

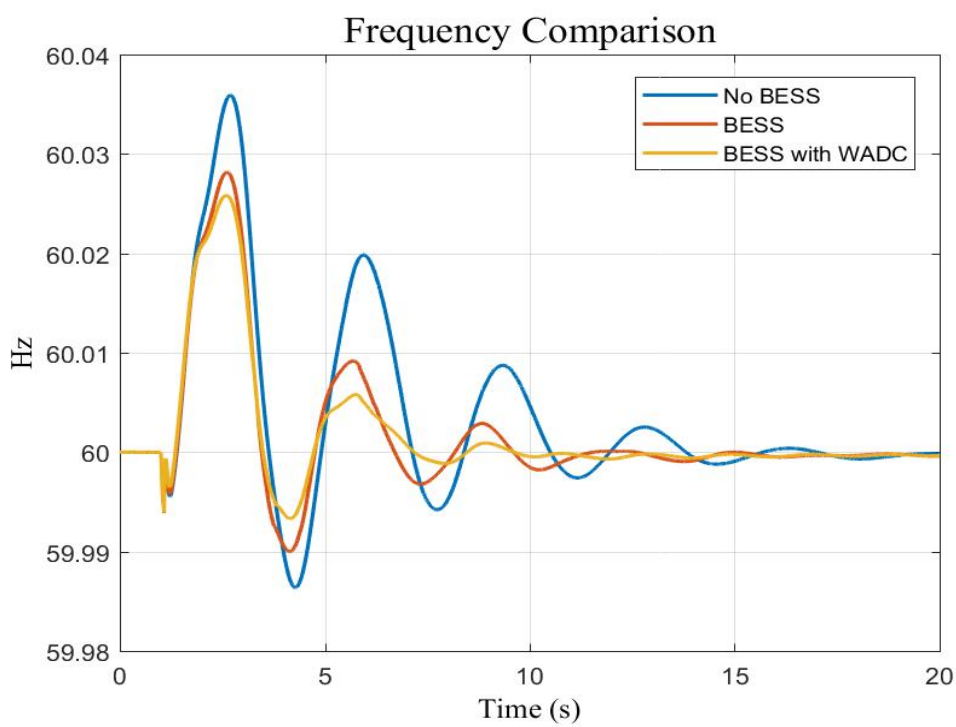


**Figure C.7:** Frequency response during line fault (WADC via BESS).

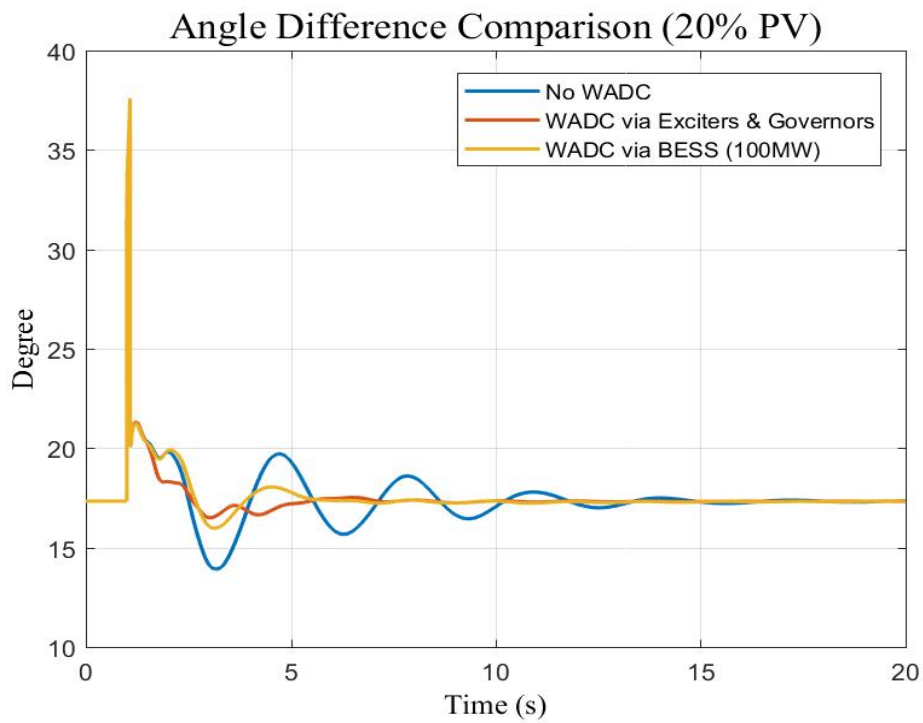


**Figure C.8:** Angle difference response during tie-line fault (20% PV with BESS).

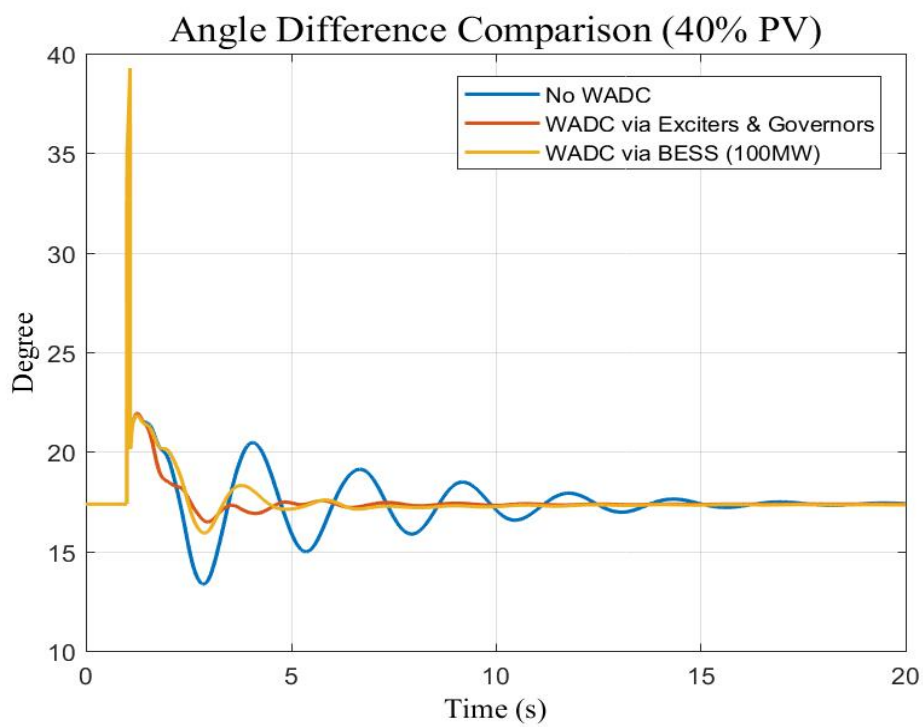


**Figure C.9:** Angle difference response during tie-line fault (40% PV with BESS).

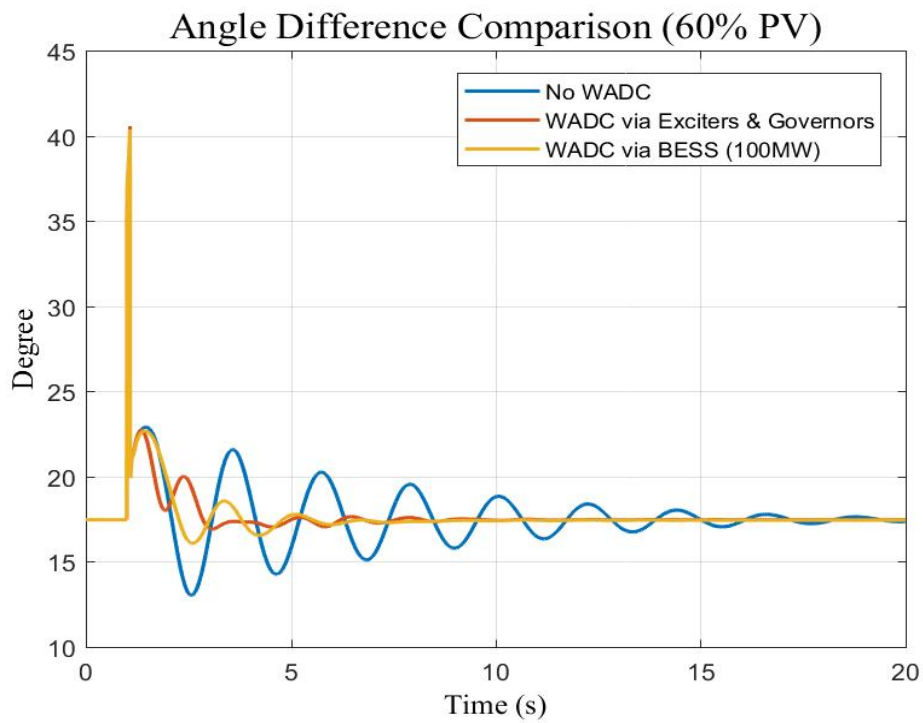


**Figure C.10:** Angle difference response during tie-line fault (60% PV with BESS).

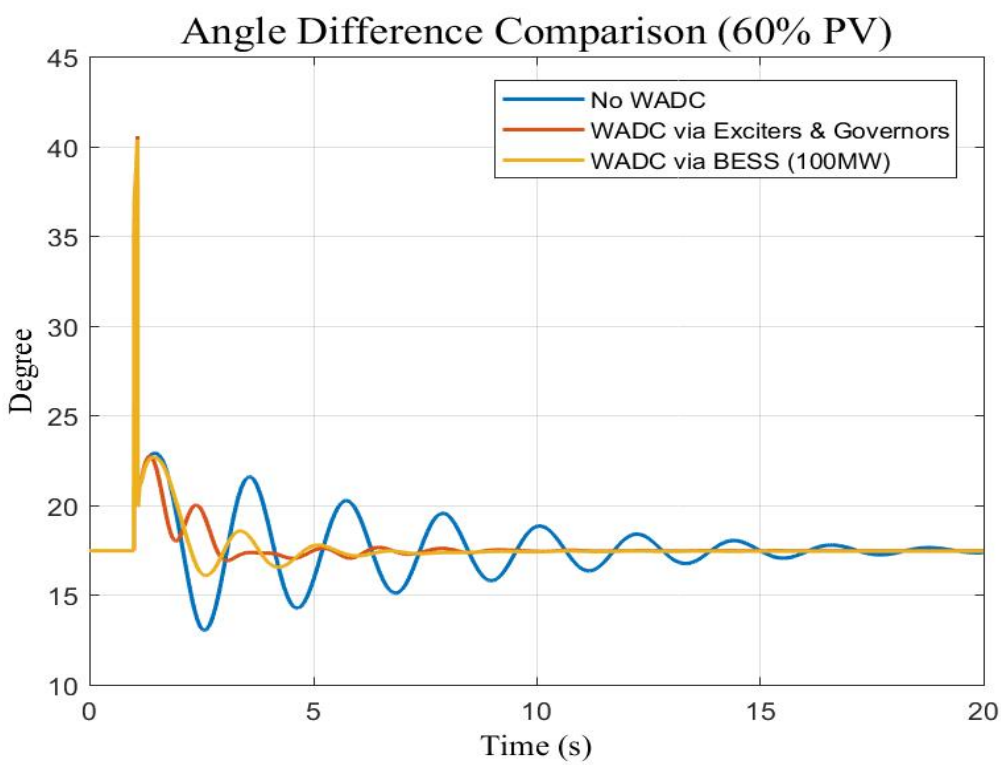


**Figure C.11:** Angle difference response during tie-line fault (60% PV with BESS).

# D Data Loss Handling Process

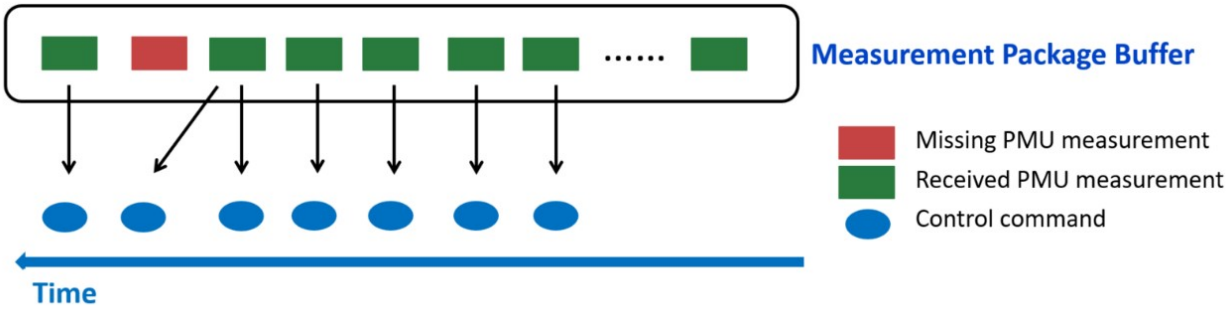


**Figure D.1:** The missing data handling process.

# Vita

Ibrahim Altarjami was born in Madinah, Saudi Arabia. He got his B.S. degree in Department of Electrical Engineering from Taibah University, Madinah, Saudi Arabia, in 2012. After that, he got the M.S. degree in the Department of Electrical Engineering and Computer Science from the University of Tennessee, Knoxville, TN, USA, in 2017. He is working towards his Ph.D. degree in the Department of Electrical Engineering and Computer Science, University of Tennessee, Knoxville, with anticipated graduation in May 2021. His research interests include power system stability and control, and renewable energy penetration.